

# **DISSERTATION**

submitted to the

Combined Faculties for the Natural Sciences and for Mathematics

of the

Ruperto-Carola University of Heidelberg, Germany

for the degree of

Doctor of Natural Sciences

presented by

M.Sc. Daniela Casarrubea

born in Palermo (Italy)

Oral examination: 1<sup>st</sup> February 2013



**A NEW MOUSE MODEL WITH GAIN OF IRON  
REGULATORY PROTEIN 1 FUNCTION**

Referees:

1. Dr. Darren Gilmour
2. Prof. Dr. Klaus Unsicker



## SUMMARY

Disorders of iron metabolism account for some of the most common human diseases, such as anemias and hemochromatosis. To maintain physiological iron balance, homeostatic mechanisms are normally in place both at the systemic and the cellular level. Cellular iron homeostasis is secured by Iron Regulatory Proteins (IRP) –1 and –2 through their binding to cis-regulatory iron-responsive elements (IRE) in target mRNAs encoding proteins with key functions in iron metabolism. In turn, the IRE-binding activity of the two IRPs is feedback regulated by the cellular labile iron pool. Mouse models with IRP deficiency have contributed valuable insights into the *in vivo* roles of the IRP/IRE system as well as mammalian iron biology. However, the physiological consequences of gain of IRP function have so far remained unexplored.

To investigate the importance of adequate IRP expression *in vivo*, we have generated a mouse model allowing conditional gain of IRP function using Cre/Lox technology. This new line expresses a flag-tagged IRP1 mutant (IRP1\*), which escapes iron-mediated regulation, being constitutively active in its IRE binding form.

Systemic expression of the IRP1\* transgene from the *Rosa26* locus yields viable animals with gain of IRE-binding activity in all organs that were analyzed. IRP1\* alters the expression of IRP target genes and is accompanied by abnormal body iron distribution. Furthermore, mice display macrocytic erythropenia with decreased hematocrit and hemoglobin levels. Flow cytometric analysis of bone marrow-derived erythroid precursors also revealed impaired erythroid differentiation. Under standard laboratory conditions, broad spectrum phenotyping of IRP1\* mice revealed that gain of IRP1 function does not affect their general health status. Yet, when challenged, mice displayed mildly altered motor coordination and reduced endurance as well as impaired neuromuscular transmission, suggesting a potential role of appropriate IRP activity in maintenance of neuromuscular function. *Ex vivo*, iron challenged bone marrow-derived macrophages showed that IRP1\* expression alters the cellular response to fluctuations in iron levels. However, when IRP1\* mice were pharmacologically administered with iron or crossed with a mouse model of chronic iron overload, IRP1\* expression did not produce any overt abnormalities in the animal response to the iron challenges.

In conclusion, this work describes the first model of gain of IRP1 function in a mammalian organism. This new mouse model further highlights the importance of appropriate IRP regulation in central organs of iron metabolism as well as for general physiology. Moreover, it opens novel avenues for study of diseases associated with abnormally high IRP activity, such as Parkinson's disease or Friedreich ataxia.

---

**ZUSAMMENFASSUNG****Ein neues Mausmodell mit erhöhter Aktivität des *Iron Regulatory Protein 1***

Störungen des Eisenstoffwechsels sind für einige der häufigsten Krankheiten des Menschen verantwortlich, wie etwa der Anämie und der Hämochromatose. Um eine physiologische Eisenbalance zu gewährleisten, spielen homöostatische Mechanismen sowohl auf der systemischen wie auch auf der zellulären Ebene eine wichtige Rolle. Dabei wird die zelluläre Eisenhomöostase durch zwei Proteine, *Iron Regulatory Proteins* (IRP -1 und -2), vermittelt. Dies geschieht durch IRP-Bindung an cis-regulatorische Elemente, *iron responsive elements* (IRE), in mRNAs die für Proteine kodieren, die ihrerseits Schlüsselfunktionen im Eisenstoffwechsel einnehmen. Gleichzeitig wird die IRE-bindende Aktivität der beiden IRPs mittels eines *feedback* Mechanismus durch den verfügbaren Eisenpool der Zelle reguliert. IRP-defiziente Mausmodelle konnten bereits wertvolle Einblicke in die Rolle des IRP/IRE Systems *in vivo* und in die RNA-Biologie von Säugetieren geben. Auf der anderen Seite blieben die physiologischen Konsequenzen einer erhöhten IRP Aktivität bislang weitgehend unbekannt.

Zur Erforschung des Einflusses einer adäquaten IRP Expression *in vivo* haben wir ein Mausmodell generiert, das eine konditional erhöhte IRP Aktivität durch Cre/Lox Technologie ermöglicht. Diese neue Mauslinie exprimiert eine mit dem *Flag* Peptid versehene IRP1 Mutante (IRP1\*), die unabhängig vom Eisenstatus konstitutiv in ihrer IRE bindenden Form vorliegt.

Systemische Expression des in den *Rosa26* Locus integrierten IRP1\* Transgen führt zur Überexpression IRE-bindender Aktivität in allen analysierten Organen. IRP1\* verändert die Expression von IRP regulierten Genen und führt zu einer anomalen Verteilung des Eisens im Körper. Ausserdem zeigen diese Mäuse eine makrozytäre Erythropenie mit erniedrigten Hämatokrit- und Hämoglobinwerten. Durch analytische Durchflusszytometrie von Erythrozytenvorläufern aus Knochenmarksgewebe entdeckten wir ausserdem eine Einschränkung der Erythrozytendifferenzierung. Unter Standardlaborbedingungen zeigte eine weitangelegte Phänotypisierung der IRP1\* Mäuse dass die zusätzliche IRP1\* Aktivität keinen generellen Effekt auf ihre Gesundheit hat. Allerdings fanden sich unter Belastungsbedingungen eine leicht verminderte motorische Koordination sowie reduzierte Ausdauer und gestörte neuromuskuläre Signalweiterleitung, was auf eine mögliche Rolle adäquater IRP-Aktivität bei der Aufrechterhaltung von neuromuskulären Funktionen hindeutet. Ex vivo zeigten aus Knochenmark gewonnene und mit Eisen oder Eisenchelatoren behandelte Makrophagen, dass die IRP1\* Expression die zelluläre Antwort auf Schwankungen der Eisenverfügbarkeit verändert. Allerdings

konnten wir beobachten, dass IRP1\* Mäuse die IRP1\* Expression weder nach pharmakologischer Gabe von Eisen noch nach Kreuzung mit einem Mausmodell chronischer Eisenüberladung zu irgendwelchen offenkundigen Abnormalitäten bei der Reaktion auf wechselnde Eisenkonzentrationen führte.

Zusammenfassend beschreibt diese Arbeit das erste Modell gesteigerter IRP1 Aktivität bei einem Säugetier. Dieses neue Mausmodell unterstreicht die Bedeutung der IRP Regulation in zentralen Organen des Eisenstoffwechsels sowie für die generelle Physiologie. Es eröffnet neue Möglichkeiten Krankheiten zu untersuchen, die mit anomal hoher IRP Aktivität verbunden sind, wie zum Beispiel Morbus Parkinson oder die Friedreichsche Ataxie.

---

---

---

**TABLE OF CONTENTS**

<b>I. LIST OF FIGURES .....</b>	<b>V</b>
<b>II. LIST OF TABLES.....</b>	<b>VI</b>
<b>III. LIST OF ABBREVIATIONS .....</b>	<b>VII</b>
<b>1. INTRODUCTION .....</b>	<b>1</b>
1.1 Iron biology.....	1
1.1.1 The light and dark side of iron biochemistry .....	1
1.1.2 Disorders of iron metabolism .....	2
1.2 Systemic iron metabolism.....	3
1.2.1 Systemic iron fluxes .....	3
1.2.2 Systemic regulation of iron homeostasis: hepcidin .....	5
1.3 Cellular iron metabolism.....	7
1.3.1 Cellular iron uptake .....	7
1.3.2 Cellular iron utilization.....	9
1.3.3 Cellular iron storage .....	10
1.3.4 Cellular iron export.....	11
1.4 Regulation of cellular iron metabolism.....	12
1.4.1 The structure of the IREs and the IRPs.....	12
1.4.2 IRP/IRE post-transcriptional regulation of “iron-genes” .....	14
1.4.3 Regulation of IRP activity .....	15
1.4.4 Expanding the IRP regulon.....	16
1.5 The IRP/IRE system in physiology and disease .....	17
1.5.1 The IRP/IRE system in erythropoiesis.....	18
1.5.2 The IRP/IRE system in duodenal iron absorption .....	23
1.5.3 The IRP/IRE system in liver function.....	25
1.5.4 The IRP/IRE system in disease.....	27
<b>1.6 AIM OF THE THESIS .....</b>	<b>31</b>
<b>2. MATERIALS AND METHODS .....</b>	<b>33</b>
<b>2.1 MATERIALS .....</b>	<b>33</b>

## TABLE OF CONTENTS

---

2.1.1 Chemicals and reagents .....	33
2.1.2 Antibodies and enzymes .....	34
2.1.3 Buffers and solutions .....	35
2.1.4 Laboratory materials and kits .....	37
2.1.5 Instruments .....	38
2.1.6 PCR primers.....	39
<b>2.2 METHODS .....</b>	<b>41</b>
2.2.1 Standard conditions and treatments of laboratory animals .....	41
2.2.2 Standard mouse phenotyping.....	42
2.2.3 Hematology and tissue biochemistry .....	43
2.2.4 Cell biology .....	44
2.2.5 Molecular biology.....	45
2.2.6 Statistical Analyses.....	51
<b>3. RESULTS .....</b>	<b>53</b>
3.1 Generation of a mouse model with gain of IRP1 function .....	54
3.1.1 Targeted expression of a conditional gain of IRP1 function allele from the mouse <i>Rosa26</i> locus.....	54
3.1.2 Mice expressing IRP1* display increased IRE-binding activity .....	58
3.2 Impact of gain of IRP1 function on iron metabolism .....	61
3.2.1 Increased IRE-binding activity alters the expression of IRP targets in vivo .....	62
3.2.2 Gain of IRP1 function promotes iron loading in liver, spleen and duodenum .....	64
3.2.3 Abnormally high IRP1 activity causes macrocytic anemia .....	66
3.2.4 IRP1 hyper-activity impairs erythroid maturation.....	67
3.3 Standard phenotyping of mice with gain of IRP1 function .....	71
3.3.1 Gain of IRP1 activity does not affect the general health status of IRP1* mice .....	71
3.3.2 IRP1* mice display altered motor coordination and reduced endurance.....	72
3.3.3 Abnormally high IRP1 activity impairs neuromuscular transmission.....	73
3.4 Impact of IRP1* expression on the response to iron loading .....	75
3.4.1 IRP1* expression alters the response of bone marrow-derived macrophages to fluctuations of iron levels ex vivo.....	75
3.4.2 IRP1* does not detectably aggravate liver iron accumulation and ensuing oxidative injury in acutely iron overloaded mice .....	79
3.4.3 Consequences of IRP1* expression in chronic iron overloaded mice.....	80

---

<b>4. DISCUSSION .....</b>	<b>85</b>
4.1 First mammalian model with primary gain of IRP1 function.....	85
4.2 Appropriate IRP1 regulation is necessary for body iron homeostasis.....	87
4.2.1 IRP1* expression affects the expression of IRP targets and alters body iron distribution.....	87
4.2.2 High IRP1 activity impairs normal erythropoiesis .....	89
4.3 The IRP1* model reveals a potential involvement of the IRP/IRE system in neuromuscular function .....	91
4.4 Impact of IRP1*expression on acute or chronic iron loading.....	93
4.5 Concluding remarks .....	95
<b>5. BIBLIOGRAPHY .....</b>	<b>99</b>
<b>6. APPENDIX .....</b>	<b>127</b>
<b>6.1 STUDY DESIGN.....</b>	<b>127</b>
<b>6.2 MATERIALS AND METHODS .....</b>	<b>128</b>
6.2.1. Body weight, food intake and body composition .....	128
6.2.2 Energy expenditure.....	128
6.2.3 Calorimeter bomb .....	128
6.2.4 Oral glucose tolerance test with insulin measurement.....	129
6.2.5 Intra peritoneal insulin sensitivity test .....	129
6.2.6 Blood analysis.....	129
6.2.7 Gross neurological examination .....	129
6.2.8 Open field test.....	130
6.2.9 Histology.....	130
<b>6.3 RESULTS .....</b>	<b>131</b>
6.3.1 Body weights and food intake .....	131
6.3.2 Energy expenditure, activity, food and water intake .....	131
6.3.3 Calorimetric bomb .....	131
6.3.4 Oral glucose tolerance test.....	131
6.3.5 Insulin sensitivity test .....	131
6.3.6 Blood analysis.....	132
6.3.7 General health and specific motor abilities.....	132

TABLE OF CONTENTS

---

6.3.8 The openfield test .....	132
6.3.9 Histology.....	132
<b>6.4 CONCLUSION .....</b>	<b>133</b>
<b>6.5 FIGURES.....</b>	<b>134</b>
<b>7. PRESENTATIONS AND PUBLICATIONS .....</b>	<b>145</b>
7.1 PRESENTATIONS.....	145
7.2 PUBLICATIONS.....	145
<b>8. ACKNOWLEDGEMENTS .....</b>	<b>147</b>

## I. LIST OF FIGURES

1.1 Systemic iron fluxes.....	4
1.2 Transcriptional regulation of hepcidin expression upon different stimuli.....	6
1.3 Cellular iron metabolism.....	8
1.4 IRE secondary structure.....	12
1.5 Crystal structure of cytosolic aconitase and the IRP1-IRE complex.....	14
1.6 The IRP/IRE system.....	15
1.7 The IRP/IRE network in erythropoiesis.....	22
1.8 The IRP/IRE network in duodenal enterocytes.....	25
1.9 The IRP/IRE system sustains hepatic and mitochondrial function.....	27
3.1. The gain-of-function IRP1* protein is a constitutive IRE-binder.....	55
3.2. Targeting of the <i>Rosa26</i> locus with a Cre/Lox inducible IRP1* expression construct.....	56
3.3. Southern-blot showing bona fide targeting of the <i>Rosa26</i> locus.....	57
3.4. Detection of the targeted <i>Rosa26</i> locus by multiplex-PCR.....	57
3.5. RT-PCR analysis confirms Cre-mediated recombination of the targeted <i>Rosa26</i> locus.....	58
3.6. IRP1* protein expression is detected by Western-blot in tissues from IRP1* mice.....	59
3.7. IRP1* shows IRE-binding activity.....	60
3.8. The IRE-binding activity of IRP1* is specific.....	60
3.9. Expression of IRP1* yields a detectable gain of IRP activity in mouse tissues.....	61
3.10. Quantification of IRP activity in IRP1* mouse tissues reveals tissue- specific differences in the degree of gain of IRP function.....	62
3.11. Impact of gain of IRP1 function on the expression of IRP target genes.....	64
3.12. Gain of IRP1 function causes iron loading in liver, spleen and duodenum.....	66
3.13. DMT1 levels are not increased in the duodenum of IRP1* mice.....	67
3.14. IRP1* expression does not alter hepcidin mRNA levels.....	68
3.15. IRP1* expression impairs normal erythropoiesis.....	69
3.16. IRP1* expression impairs erythroblastic maturation.....	70
3.17. TfR1 levels are increased in erythroblast progenitors of IRP1* mice.....	71

<b>3.18. IRP1* mice display altered motor coordination.....</b>	<b>73</b>
<b>3.19. IRP1* expression decreases motor endurance.....</b>	<b>74</b>
<b>3.20. IRP1* mice display normal muscle strength calibrated over weight.....</b>	<b>74</b>
<b>3.21. IRP1* expression impairs neuromuscular transmission.....</b>	<b>75</b>
<b>3.23. IRP1* expression alters the pattern of expression of IRP target genes in BMDM exposed to changes in iron levels ex vivo.....</b>	<b>77</b>
<b>3.24. Total IRP activity remains high in IRP1* BMDM upon ex vivo iron loading.....</b>	<b>78</b>
<b>3.25. IRP1* mRNA levels from the <i>Rosa26</i> promoter are not affected by changes in iron levels.....</b>	<b>79</b>
<b>3.26. IRP1* protein levels are diminished upon hemin treatment ex vivo.....</b>	<b>79</b>
<b>3.27. IRP1* expression does not aggravate liver iron accumulation and lipid peroxides levels in response to acute iron loading.....</b>	<b>80</b>
<b>3.28. Primary iron loaded mice with high IRP1 activity show strong hepatic iron accumulation, similarly to HFE KO animals.....</b>	<b>82</b>
<b>3.29. Hepcidin levels are unchanged in primary iron loaded mice with hyper- active IRP1.....</b>	<b>83</b>

## II. LIST OF TABLES

<b>Table 2.1 Enzymes used for western blot.....</b>	<b>35</b>
<b>Table 2.2 Enzymes used for flow cytometry.....</b>	<b>35</b>
<b>Table 2. 3 Primer sequences.....</b>	<b>40</b>
<b>Table 3.1 IRP1* mice are obtained in Mendelian ratios.....</b>	<b>58</b>
<b>Table 3.2. IRP1* mice display moderate macrocytic erythropenia.....</b>	<b>67</b>
<b>Table 3.3. Serum iron parameters in IRP1* mice.....</b>	<b>68</b>
<b>Table 3.4. Serum iron, ferritin and transferrin saturation are elevated in primary iron loaded mice with gain of IRP1 function.....</b>	<b>82</b>

**III. LIST OF ABBREVIATIONS**

ABCB7	ABC transporter
ACO2	aconitase
AD	Alzheimer's disease
ALAS	aminolevulinic acid synthase
ALS	amyotrophic lateral sclerosis
APP	$\beta$ -amyloid precursor protein
BMDM	bone marrow-derived macrophages
BMPs	bone morphogenetic proteins
CMAP	compound muscle action potential
Cdc14A	cell division cycle 14A
cDNA	copy deoxyribonucleic acid
CIA	cytosolic iron-sulfur cluster assembly
COPD	chronic obstructive pulmonary disease
Ctr	control
DcytB	duodenal cytochrome B
DFO	desferrioxamine
DMT1	divalent metal iron transporter
eALAS	erythroid 5-aminolevulinatase synthase
ECG	electrocardiography
ES	embryonic stem cell line
EMSA	electrophoretic mobility shift assay
EPO	erythropoietin
ERK	extracellular signal-regulated kinase
ETC	electron transport chain
EMPreSS	European mouse phenotyping of standardised screens
FA	Friedreich's ataxia
FACS	fluorescence-activated cell sorting
FBXL5	F-box and leucine repeat protein 5
FCS	forward scatter
FECH	ferrochelatase

## LIST OF ABBREVIATIONS

---

Fe	iron
<sup>59</sup> Fe	radioactively-labelled iron
Fe-S	iron sulfur cluster
FLAG-tag	polypeptide protein tag
FLVCR	feline leukemia virus subgroup receptor 1
FPN	ferroportin
FPN1A	FPN transcript isoform 1A (with IRE)
FPN1B	FPN transcript isoform 1B (no IRE)
FTH	ferritin heavy chain
FTL	ferritin light chain
FXN	frataxin
GLRX5	glutaredoxin 5
hALAS	housekeeping aminolevulinic acid synthase
HAMP	hepcidin gene
HH	hereditary hemochromatosis
HIF2a	hypoxia-inducible factor 2a
HJV	hemojuveline
Hprt	hypoxanthine-guanine phosphoribosyltransferase
HRE	hypoxia response elements
H <sub>2</sub> O <sub>2</sub>	hydrogen peroxide
IgG	immunoglobulin G
IL6	interleukin 6
IRE	iron regulatory element
IRES	internal ribosome entry site
IRP	iron regulatory protein
IRP1*	IRP1 gain-of-function
IPR1A	IRP1 fly homologue
ISCU	iron-sulfur cluster scaffold protein
JAK	janus kinase
kb	kilobase
KO	knockout

---

LIP	labile iron pool
mAco	mitochondrial aconitase
MAPK	mitogen-activated protein kinase
MCV	mean cell volume
MCH	mean cell hematocrit
MDA	malondialdehyde
Mfn	mitoferrin
mM	millimolar
MRCKa	Cdc42-binding kinase a
mRNA	messenger ribonucleic acid
NS	not significant
nt	nucleotide
NTBI	non-transferrin bound iron
O <sub>2</sub> <sup>-</sup>	oxide ion
O <sub>2</sub>	oxygen
OGTT	oral glucose tolerance test
IPIST	intraperitoneal insulin sensitivity test
PCBP1	poly(rC)-binding protein 1
Pcm	polycythemia
PCR	polymerase chain reaction
PD	Parkinson's disease
PHD	prolyl-hydroxylases
PPIX	protoporphyrin IX
qPCR	quantitative polymerase chain reaction
qNMR	quantitative nuclear magnetic resonance
RBC	red blood cells
RE	response elements
RNA	ribonucleic acid
RT	reverse transcription
SDH	succinate dehydrogenase
SEM	standard error of the mean
Sla	sex-linked anemia
SLC48A1	solute carrier family member 48A1
SNVC	sensitive nerve conduction velocity

## LIST OF ABBREVIATIONS

---

SOD1	superoxide dismutase
STAT	signal transducer and activator of transcription
TBARS	thiobarbituric acid reactive substances
TCA	tricarboxylic acid
TfR1	transferrin receptor 1
TfR2	transferrin receptor 2 (no-IRE TfR1 homolog)
TG	targeted
TIBC	total iron binding capacity
UIBC	unbound iron binding capacity
UTR	untranslated region
WT	wild type

---



## 1. INTRODUCTION

### 1.1 Iron biology

#### 1.1.1 The light and dark side of iron biochemistry

Iron is the second most abundant metal in the earth's crust and is also an essential micronutrient for life. The high incidence of human diseases caused by imbalances of iron homeostasis demonstrates the biological importance (Fleming and Ponka, 2012).

As a transition metal, iron can adopt different oxidation states of which the most common are ferrous ( $\text{Fe}^{2+}$ ) and ferric ( $\text{Fe}^{3+}$ ) ion forms. The ability of iron to readily accept and donate electrons makes iron an essential cofactor for electron transfer while its flexible coordination chemistry is key to its versatility in binding to biological ligands. Iron plays part in a wide range of biological processes either as cofactor or more often as part of prosthetic groups, for instance as heme and Fe-S clusters (Ponka, 1997; Sheftel et al., 2010). Hemoproteins are implicated in diverse biological functions such as oxygen transport (hemoglobin and myoglobin), electron transfer along the mitochondrial respiratory chain (cytochromes) and antioxidant defense (superoxide dismutase, peroxidase and catalase) (Ponka, 1997). Fe-S proteins are involved in electron transfer reactions as well as DNA/RNA synthesis, nucleotide metabolism, citric acid cycle and regulation of iron homeostasis (Rouault and Tong, 2008).

Paradoxically, the same chemical properties that make iron biologically essential also underlie the toxicity of iron excess. Ferrous iron can in fact react with hydrogen peroxide and generate highly reactive hydroxyl radicals via Fenton chemistry (Merkofer et al., 2006):



Reactive oxygen species readily attack nucleic acids, proteins and lipid membranes leading to damage and eventually cell death and organ injury (Galaris and Pantopoulos, 2008).

Hence, due to its dual nature, iron levels must be maintained in a tight physiological range to avoid the detrimental consequences of both iron deficiency and excess.

### **1.1.2 Disorders of iron metabolism**

Iron mismanagement belongs to some of the most common human diseases worldwide. Iron deficiency mostly causes anemia, which is a major public health problem affecting billions of people around the globe (WHO, 2005). Commonly, insufficient dietary iron intake or heavy blood loss results in iron deficiency. It disproportionally affects individuals with marginal basal iron levels (or higher iron requirements), such as young children and menstruating or pregnant women (WHO, 2005). Genetic defects involving crucial iron-managing proteins are also recognized as causes of various forms of anemia (Andrews, 2008).

Unlike iron deficiency, the etiology of iron-overload disorders is typically genetic, although environmental factors can contribute to the manifestation of the disease as in the case of hemochromatosis. Systemic iron accumulation typically results in unrestricted access of iron into organs, such as liver, heart and endocrine glands with ensuing severe tissue damage (Fleming and Ponka, 2012).

At the interface between iron deficiency and iron overload is a series of pathologies characterized by defects of iron distribution. This can lead to iron loading in certain tissues, coexisting with iron deficiency in other organs. Iron mislocalization can also occur intracellularly where it results in abnormal iron distribution in different intracellular compartments, such as cytosol and mitochondria. Examples of disorders of systemic iron distribution are the acquired anemia of chronic disease and the inherited iron-refractory iron deficiency anemia. Both disorders are characterized by iron retention in the reticulo-endothelial system and iron shortage in interstitial fluids and plasma (Weiss and Goodnough, 2005; Finberg, 2009). Deficiency in proteins responsible for intracellular iron utilization leads to iron misdistribution between the cytoplasmic and mitochondrial compartments thereby causing degenerative diseases like Friedreich Ataxia (Ye and Rouault, 2010). Furthermore, localized iron accumulation has also been associated with and implicated in the pathogenesis of neurological disorders such as neurodegeneration with brain iron accumulation as well as Alzheimer's and Parkinson's diseases (Youdim, 2008; Gregory and Hayflick, 2011; Batista-Nascimento et al., 2012).

Inadequate iron management is a common denominator of a wide spectrum of hematological, metabolic and neurodegenerative human diseases. To avoid the pathological consequences of iron imbalance, homeostatic mechanisms have evolved to tightly regulate body iron levels.

## 1.2 Systemic iron metabolism

### 1.2.1 Systemic iron fluxes

Each cell in an organism requires iron for fundamental metabolic processes. A network of iron fluxes exists between the sites of iron absorption (the small intestine), utilization (erythroblasts in the bone marrow), recycling (macrophages of the spleen) and storage (the liver) (Fig. 1.1).

Primary sites of dietary iron absorption are the duodenal enterocytes. Although heme is the most bioavailable source of iron, the mechanism of dietary heme absorption is still ill understood (Hallberg, 1981). By contrast, the mechanism of inorganic iron absorption is well characterized. Upon reduction of dietary ferric iron by the membrane-bound ferric reductase DcytB (duodenal cytochrome B) (Latunde-Dada et al., 2002), ferrous iron is transported across the apical side of duodenal enterocytes through the transmembrane divalent metal iron transporter (DMT1) (Gunshin et al., 2001). On the basolateral side of the absorptive cell, iron is exported to the blood stream through the (sole) iron exporter ferroportin (FPN) (Abboud and Haile, 2000; Donovan et al., 2000; McKie et al., 2000). This step requires iron oxidization back to its ferric form by the multi-copper ferroxidase hephaestin (Vulpe et al., 1999). In all other cells, FPN-mediated iron export is assisted by the ferroxidase ceruloplasmin, which is synthesized in the liver and released into circulation (Harris et al., 1999).

Once in the blood stream, iron typically circulates through the body bound to the divalent glycoprotein transferrin, which buffers it in a soluble and non-toxic form (Bartnikas, 2012). In pathological states when plasma iron exceeds the total iron binding capacity (TIBC) of serum transferrin, iron starts to accumulate in the form of non-transferrin bound iron (NTBI) (Brissot et al., 2012). All cells and tissues in the body take up iron-bound transferrin through the ubiquitously expressed transferrin receptor 1 (TfR1) (Cheng et al., 2004).

About 10% of total body iron is contained within the skeletal muscle, where iron is mainly located in myoglobin. This hemoprotein is involved in oxygen storage and diffusion from capillaries to mitochondria, where cellular respiration generates the energy necessary to fuel the contractile activity of the muscle (Ordway and Garry, 2004). However, the majority of body iron (~75%) is used for hemoglobinisation of nascent red blood cells within the bone marrow (Hentze et al., 2004). Of note, the amount of iron used for erythropoiesis greatly exceeds the iron that is absorbed from the diet (Fig. 1.1); therefore iron recycling is essential to sustain the high erythropoietic iron needs. Continuously, senescent and damaged erythrocytes are engulfed by macrophages of the reticulo-endothelial system, present in the spleen, liver and bone marrow

## 1. INTRODUCTION

(Knutson et al., 2003). In the macrophages, heme oxygenase extracts iron contained in the heme (Poss and Tonegawa, 1997), which is then recycled and returned to plasma transferrin. While macrophages of the liver, spleen and bone marrow normally hold a transient fraction of iron, the body iron excess is safely stored in liver hepatocytes within ferritin shells and is ready to be mobilized upon demand (Pantopoulos et al., 2012).

A controlled physiological mechanism of iron excretion from the body does not exist and iron is normally only lost through cell shedding and minor bleeding (Hentze et al., 2010). To compensate for the iron losses, duodenal iron absorption must be tightly controlled to ensure that erythroid iron demand is met and hepatic iron stores are replete.

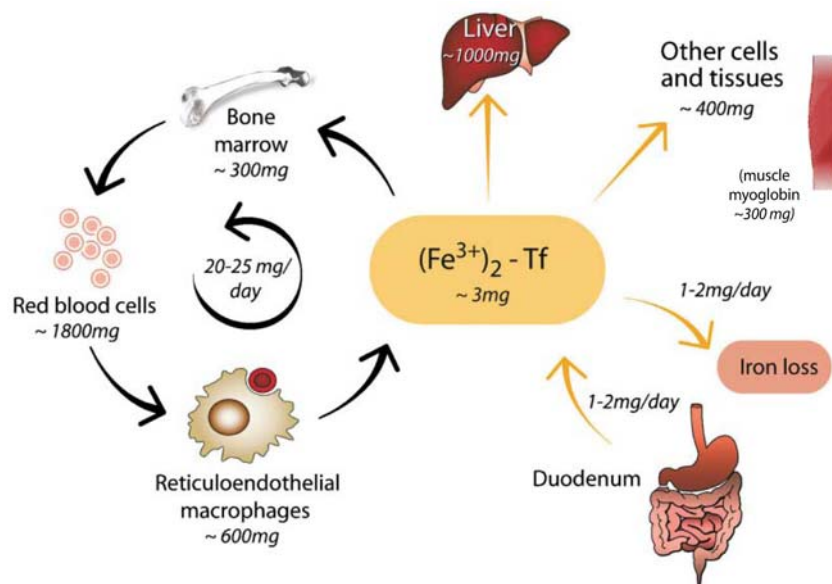


**Figure 1.1 Systemic iron fluxes.** Schematically depicted is the distribution of total body iron content among tissues. Central organs of iron metabolism are represented, including the site of iron absorption (the duodenum), usage (erythrocytes), recycling (macrophages) and storage (the liver). Values correspond to the approximate tissue iron content and daily fluxes of iron of an adult person.  $(\text{Fe}^{3+})_2\text{-Tf}$ : diferric-transferrin. Picture modified from Hentze et al., 2004.

### **1.2.2 Systemic regulation of iron homeostasis: hepcidin**

Central coordinator of systemic iron fluxes is hepcidin, a small peptide hormone primarily produced in the liver. Upon synthesis, hepcidin is secreted into the blood stream where it targets FPN, mainly on the surface of enterocytes, macrophages and hepatocytes. Hepcidin binding to FPN induces its internalization and lysosomal degradation (Nemeth et al., 2004), thus directly inhibiting iron release into the circulation from the sites of iron absorption, recycling and storage. Therefore, hepcidin expression catalyzes a systemic response to reduce iron fluxes into circulation in iron-replete conditions. Convincing evidence of the primary importance of hepcidin for systemic iron balance was offered by targeted deletion of hepcidin in mice. Animals completely lacking hepcidin expression suffered from severe iron overload in multiple organs, which was concurrent with iron depletion in spleen macrophages (Lesbordes-Brion et al., 2006).

Hepcidin production must respond to various body signals to coordinate iron absorption from the diet and release from the reticulo-endothelial system and the hepatic stores (Fig 1.2). Physiologically, hepcidin expression is modulated by systemic iron availability as both elevated transferrin saturation and high hepatic iron stores have been implicated in direct activation of hepcidin expression (Ramos et al., 2011). Conversely, erythropoietic activity and hypoxia have been shown to reduce hepcidin expression (Pak et al., 2006; Peyssonnaud et al., 2007), which allows an increase of systemic iron influx to sustain the erythropoietic iron needs. In addition, hepcidin also reacts to pathological stimuli (Fig 1.2). Noteworthy, hepcidin was initially discovered as a peptide associated to inflammation and its bactericidal properties earned it the original name of anti-microbial peptide (Krause et al., 2000; Park et al., 2001). Inflammatory cues and infection have been shown to induce hepcidin expression (Nicolas et al., 2002), thus resulting in restricted iron availability through a mechanism likely evolved as host-response to pathogen invasion. Overall, these different regulatory signals are detected and integrated by hepatocytes through a panel of different sensory molecules on their cell surfaces. A network of intracellular signaling cascades, involving extracellular signal-regulated kinase (ERK)/ mitogen-activated protein kinase (MAPK), bone morphogenetic proteins (BMPs) as well as Janus kinase (JAK)/signal transducer and activator of transcription (STAT), converge into the regulatory elements on hepcidin promoter (Fig. 1.2) (Hentze et al., 2010; Ganz and Nemeth, 2012). The resulting hepcidin transcriptional output is normally adequate to adjust systemic iron levels to the current body iron requirements.

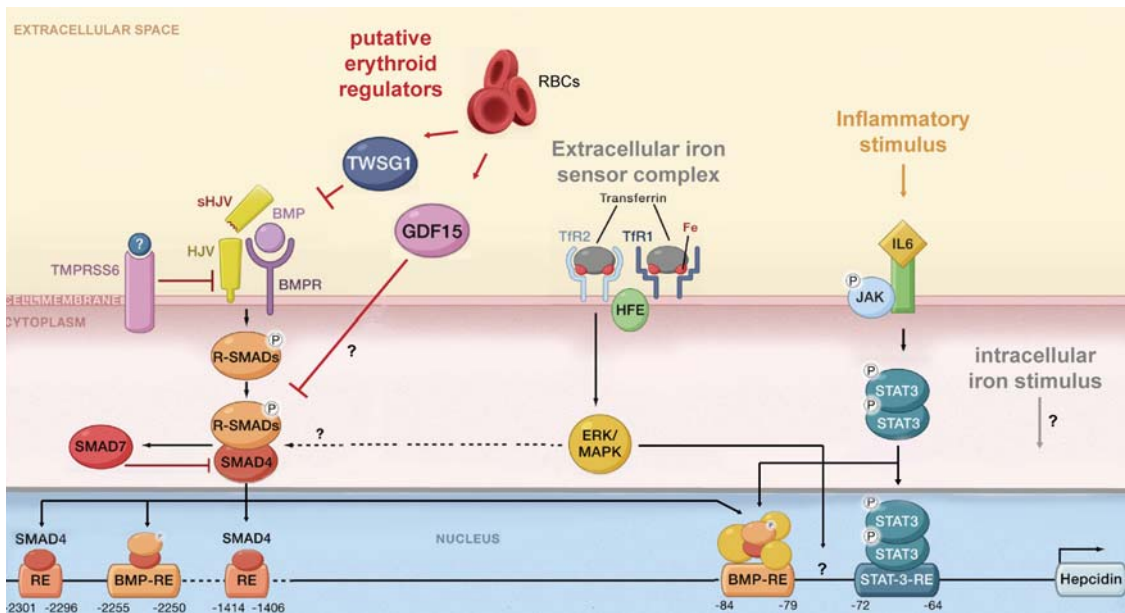


**Figure 1.2 Transcriptional regulation of hepcidin expression upon different stimuli.** Hepcidin expression in hepatocytes is transcriptionally regulated by multiple signals. Intra- and extra-cellular iron concentration, as well as inflammation, induce hepcidin expression, while erythropoiesis represses hepcidin expression. On the left: putative erythroid regulators released by erythroid precursors and acting on BMP-activated SMAD cascade, which induces hepcidin expression by binding to response elements (RE) on the hepcidin promoter. The BMP signaling is considered critical for hepcidin regulation in response to increased iron stores. Hemojuvelin (HJV) is a BMP coreceptor and can be cleaved by the matriptase TMPRSS6, with consequent inhibition of hepcidin expression. In the middle: upon increased transferrin-iron binding to Tfr1, HFE is displaced and binds to Tfr2 (IRE-free Tfr1 homolog, preferentially expressed in the liver), thereby activating hepcidin expression via ERK/MAPK and SMADs signaling. On the right: inflammatory cytokines, such as interleukin 6 (IL6), activate hepcidin transcription via the Jak/STAT pathway. (Hentze et al., 2010) RBCs: red blood cells. Picture modified from Hentze et al., 2010.

Being central to the regulation of systemic iron homeostasis, it is not surprising that failure to modulate hepcidin expression results in life threatening diseases with systemic iron overload, such as hereditary hemochromatosis (HH) (Camaschella, 2005). The underlying cause of HH is an inappropriately low synthesis of hepcidin, which leads to FPN overexpression on the surface of enterocytes and macrophages. Consequently, dietary iron is absorbed and released into the blood in an uncontrolled manner, thus rising, over time, transferrin saturation. Accordingly, NTBI starts to build up in the plasma and also accumulates in parenchymal organs, such as liver, heart and pancreas. If not treated with iron-depletion therapies, like phlebotomy, HH can lead to fatal complications such as liver cirrhosis, heart failure and diabetes (Pietrangelo, 2010).

Family studies of HH patients have implicated four genes, besides *HAMP* (hepcidin) itself (Roetto et al., 2002), in the etiology of the disorder. These include genes encoding sensory molecules located on hepatocyte surface such as *HFE* (Simon et al., 1977; Feder et al., 1996), transferrin receptor-2 (*TfR2*) (Camaschella et al., 2000) and hemojuvelin (*HJV*) (Papanikolaou et al., 2003), which thus emerged as critical regulators of hepcidin expression (Fig. 1.2). In addition, hepcidin's molecular target *FPN*, when mutated on aminoacid residues responsible for hepcidin interaction, determines a rare and dominant form of HH characterized by hepcidin resistance (Montosi et al., 2001; Njajou et al., 2001). Mouse models of the HH disease exist in which *Hamp*, *Hfe*, *TfR2*, *Hjv* and *Fpn* have been individually mutated (Donovan et al., 2005; Huang, 2005; Kawabata et al., 2005; Niederkofler, 2005; Lesbordes-Brion et al., 2006; Zohn et al., 2007; Vujić Spasić et al., 2008). Their study, complemented by biochemical in vitro approaches, has allowed the outlining of the molecular mechanisms regulating hepcidin activation as well as the dynamics of hepcidin-mediated regulation.

### **1.3 Cellular iron metabolism**

A network of iron fluxes is not only present at the systemic level and also cellular iron homeostasis comprises analogous tasks of iron import, utilization, storage and export (Fig. 1.3). Depending on the cell-type, some of these tasks involve different molecular players, which reflects the tissue-specificities of systemic iron metabolism.

#### **1.3.1 Cellular iron uptake**

Iron circulates in the blood stream mainly bound to transferrin; thus, cellular iron uptake typically occurs via binding of diferric-transferrin to high-affinity TfR1 and subsequent clathrin-dependent internalization of the whole complex (Fig. 1.3) (Chen and Paw, 2012). Following acidification of the endocytosed vesicles, ferric iron is released from transferrin (Dautry-Varsat et al., 1983) and reduced to its ferrous form by the STEAP family of metalloreductases (Ohgami et al., 2005, 2006). Ferrous iron is then transported into the cytoplasm through the DMT1 iron-channel. Hence, DMT1 has a dual function: as key absorbing molecule transporting dietary iron across the apical membrane of duodenal enterocytes as well as, in all other cell-types, acting as endosomal protein involved in the iron transfer from the endosome to the cytosol. Inactivation of DMT1, both in mice and humans, leads to iron deficiency anemia due to impaired intestinal iron

## 1. INTRODUCTION

absorption and usage by the erythron (Fleming et al., 1997; Gunshin et al., 2005; Mims et al., 2005). Following iron release, the vesicles containing apo-transferrin and TfR1 are recycled back to the cellular surface where apo-transferrin is released into the circulation and TfR1 is ready for a new cycle (Fig. 1.3). Although ubiquitously expressed, the major role of TfR1 resides in maturing erythroblasts that highly express it on their surface to take up large amounts of iron required for hemoglobin synthesis. Targeted disruption of TfR1 in mice leads to embryonic lethality, mainly due to erythropoietic defects. This demonstrates that TfR1 is essential for erythropoiesis but can be dispensable for iron acquisition in non-erythroid cells (Levy et al., 1999). As previously mentioned, iron can be also acquired in the form of heme and NTBI. Biochemical and genetic studies have proposed several molecular candidates for both heme and NTBI uptake (Hentze et al., 2010), which suggests redundancy in the underlying mechanisms rather than an exclusive pathway.

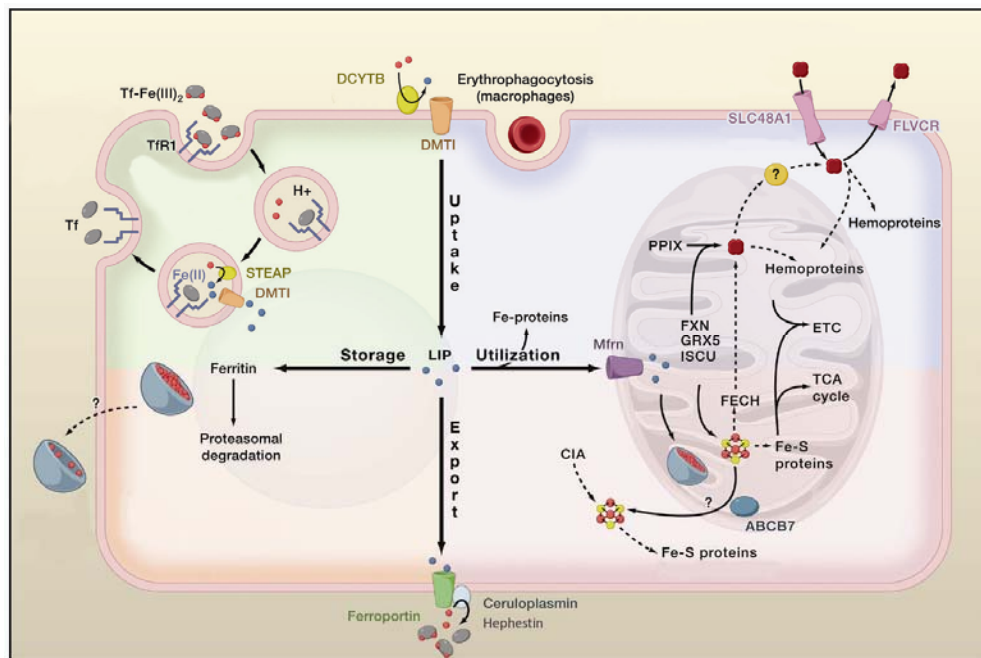


**Figure 1.3 Cellular iron metabolism.** Depicted are the main pathways of iron uptake, utilization, storage and export in a generic cell. DCYTB: duodenal cytochrome B; Tf: transferrin; TfR1: transferrin receptor 1; LIP: labile iron pool; CIA: cytosolic iron-sulfur cluster assembly machinery; ETC: electron transport chain; TCA cycle: tricarboxylic acid cycle; FECH: ferrochelatase; FXN: frataxin; GLRX5: glutaredoxin 5; ISCU: iron-sulfur cluster scaffold protein; PPIX: protoporphyrin IX; Mfrn: mitoferrin; FLVCR: Feline leukemia virus subgroup receptor -1 (heme exporter); SLC48A1: solute carrier family member 48A1 (the only bona fide heme importer identified so far) (Rajagopal et al., 2008). Picture modified from Hentze et al., 2010.

### 1.3.2 Cellular iron utilization

Independent of the mechanism of cellular uptake, once in the cytosol iron is mainly routed to the major site of cellular iron usage, i.e. the mitochondria. Iron is transported into the mitochondria by members of the mitochondrial solute carrier family, i.e. mitoferrin -1 and -2 (Shaw et al., 2006; Paradkar et al., 2009). Once inside the mitochondrial organelle, iron is used to produce heme and Fe-S clusters (Fig. 1.3).

The biogenesis of heme comprises a series of steps, some of which occur in the cytoplasm. The rate limiting step of heme synthesis is catalyzed by the mitochondrial matrix enzyme 5-aminolevulinic acid synthase (ALAS). Two isoforms of ALAS exist, produced either by the ubiquitously expressed (housekeeping) gene hALAS or by the erythroid-specific eALAS. Dysfunction of eALAS in humans results in impaired heme synthesis and leads to X-linked sideroblastic anemia, a disease characterized by ineffective erythropoiesis and mitochondrial iron deposition in maturing erythroblasts (Cotter et al., 1992). The last step of heme synthesis is the insertion of ferrous iron into the protoporphyrin ring by mitochondrial ferrochelatase (Dailey et al., 1994). Shortage of ferrochelatase activity in humans causes toxic accumulation of protoporphyrin IX that results in erythropoietic protoporphyria (Lamoril et al., 1991).

Besides heme, iron is used in the mitochondria to generate another important cofactor, the Fe-S cluster. The biogenesis of Fe-S cluster has been extensively studied in prokaryotic and yeast models (Vickery and Cupp-Vickery, 2007; Lill and Mühlenhoff, 2008), leading to the discovery of many crucial players of this biosynthetic machinery. The validity of the proposed molecular players has been subsequently confirmed and further emphasized in higher eukaryotes, including animal models and human patients with defective Fe-S cluster biogenesis (Rouault and Tong, 2008; Sheftel et al., 2010). In essence, the process includes a series of early events that leads to the synthesis of Fe-S cluster intermediate on a scaffold protein called ISCU (Agar et al., 2000). During this early phase, the protein frataxin (FXN) has been proposed to take part as possible iron-donor (Bulteau et al., 2004). Once assembled on ISCU, the transient Fe-S cluster must be transferred and coordinated onto apo-proteins through a process assisted by glutaredoxin-5 (GLRX5) (Mühlenhoff et al., 2003). In contrast to mitochondrial Fe-S proteins, it is still unclear how Fe-S clusters are coordinately assembled on cytosolic and nuclear apo-protein. A cytosolic assembly machinery (called CIA) has been identified (Lill and Mühlenhoff, 2008), which seems to be connected to the mitochondrial apparatus at least via one component, the ABC transporter ABCB7. In fact, ABCB7 is located in the mitochondrial inner membrane and transports an

unknown intermediate “x”, containing the sulfur moiety necessary for the formation of cytosolic and nuclear Fe-S cluster proteins (Kispal et al., 1997). Defects in the Fe-S cluster biogenesis machinery not only impair the function of Fe-S cluster containing enzymes, but also lead to deregulation of cellular iron metabolism (Richardson et al., 2010). Remarkably, mutations of some specific components, such as FXN, ISCU, GLRX5 and ABCB7, have been associated with hematological and neurodegenerative disorders (see 1.5.4) (Campuzano et al., 1996; Camaschella et al., 2007; Mochel et al., 2008; Olsson et al., 2008; Bekri et al., 2009).

### **1.3.3 Cellular iron storage**

Iron exceeding the cellular needs can be either exported or safely stored in a redox-inactive form inside ferritin shells (Fig. 1.3). Heteropolymers of 24 ferritin heavy (FTH) and light (FTL) subunits can accommodate up to 4500 iron atoms (Harrison and Arosio, 1996). The iron, which has been proposed to be chaperoned to ferritin by PCBP1 [poly(rC)-binding protein-1] (Shi et al., 2008), is first oxidized by FTH, while FTL provides a nucleation center for its deposition. Despite being ubiquitously expressed, FTH and FTL levels vary among tissues, with FTH being predominant in the heart while FTL is expressed mostly in the liver (Arosio et al., 1976). A mitochondrial form of ferritin also exists, encoded by a distinct nuclear gene and with a very restricted tissue expression (Levi et al., 2001). Although its cellular role in normal conditions remains elusive, mitochondrial ferritin levels are found to be increased in sideroblastic anemia (Arosio and Levi, 2010). In addition, a glycosylated form of FTL is secreted into the serum (Meyron-Holtz et al., 2011); recent experiments in mice suggested that serum FTL derives primarily from macrophages, but its physiological function is still unclear (Cohen et al., 2010). Serum FTL is elevated in systemic iron loading and inflammation (Torti and Torti, 1994) and is commonly used as clinical marker of body iron stores. In the cell, iron stored in ferritin can be mobilized for metabolic purposes upon lysosomal or proteasomal ferritin degradation (Rudeck et al., 2000; Zhang et al., 2010). By sequestering redox-active iron, ferritin plays a fundamental role as cellular antioxidant. Its expression is regulated both transcriptionally (via antioxidant response elements, among others) and post-transcriptionally (Torti and Torti, 2002). Recently, an internal ribosome entry site (IRES) has been found within the untranslated region (UTR) of FTL mRNA, which suggests that FTL translation might be promoted under stress conditions (Daba et al., 2012). The biological importance of ferritin is further emphasized by the embryonic lethality of genetic deletion of FTH in mice (Ferreira et al., 2000), while its conditional ablation in the hepatocytes results in iron-induced oxidative damage of the liver (Darshan et al., 2009). In

humans, mutations of FTL are associated with a neurodegenerative disorder, i.e. ferritinopathy, characterized by brain iron overload and ferritin inclusion bodies in the nucleus of cells mainly belonging to the central nervous system (Curtis et al., 2001).

#### **1.3.4 Cellular iron export**

Cellular iron export removes excess iron that is neither used nor stored by the cell. In specialized cells, such as duodenal enterocytes and macrophages, iron export is instrumental in maintaining adequate plasma iron levels. As previously mentioned (see 1.2.1), iron export occurs through the only known iron export channel in vertebrates, FPN (Fig. 1.3) (Abboud and Haile, 2000; Donovan et al., 2000; McKie et al., 2000). Targeted disruption of FPN in mice is embryonic lethal (Donovan et al., 2005), which reflects its unique function as the sole iron exporter. Besides elemental iron, cells may also export iron bound to ferritin (through a yet elusive mechanism) as well as heme. FLVCR1 (Feline leukemia virus subgroup receptor -1) facilitates heme export in differentiating erythroblasts and in macrophages, thus maintaining proper iron levels for erythropoiesis as well as ensuring heme iron recycling, respectively (Keel et al., 2008). While mice with FLCVR1 ablation die embryonically and lack definitive erythropoiesis, FLCVR1 deletion after birth causes severe macrocytic anemia associated with an early erythropoietic blockade (Keel et al., 2008).

At the crossroad between the intracellular fluxes of iron uptake, usage, storage and export lies the labile iron pool (LIP) (Fig. 1.3). The LIP is a redox-active form of iron serving immediate metabolic needs (Breuer et al., 2008) and is localized both in the cytoplasm and the mitochondria (Rauen et al., 2007). Coordination of cellular iron fluxes is necessary to ensure that cellular iron requirements are met, while avoiding the expansion of the redox active iron pool. The LIP, whose size mirrors the intracellular iron content, is the iron entity that can be sensed by the cellular iron homeostatic machinery (Wang and Pantopoulos, 2011).

## 1.4 Regulation of cellular iron metabolism

The maintenance of cellular iron homeostasis is orchestrated by an iron-sensitive post-transcriptional regulatory machinery modulating the expression of key proteins involved in cellular iron metabolism. The system is driven by iron regulatory proteins (IRPs) -1 and -2 through their binding to cis-iron regulatory elements (IREs) located within the 5'- or 3'- UTR of the target mRNAs (Hentze et al., 2010; Anderson et al., 2012). A combination of biochemical, mutagenetic and structural approaches has allowed extensive *in vitro* exploration of the characteristics, function and regulation of this conserved cellular homeostatic machinery.

### 1.4.1 The structure of the IREs and the IRPs

IREs are evolutionarily conserved RNA hairpin structures of about 15-30 nucleotides contained in the UTR of various mRNAs. A typical IRE is defined by both sequence and structure (Bettany et al., 1992; Theil, 1994) and consists of a 6-nucleotide apical loop on a stem of 5 paired nucleotides, separated by an unpaired cytosine bulge from a lower stem of variable length (Fig. 1.4) (Hentze et al., 1988; Address et al., 1997). Study of the phylogenetic distribution of the IRE element of different genes revealed that the structure of the ferritin IRE might be the ancestral version that was then adopted by other genes through convergent evolution (Piccinelli and Samuelsson, 2007).

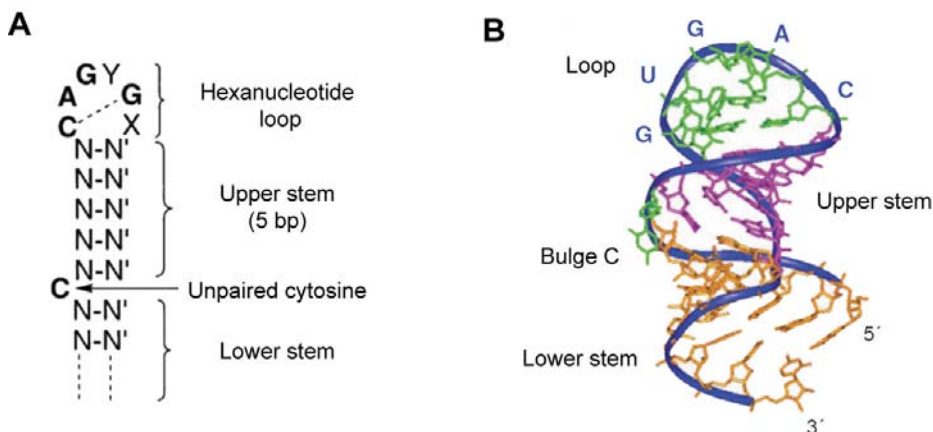


**Fig. 1.4 IRE secondary structure.** A) The secondary structure of a schematic consensus IRE is shown. The 6 nucleotide upper loop usually contains a sequence CAGYGX, with Y being either a U or a C and X representing any residue except G. The upper stem contains 5 paired nucleotides consisting of variable residues (N). The stem below the unpaired cytosine can have variable length. B) The nuclear magnetic

resonance structure of the consensus IRE is depicted (Address et al., 1997). The 6-nucleotide conserved sequence form an apical loop sitting on top of two A-conformation helical stems. The upper stem seems to work as a molecular ruler to orient the C bulge and the loop for optimal interaction with the IRPs. Figure adopted from Rouault, 2006.

IRP1 and IRP2 are ubiquitously expressed proteins and members of the gene family of aconitases (Gruer et al., 1997), which catalyze the conversion of citrate to iso-citrate in the tricarboxylic acid (TCA) cycle. It appears that the *IRP1* gene diverged from mitochondrial aconitase (*mACO*) following an early duplication event and subsequent acquisition of the IRE-binding function. In turn, *IRP2* originated from a second duplication in higher eukaryotes, but lost the aconitase activity some time during evolution (Gruer et al., 1997). The aconitase function of IRP1 is analogous to the enzymatic activity of mACO (Kennedy et al., 1992), but, in contrast to the mACO, IRP1 is prone to Fe-S cluster loss upon iron depletion (Rouault et al., 1992). The crystal structure of IRP1 in the cytosolic aconitase form (Fig. 1.5A) confirmed the high similarity with mACO (Dupuy et al., 2006), which was predicted on the basis of the sequence conservation (Rouault et al., 1991). Similar to mACO, IRP1 contains four globular domains, with a cleft formed at the interface between domains 1-3 and 4 (Dupuy et al., 2006). The Fe-S cluster is bound inside the cleft, which constitutes the aconitase catalytic site. Disassembly of the Fe-S cluster, upon iron depletion, leads IRP1 to switch to an open conformation and expose its IRE-binding site (Fig. 1.5B) (Walden et al., 2006). The conversion of IRP1 between cytosolic aconitase and RNA-binding conformations is reversible, making IRP1 a bifunctional protein (Rouault et al., 1992). Mutagenesis experiments have revealed that three cysteines (C437, C503 and C506) are responsible for Fe-S cluster coordination and whose substitution turns IRP1 into a constitutive IRE-binding protein (Philpott et al., 1993; Hirling et al., 1994). Experimental approaches including mutagenesis, crosslinking and chemical modification of IRP1 indicated that the aconitase active site and the RNA-binding site overlap (Hirling et al., 1994; Basilion et al., 1994; Philpott et al., 1994), thus making the two IRP1 activities mutually exclusive. These earlier evidences have been then validated by comparison of the crystal structures of the cytosolic aconitase and the IRP1 bound to IRE (Fig. 1.5) (Walden et al., 2006). From analysis of the two crystal structures, it is evident that the switch of IRP1 between the two forms is associated with extensive conformational rearrangements. Although IRP2 has not been crystallized yet, the structural definition of the IRP1-IRE complex has enabled modeling of the structure of IRP2 (Zumbrennen et al., 2009). Despite the great degree of identity (~64%) between the two IRPs,

IRP2 does not assemble a Fe-S cluster and does not retain aconitase active-site residues (Dupuy et al., 2006). Also, close to its N-terminus, IRP2 contains a cysteine- and proline-rich stretch of 73 amino acids, which is encoded by a separate exon and appears to be unstructured. Initially thought to be involved in iron-mediated degradation of IRP2 (Iwai et al., 1998), the role of this specific structural characteristic for IRP2 function is unknown.

Both IRP1 and IRP2 bind IRE sequences with very high affinity (Butt et al., 1996). This was shown using electrophoretic mobility shift assays (EMSAs) with radiolabeled and in vitro transcribed IRE sequences as bait to “fish” active IRE-binding IRPs. There is a hierarchy in the binding affinities of different IRE sequences to the IRPs (Goforth et al., 2010), suggesting a differential regulation of distinct IRP-target genes according to various biological situations.

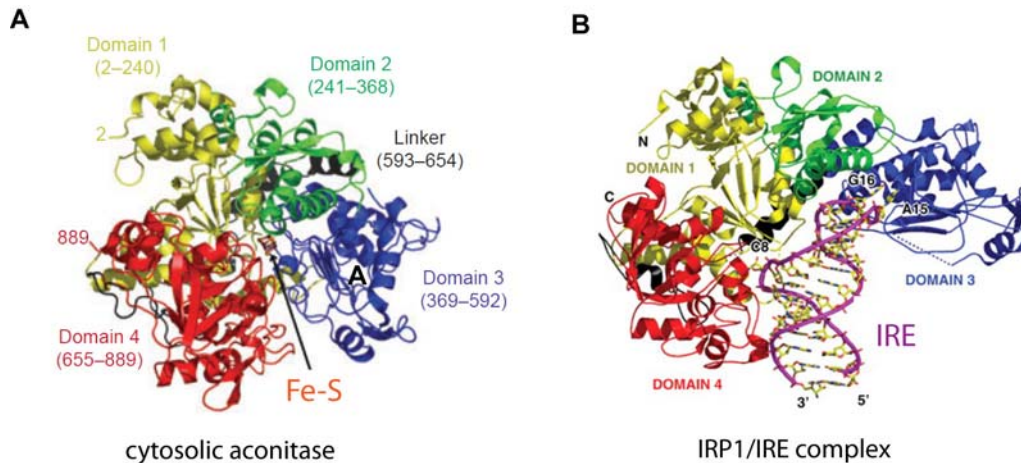


**Figure 1.5 Crystal structure of cytosolic aconitase and the IRP1-IRE complex.** A) Represented is the crystal structure of IRP1 in its closed conformation bound to the Fe-S cluster. B) Upon Fe-S cluster disassembly, IRP1 assumes an open conformation and accommodate the IRE. To help the conformational change, a flexible hinge linker (in black) connects domains 1-3 to domain 4. Figures adopted from Dupuis et al., 2006 (cytosolic aconitase) and Walden et al, 2006 (IRP1-IRE complex).

#### 1.4.2 IRP/IRE post-transcriptional regulation of “iron-genes”

IRPs and IREs work together to modulate the expression of key iron metabolism genes and coordinately regulate iron uptake, storage and export (Fig. 1.6). Typical targets of IRP post-transcriptional regulation are mRNAs encoding proteins involved in iron uptake (TfR1 and DMT1), utilization (eALAS), storage (FTL and FTH) and export (FPN) (Hentze et al., 2004). The interaction of the IRPs with IRE hairpin structures is promoted under iron-scarce conditions and abolished during iron repletion by different mechanisms (see 1.5.2). Binding of the IRPs to 5’-

IRE mRNAs (e.g. FTL and FPN) hinders the recruitment of the small ribosomal subunit, preventing translational initiation of the target mRNA (Muckenthaler et al., 1998). Conversely, IRP binding to 3'-IRE mRNAs (eg. TfR1) stabilizes the target mRNA against degradation (Hentze and Kuhnt, 1996). Therefore, the IRP-IRE interaction enhances TfR1-mediated iron uptake while diminishing storage into ferritin and export through FPN. Consequently, cellular iron availability increases, rescuing the cell from iron starvation. Conversely, in iron-replete conditions, iron uptake is decreased due to TfR1 mRNA degradation, while safe storage and export are promoted by actively translated ferritin and FPN, respectively. Therefore, loss of IRP-IRE interaction under iron sufficiency prevents dangerous surfeit of redox active iron.

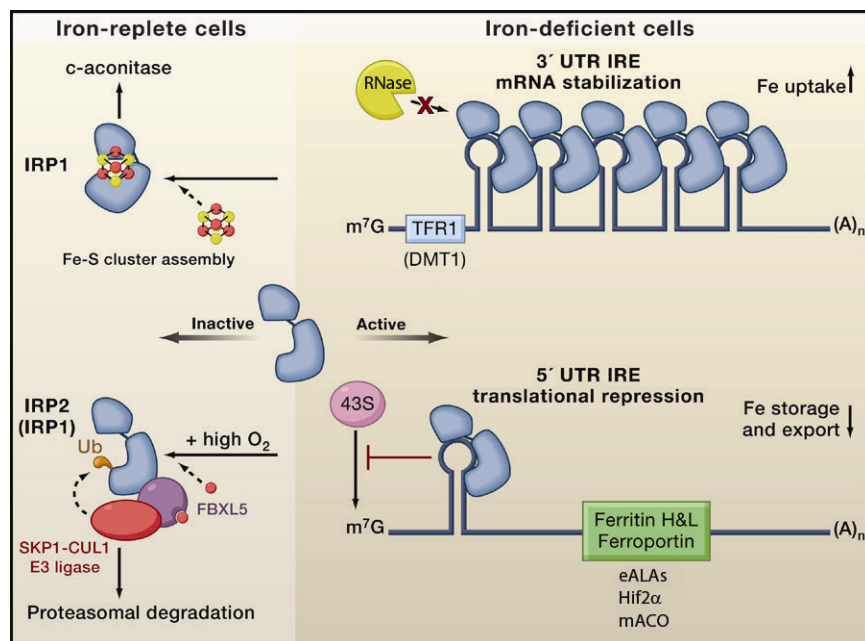


**Figure 1.6 The IRP/IRE system.** In iron-deficient cells (right) IRPs are active and bind IRE-containing mRNAs within their 3' or 5' UTR, thus determining stabilization of the target (e.g. TfR1) or translational repression (e.g. ferritin -H and -L, ferroportin). Upon iron-repletion (left), the interaction between IRPs and the IRE-targets is prevented as IRP1 is mainly converted to cytosolic aconitase by Fe-S cluster assembly, while IRP2 is targeted for proteasomal degradation via the E3 ubiquitin-ligase complex (see 1.4.3). Picture modified from Hentze et al., 2010.

### 1.4.3 Regulation of IRP activity

For the IRP/IRE system to efficiently coordinate cellular iron fluxes, IRP activity must be coupled to the cellular iron status. The cellular iron pool regulates IRE-binding of the two IRPs through distinct mechanisms (Fig. 1.6).

The reversible Fe-S cluster switch is the main mechanism regulating IRP1 activity (Paraskeva and Hentze, 1996); under physiological iron (and oxygen) conditions, IRP1 predominantly exists in the cytosolic aconitase form (Meyron-Holtz et al., 2004a, 2004b). The cytosolic aconitase pool can be up to 100-fold more abundant than the IRE-binding form of IRP1 (Chen et al., 1997), thus representing a large latent pool of activatable IRP1. This reserve of IRE-binding activity could in principle allow a faster IRP-regulatory response upon substantial cellular demand. However, there is at most a 4-fold increase in IRP1 IRE-binding activity in response to iron deficiency (Chen et al., 1997). The biological significance of such an excess of cytosolic aconitase activity remains unanswered, especially in the light of the lack of abnormalities following IRP1 ablation in mice (see 1.5).

By contrast to IRP1, IRP2 is regulated in an irreversible manner at the level of protein stability. This has recently been shown to involve FBXL5 (F-box and leucine-rich repeat protein 5), which is part of an E3 ubiquitin-ligase complex and contains an iron-sensitive hemerythrin-like domain (Salahudeen et al., 2009; Vashisht et al., 2009). In iron/oxygen deficient conditions, the diiron centre of the hemerythrin domain is destabilized, which results in FBXL5 degradation and IRP2 stabilization (Chollangi et al., 2012; Shu et al., 2012; Thompson and Bruick, 2012). Upon iron/oxygen repletion, accumulating FBXL5 interacts with IRP2 and targets it for proteasomal degradation (Salahudeen et al., 2009; Vashisht et al., 2009). While IRP1 is mainly regulated by the reversible Fe-S cluster switch, apo-IRP1 (the RNA-binding form of IRP1) is also targeted by FBXL5 (Salahudeen et al., 2009; Vashisht et al., 2009). This might represent a safety mechanism to avoid excessive activation of IRP1-IRE binding in conditions when the Fe-S cluster biogenesis is impaired.

Besides inorganic iron and Fe-S cluster, a series of iron-dependent, like heme (Ishikawa et al., 2005), and iron-independent mechanisms, like phosphorylation, oxygen and nitrogen reactive species (Drapier et al., 1993; Eisenstein et al., 1993; Pantopoulos et al., 1997), regulate the activity of the two IRPs (Anderson et al., 2012). The ability of IRPs to respond to multiple signals indicates their capacity to modulate their activity in response to a wide range of physiological conditions, thereby maintaining optimal cellular iron balance.

#### **1.4.4 Expanding the IRP regulon**

IRE motifs were initially identified in the 5' and 3' UTR of ferritin and TfR1 (the latter being the only mRNA found to possess multiple IREs), respectively, and in other genes connected to iron metabolism, including DMT1, eALAS and FPN (Hentze et al., 2004). Of note,

genes apparently less related to iron metabolism also contain IRE sequences, including the mitochondrial aconitase (mACO – TCA cycle) (Kim et al., 1996), Cdc14A (mitotic phosphatase – cell cycle) (Sanchez et al., 2006), MRCK $\alpha$  (Cdc42-binding kinase  $\alpha$  – cytoskeleton remodeling) (Cmejla et al., 2006), HIF2 $\alpha$  (hypoxia-inducible factor 2 $\alpha$  - hypoxia adaptation) (Sanchez et al., 2007a),  $\beta$ -amyloid precursor protein (APP – Alzheimer’s disease) (Rogers et al., 2002),  $\alpha$ -synuclein (Parkinson’s disease) (Friedlich et al., 2007) and *Drosophila* succinate dehydrogenase (Kohler et al., 1995) (SDH – TCA cycle and mitochondrial electron transport chain). The definition of the structural requirements for IRPs recognition of IRE elements has been instrumental in the identification of genes containing IRE-like motifs. Most of these discoveries are based on directed approaches during the study of iron-regulated genes and specific bioinformatic searches (Dandekar et al., 1998; Campillos et al., 2010). More recently, a systematic transcriptome-wide approach has allowed the identification of 35 novel putative IRE-containing mRNAs (Sanchez et al., 2011). The experimental strategy included immunoselection of IRP-IRE ribonucleoprotein complexes from mouse tissues, followed by microarray identification of the mRNA composition and bioinformatic identification of IRE-like motifs (Sanchez et al., 2011). While the role of many of these IREs still remains to be determined *in vivo*, the presence of IRE sequences in such a variety of genes is suggestive of a much broader competence of the IRP/IRE regulatory system beyond iron metabolism *per se*.

### **1.5 The IRP/IRE system in physiology and disease**

The IRP/IRE regulatory system has been extensively studied in cultured cells, forming the basis for the molecular understanding of its central importance in cellular iron homeostasis (see 1.4). In addition to maintaining cellular iron balance, the role of the IRP/IRE system has also important implications on systemic processes, including erythropoiesis, duodenal iron absorption and liver iron storage. Most of the knowledge that we currently have regarding the role of the IRP/IRE system in body physiology has been gained through the generation of animal models with IRP1 and IRP2 ablation. Mice lacking either of the two IRPs are viable and fertile, demonstrating that IRP1 and IRP2 can largely compensate for each other (LaVaute et al., 2001; Meyron-Holtz et al., 2004a; Galy et al., 2005b). Interestingly, IRP1-deficient mice display no overt phenotypic abnormalities under standard laboratory conditions, whereas mice with constitutive IRP2 deficiency exhibit altered body iron distribution and microcytic anemia (Cooperman et al., 2005; Galy et al., 2005b). These findings suggest a predominant role of IRP2

in the regulation of iron metabolism. However, ablation of both IRPs leads to embryonic lethality at blastocyst stage, showing that the IRP/IRE system is essential for viability (Smith et al., 2006; Galy et al., 2008). To study the effects of double IRP deficiency in vivo and overcome the embryonic lethality of double IRP ablation, mouse lines with tissue-specific deletion of the IRPs have been generated (Galy et al., 2008, 2010; Ferring-Appel et al., 2009). Together with the systemic IRP2 deficiency, models with conditional ablation of IRPs have provided fundamental insights into the role of the IRP/IRE system in key tissues involved in systemic iron metabolism, as discussed below.

### **1.5.1 The IRP/IRE system in erythropoiesis**

Most of the iron in the body is employed in the erythropoiesis. Circulating erythrocytes carry hemoglobin-bound oxygen and deliver it to all cells in the body, thus securing proper oxygenation of the tissues. A feedback loop exists that modulates the erythropoietic activity according to the degree of tissue oxygenation. In the kidney hypoxia-inducible factor 2 $\alpha$  (Hif2 $\alpha$ ), which is a known IRP-target gene (Sanchez et al., 2007b), is the major oxygen sensor that transcriptionally regulates the expression of the hematopoietic hormone erythropoietin (EPO) (Scortegagna et al., 2003a, 2003b). In normoxia, Hif2 $\alpha$  has a very short half-life because it is hydroxylated by the prolyl-hydroxylases (PHDs) and targeted for proteasomal degradation (Kallio et al., 1999). Under low oxygen and iron concentration (as iron is a PHD cofactor), PHD activity is reduced, thus resulting in HIF2 $\alpha$  stabilisation (Semenza, 2011). Accumulated HIF2 $\alpha$  translocates into the nucleus where it directly binds (as heterodimer with the constitutively expressed HIF1 $\beta$  subunit) to the hypoxia response elements (HRE) on the EPO promoter, thereby activating EPO expression (Warnecke et al., 2004). EPO secretion results in a direct stimulation of the proliferation and maturation, in the bone marrow, of early hematopoietic precursor cells expressing the EPO receptor on their surface (Fraser et al., 1988). As a consequence, an increased number of mature erythrocytes is released into the circulation with an ensuing net increase of the oxygen-carrying capacity of the blood.

Systemic ablation of HIF2 $\alpha$  in mice leads to anemia (Gruber et al., 2007), while conditional deletion in hepatocytes, as second minor source of EPO (Koury et al., 1991; Fandrey, 2004) specifically reduce hepatic EPO expression (Rankin et al., 2007). In addition to the PHD-mediated post-translational regulation, HIF2 $\alpha$  is also subjected to IRP-mediated translational regulation due to an IRE in the 5'UTR of its mRNA (Sanchez et al., 2007b). In kidney cells, under low iron conditions, IRP-driven translational repression of HIF2 $\alpha$  may thus lead to

decreased EPO synthesis and diminished erythropoietic activity (Fig. 1.7). Hence, the IRP/IRE system has potential to control EPO expression via HIF2 $\alpha$  and reduce the rate of red blood cell production in conditions of scarce iron availability. Because iron is necessary for the synthesis of heme and hemoglobin, this would avoid the generation of microcytic (smaller) and hypochromic (with low hemoglobin) erythrocytes. While the regulatory loop including IRP- HIF2 $\alpha$ -EPO and erythropoiesis has not been demonstrated in vivo, mice with systemic ablation of IRP2 develop microcytic anemia (Cooperman et al., 2005; Galy et al., 2005b). However, when the IRP2 deficiency is limited to either hepatocytes, enterocytes or macrophages, mice do not display any hematological abnormalities (Ferring-Appel et al., 2009). Therefore, the macrocytic anemia of IRP2 KO mice is considered to be principally due to a local defect in maturing erythroblasts.

Developing erythroid cells in the bone marrow have very special iron requirements as they need to continuously uptake large amounts of iron to ensure heme and hemoglobin synthesis and finalize their maturation. To achieve this task, erythroid precursors highly express TfR1 on their surface, allowing avid iron uptake. The importance of TfR1-mediated iron uptake for erythropoiesis is highlighted by mouse models with deficiency of transferrin (the serum iron-carrier) or TfR1 (necessary for transferrin-bound iron uptake). Hypotransferrinemic mice display severe anemia with microcytic hypochromic erythrocytes and tissue iron deposition (Trenor et al., 2000), showing that while other cells in the body have alternative ways for NTBI uptake, erythroid precursors rely on transferrin-bound iron uptake. TfR1-deficiency in mice results in a more severe phenotype, which affects both erythropoiesis and neurological development (Levy et al., 1999). Connected to its function in the transferrin cycle, where DMT1 exports iron from the the endocytic vesicle to the cytoplasm, DMT1 mutant mice display impaired iron uptake into erythroblasts (Fleming et al., 1998). As both TfR1 and DMT1 are IRP target genes, their IRP-mediated stabilization (via the 3'IRE in their mRNAs) in erythrocyte precursors could promote iron-uptake and facilitate their maturation process (Fig. 1.7). Consistently, the macrocytic anemia of IRP2 KO mice is associated with decreased TfR1 mRNA and iron levels in the bone marrow (Cooperman et al., 2005; Galy et al., 2005b), thus showing a failure to stabilize TfR1 against degradation and a consequent impaired iron uptake in IRP2 KO erythroblasts. The bone marrow of IRP2 KO mice also contained higher levels of ferritin, which is consistent with loss of IRP-mediated translational repression (Cooperman et al., 2005; Galy et al., 2005b). Ferritin upregulation could contribute to the hematological defect of IRP2 KO mice by sequestering intracellular iron and preventing its use for hemoglobin production (Fig. 1.7).

In maturing erythroblasts, TfR1, ferritin and eALAS synthesis must be especially coordinated to guarantee efficient production of hemoglobin. A study on primary murin erythroid progenitors showed an apparent uncoupling of ferritin and eALAS synthesis compared to the IRP/IRE regulatory paradigm (Schranzhofer et al., 2006). Under conditions of IRP activation, TfR1 levels were enhanced and ferritin repressed, which is consistent with IRP-mediated stabilization of TfR1 and repression of ferritin via their 3'- and 5'- IREs, respectively. However, eALAS was efficiently translated despite a 5'IRE. To explain this unexpected finding, the authors proposed a mechanistic hypothesis accounting for the massive transcription of eALAS in maturing erythroblast which may lead to an excess of IRE sites over available IRP molecules (Schranzhofer et al., 2006). In addition, the eALAS-IRE has a lower binding affinity to IRPs compared to the IRE sequences of ferritin and TfR1 (Cox et al., 1991). This may allow eALAS to escape IRP-mediated repression under the experimental conditions (Schranzhofer et al., 2006). The results of this *ex vivo* study are still a bit controversial when compared to the findings of others research. In support of the importance of IRP-mediated regulation of eALAS, primary erythroid precursors from IRP2 KO mice display a strong increase in eALAS expression and accumulation of protoporphirin IX (Cooperman et al., 2005). This suggests that IRP-mediated repression of eALAS may avoid the production and toxic accumulation of heme-intermediates under iron scarce conditions. Also, although IRP1 KO mice have normal blood values, the macrocytic anemia of IRP2 KO mice is more severe when one of the two IRP1 alleles is mutated in addition (Smith et al., 2004). This indicates also IRP1 has a role in erythropoiesis like IRP2. Moreover, the importance of IRP1 for hemoglobin synthesis is shown in a zebrafish model with a secondary abnormal increase of IRP1 activity (Wingert et al., 2005). IRP1 activation due to a primary defect in Fe-S cluster synthesis (caused by *Glrx5* deletion) and, with genetic complementation assay, shown to directly reduce eALAS expression and cause anemia (Wingert et al., 2005).

Regulation of iron export in erythroid precursors may also play a role in erythropoiesis along with iron uptake, sequestration and use for hemoglobin synthesis. In support of this argument, FPN has recently been shown to be expressed also in erythroblasts (Zhang et al., 2009). Bearing an IRE within its 5'UTR, FPN is normally subjected to IRP-mediated translational repression (Abboud and Haile, 2000; Donovan et al., 2000; McKie et al., 2000). Hence, FPN synthesis and function in erythroblasts would only be allowed upon intracellular iron accumulation and ensuing IRP inactivation. Therefore, FPN expression in erythroid precursors may represent a safety valve to avoid toxic iron accumulation in cases when the rate of iron

uptake exceeds iron usage in the mitochondria. Being also subjected to hepcidin-mediated translational regulation, FPN is degraded by hepcidin upon increased plasma iron levels (Zhang et al., 2011). Conversely, upon systemic iron depletion, FPN expression in erythroid precursors is reduced to possibly partially suppress erythropoiesis when non-erythropoietic tissues risk to develop iron deficiency (Zhang et al., 2011). Intriguingly, alternative splicing generates a FPN transcript lacking the IRE (named FPN1B) preferentially in erythroid precursors (and, to a lower extent, in duodenal enterocytes) (Zhang et al., 2009). The predominant expression of FPN1B in early erythroid progenitors represents a way to by pass IRP-mediated repression during early stages when precursor cells commit to proliferation and erythroid differentiation. During terminal erythroid differentiation, FPN1A (containing the 5'IRE) predominates, which allows erythroid cells to limit iron export (by IRP-mediated FPN1A repression) and to efficiently manufacture heme without developing microcytic anemia (Zhang et al., 2009). These findings are in agreement with an earlier observation in the polycythemia (Pcm) mouse that bears a radiation-induced deletion in the FPN promoter that eliminates the 5'IRE (Mok et al., 2004). Associated with a loss of IRP-mediated repression of FPN iron export, the Pcm mouse suffers from a transient hypochromic and microcytic anemia. The latter spontaneously corrects in young adult mice due to increased hepcidin expression. Hence, the loss of IRP-mediated translational control of FPN is compensated by increased hepcidin-mediated FPN degradation. The evidences from the Pcm mouse model show the importance of IRP-mediated regulation of FPN in erythroid cells, especially in early stages of life when hepcidin expression is not sufficient to effectively suppress FPN (Mok et al., 2004).

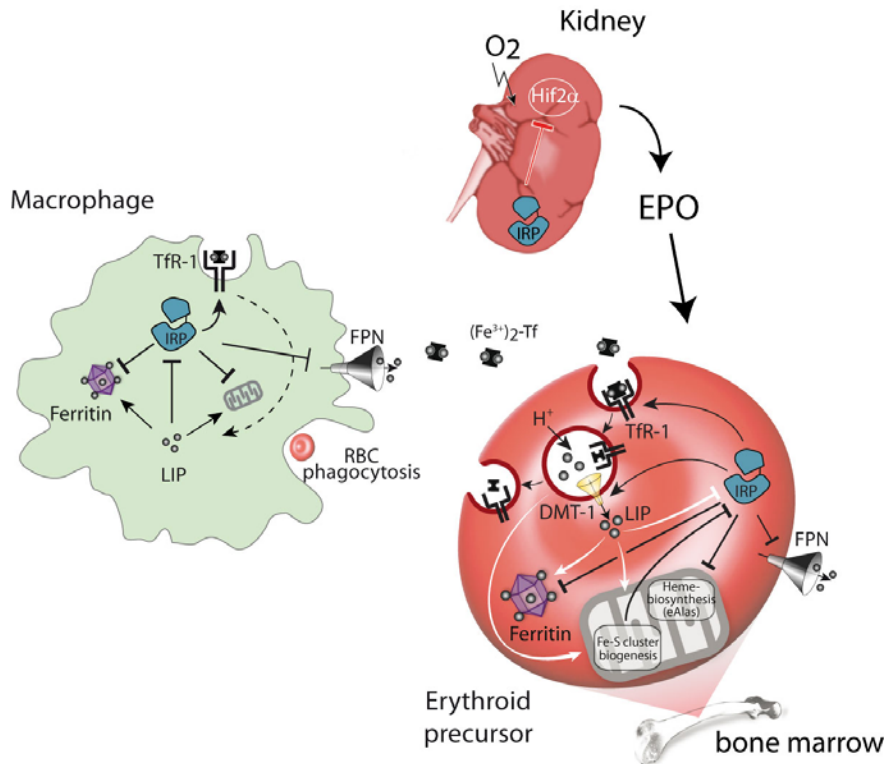


**Figure 1.7 The IRP/IRE network in erythropoiesis.** IRPs can influence erythropoiesis: by controlling, the synthesis of HIF2 $\alpha$ , the transcription factor that modulates the expression of the hematopoietic hormone erythropoietin (EPO) in the kidney; by regulating the expression of Tfr1, DMT1, ferritin, FPN and eALAS in developing erythroid precursors; by influencing the iron recycling capacity of macrophages, mainly via FPN regulation.  $(Fe^{3+})_2-Tf$ : diferric-transferrin; RBC: red blood cell. Figure modified from Muckenthaler et al., 2008.

Adequate macrophage recycling function may also be regarded as a crucial determinant for erythropoietic activity. Erythropoiesis is largely sustained by the continuous supply of iron recycled from senescent or damaged erythrocytes by the macrophages of the reticulo-endothelial system (Fig. 1.1). Therefore, a defect in the iron recycling capacity of macrophages might jeopardize the maturation of red blood cells. Besides erythrophagocytosis, macrophages continuously absorb large amount of iron via multiple mechanisms, including scavenging of hemoglobin (Kristiansen et al., 2001) and heme derived from intravascular hemolysis (Hvidberg et al., 2005). For this reason, macrophages are considered as a transient iron storage compartment and, in agreement, ferritin is among the most abundant transcripts found in these cells (Hashimoto et al., 1999). The degree of iron sequestration within ferritin might in principle influence macrophage iron recycling and could in turn be affected by IRP translational regulation of

ferritin. However, FPN is considered as the critical determinant for macrophage function and mice with targeted deletion of FPN show marked iron retention in macrophages of the liver and spleen (Donovan et al., 2005). As a consequence, erythroid precursors are deprived of iron, resulting in the anemic phenotype of FPN-deficient mice (Donovan et al., 2005). Although FPN is subjected to IRP-mediated translational repression, spleen and bone marrow macrophages from IRP2 KO mice unexpectedly display reduced FPN and elevated ferritin expression, associated with reduced iron stores (Galy et al., 2005b). While the underlying mechanism remains unclear, this is unlikely to be due to a direct effect of IRP deficiency in macrophages, as suggested by the fact that macrophage-specific deletion of IRP2 does not recapitulate this phenotype (Ferring-Appel et al., 2009).

### **1.5.2 The IRP/IRE system in duodenal iron absorption**

As there is no controlled mechanism of body iron excretion, duodenal iron absorption is tightly controlled via a complex network of transcriptional, post-transcriptional and post-translational mechanisms, with some of the key molecules involved being IRP-target genes (Fig. 1.8).

A representative example of such a complex regulatory network is DMT1, the channel mediating the transport of dietary iron across the apical membrane of duodenal enterocytes (see 1.2.1). DMT1 is a special target of IRP regulation as it can be controlled by IRPs in different ways. First, DMT1 is encoded by a 3'IRE-mRNA, which mediates positive regulation by IRPs in a fashion similar to TfR1 (Galy et al., 2008). More indirectly, IRPs can also influence DMT1 expression via HIF2 $\alpha$ . DMT1 belongs in fact to the targets of HIF2 $\alpha$  transcriptional regulation, which emerged to have a critical role in maintaining systemic iron balance (Mastrogiannaki et al., 2009). Specific deletion of HIF2 $\alpha$  in the gut epithelium of mice leads to a decrease in serum and liver iron levels and a marked decrease in liver hepcidin expression, indicating an attempt to counteract the systemic iron deficiency (Mastrogiannaki et al., 2009). HIF2 $\alpha$  mRNA contains a 5'IRE that subjects it to IRP-mediated repression (Sanchez et al., 2007b). Therefore, IRPs can indirectly negatively influence DMT1 expression by repressing HIF2 $\alpha$ . Interestingly, DMT1 can come in different flavors, as four isoforms of its mRNA can be generated by different mechanisms (Hubert and Hentze, 2002). Two 5' variants are being generated by alternative transcriptional start site usage and are named DMT1-A and B. Two additional 3' variants, with or without IRE, are instead produced by alternative splicing (Hubert and Hentze, 2002). In the duodenum, the IRE-containing isoforms of DMT1 prevail over the others (Galy et al., 2008).

Although control of dietary iron absorption is crucial for maintenance of systemic iron balance, DMT1 regulation appears to be directly dependent on the local iron status within enterocytes. This is evident in mice lacking hephaestin (sla mice) (Chen et al., 2003), which is the ferroxidase required for efficient FPN-mediated iron export across the basolateral membrane of enterocytes. In the absence of hephaestin, the duodenal enterocytes of sla mice fail to efficiently transport the iron absorbed from the diet to the circulation. As a consequence, sla mice display severe systemic iron deficiency due to iron accumulation within the enterocytes. In spite of that, DMT1 levels are not increased with the local iron loading in the duodenum (and the ensuing loss of IRP-mediated stabilization) (Chen et al., 2003). From the observations in the sla mouse model, it is clear that FPN is a crucial connection required to couple duodenal iron absorption to systemic iron demand and make duodenal enterocytes competent for systemic iron supply. In fact, it is not a coincidence that FPN is the molecular target of the systemic regulator of iron homeostasis hepcidin (Nemeth et al., 2004). In addition, FPN expression is also modulated by the IRP/IRE system (Abboud and Haile, 2000; Donovan et al., 2000; McKie et al., 2000). Yet, as aforementioned (see 1.5.1), a FPN variant lacking the IRE (FPN1B) is expressed, along with the IRE variant, in enterocytes and erythroid precursors (Zhang et al., 2009). In the duodenum, the presence of a FPN isoform with no 5'IRE might be a way to escape IRP-mediated repression in conditions of systemic iron scarcity. This would allow local iron deficiency in enterocytes to be ignored (by not repressing FPN in order to facilitate local iron increase) to favor iron flux into the bloodstream and satisfy the systemic iron demand.

The role of the IRP/IRE system in duodenal function was investigated in mice with conditional ablation of IRP2 or both IRPs in enterocytes. Deletion of IRP2 in the intestine resulted in duodenal iron loading (as in the constitutive IRP2 KO model) associated with increased ferritin levels (Galy et al., 2005b; Ferring-Appel et al., 2009). The cell-autonomous nature of this phenotype was further confirmed by the fact that the duodenal iron loading was not recapitulated when IRP2 was specifically ablated in macrophages and hepatocytes (Ferring-Appel et al., 2009). Intestine-specific ablation of both IRPs resulted in a more severe phenotype, as mice displayed growth defects already at 7 days post partum and died shortly after weaning (likely because of dehydration) (Galy et al., 2008). This shows that IRPs are crucial for intestinal function and organismal survival. Histologically, duodenal samples displayed less structured crypts and villi, as well as increased apoptosis, while ultrastructural analysis revealed signs of mitochondriopathy (mitochondria appeared swollen and with unstructured cristae). At the molecular level, IRP-target genes displayed the expected pattern of a loss of IRP function, including induction of ferritin and FPN as well as reduction of TfR1 and DMT1 levels. Locally,

this results in a situation of cellular iron starvation because iron is sequestered into ferritin, while less dietary iron is absorbed and more iron is exported via FPN. At the systemic level, the increase in FPN-mediated iron export may compensate for the decreased dietary iron absorption, as mice do not show any signs of systemic iron deficiency. Findings from this study show that while hepcidin is considered the principal regulator of systemic iron homeostasis, IRP-mediated regulation of the same molecular target FPN is also important to secure systemic iron supply (Galy et al., 2008).

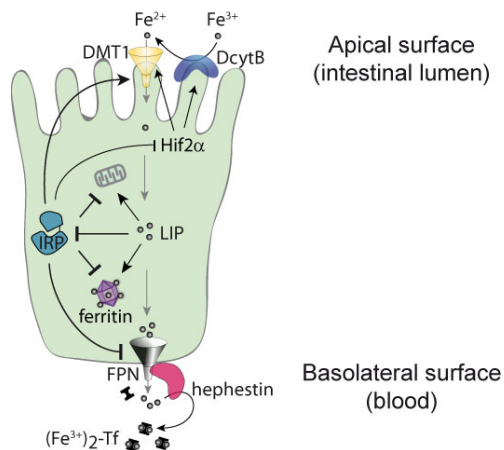


**Figure 1.8 The IRP/IRE network in duodenal enterocytes.** The IRP/IRE system critically influences duodenal function by post-transcriptionally regulating key molecules involved in iron absorption (DMT1 and Hif2α), intracellular iron sequestration (ferritin) and usage (in the mitochondrion) and iron export into the circulation (FPN). Picture modified from Muckenthaler et al., 2008.

### 1.5.3 The IRP/IRE system in liver function

The liver is the body iron storage organ and is also the principal site of expression and secretion of the systemic regulator of iron homeostasis hepcidin, as well as the serum iron-carrier transferrin and the ferroxidase ceruloplasmin. Therefore, the liver represents a crucial node for systemic iron metabolism as well as general body metabolism. It is not surprising that dysregulation of local iron management in hepatocytic cells (Fig. 1.9) can have detrimental systemic consequences.

Conditional ablation of the two IRPs in the hepatocytes is lethal to mice as they die within 2 weeks after birth (Galy et al., 2010). From the liver biopsies and blood biochemical analyses, the animal death associated with profound liver damage, internal bleeding and hepatic steatosis (fatty liver). On further examination, the hepatocytes displayed the typical molecular footprint of

loss of IRP function, including increased ferritin and ferroportin (due to loss of IRP-mediated repression), and reduced TfR1 and DMT1 (coherent with loss of IRP-mediated stabilization). Due to the ensuing increase in iron storage and export, alongside reduced iron import, the hepatocytes became iron-starved. Consequently, cellular iron starvation has detrimental effects on organelles such as the mitochondria. The mitochondrion requires iron as a main building block for the synthesis of heme and Fe-S clusters. The IRP double KO hepatocytes additionally presented with a reduction in the mitochondrial iron transporter mitoferrin 2 (although it is not an IRP-target) and thus contributed to further decrease in the iron content of the mitochondrial compartment. As expected, mitochondrial iron deficiency correlated with a decrease of heme- and Fe-S- proteins, including components of the mitochondrial electron transport chain and the TCA cycle, as well as the mitochondrial ferredoxin and cytoplasmic Fe-S proteins, such as xanthine dehydrogenase. Likely, the deficit of mitochondrial energy metabolism caused the severe mitochondriopathy, which in turn represented the leading cause of the hepatic failure (Galy et al., 2010). Interestingly, mice with double IRP deficiency in the intestine also showed signs of mitochondriopathy, as mitochondria of the enterocytes contained numerous round electron-dense deposits and disfigured structure of the cristae (Galy et al., 2008). Hence, both in the intestine and the liver, double IRP ablation was associated with mitochondrial dysfunction and had severe consequences for the specific tissues, leading to death caused by malabsorption and liver failure (Galy et al., 2008, 2010), respectively.

The importance of the IRP/IRE system for liver function and viability is also highlighted by a more recent mouse model with targeted FBXL5 deletion (Moroishi et al., 2011). Being involved in iron-mediated degradation of IRP2 (and apo-IRP1) (Salahudeen et al., 2009; Vashisht et al., 2009) (see 1.4.3), FBXL5 ablation determines a secondary increase of IRP2 expression. While systemic FBXL5 deficiency is lethal, its conditional deletion in hepatocytes has also detrimental consequences and leads to fatal liver failure (Moroishi et al., 2011). Interestingly, combined ablation of IRP2 rescues FBXL5 KO mice from death, showing that IRP2 overexpression plays a major role in the fatal consequences of FBXL5 deletion (Moroishi et al., 2011). However, it cannot be excluded that FBXL5 is also involved in the degradation of other proteins whose upregulation could contribute to the defects of the FBXL5 KO model.

Overall, the conditional IRP ablation in the hepatocytes unraveled the importance of the IRP/IRE system in liver physiology. More in general, it demonstrated a crucial role of the IRP/IRE system for securing adequate iron supply to sustain mitochondrial function.

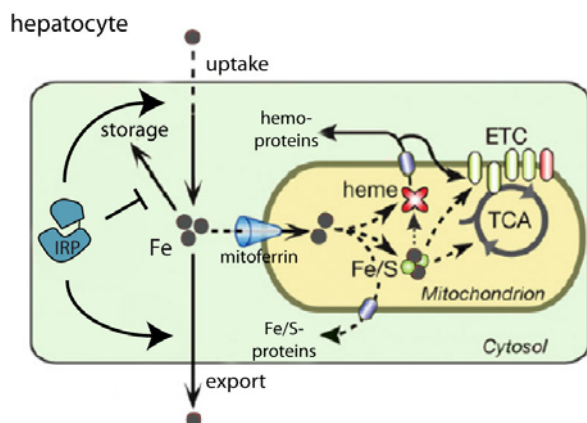


**Figure 1.9 The IRP/IRE system sustains hepatic and mitochondrial function.** The IRP/IRE system critically influences liver function by regulating cellular iron fluxes. The cellular iron regulatory machinery secures hepatocytic iron balance and, in particular, adequate iron supply to the mitochondrial compartment to sustain the synthesis of heme and Fe-S proteins necessary for energy metabolism. TCA: tricarboxylic acid cycle, ETC: electron transport chain. Modified from Galy et al., 2010.

#### 1.5.4 The IRP/IRE system in disease

While animal models with targeted deletion of the IRPs have provided valuable insights into the role of the IRP/IRE system in body physiology (see 1.5.3), disturbed IRP/IRE regulation has also been reported in some human conditions, as described below.

As many as 21 different mutations have been identified in the 5'UTR of the *FTL* gene, including single or double point substitutions as well as longer deletions (Cazzola et al., 1997; Cremonesi et al., 2003b). Some of them specifically affect the structure of the IRE sequence and have been associated with the autosomal dominant hyperferritinemia cataract syndrome (Beaumont et al., 1995; Girelli et al., 1995; Cazzola et al., 1997). This disease is characterized by early on-set bilateral cataract associated with abnormal FTL accumulation in the serum. Disruption of the interaction between the mutant FTL-IRE and IRP is consistent with a decreased repression of FTL and it has been confirmed in cultured lymphoblastoid cells from the affected patients (Cazzola et al., 1997). Yet, the reason why FTL specifically accumulates in the lens and it causes the cataract remains unclear.

In contrast to FTL, just one single mutation of the FTH-IRE has been implicated in disease. Such a mutation has been identified in four members of a Japanese family affected by autosomal dominant iron overload (Kato et al., 2001). Surprisingly, this mutation in the FTH-IRE was found to increase the binding affinity to IRP and to be associated with FTH downregulation in the liver.

Also, serum ferritin was shown to be increased in the affected patients (Kato et al., 2001). While the reason underlying increased serum ferritin is not clear, it is consistent with a mouse model with reduced FTH expression (Ferreira et al., 2001). However, a larger study of subjects with abnormally high serum ferritin and iron levels could not identify point mutations in the FTH-IRE sequence (Cremonesi et al., 2003a). This suggests that mutations of the IRE sequence of the FTH gene are rather infrequent in human patients as compared to FTL-IRE and gives a hint to the importance of preserving the IRP-mediated regulation of FTH.

Large studies including single nucleotide polymorphism identification and genome wide association studies have identified polymorphisms in the *IRP2* promoter and coding sequence that could affect IRP2 expression. Interestingly, these polymorphisms associate with increased susceptibility to chronic obstructive pulmonary disease (COPD) and potentially explain the altered expression levels of IRP2 observed in the lung of COPD patients (DeMeo et al., 2009). Polymorphisms of the *IRP2* gene are also associated with Alzheimer's disease (AD) (Coon et al., 2006). Curiously, analysis of brain necropsies from AD patients showed altered distribution of IRP2, which co-localizes with the characteristic histopathological features of AD (Smith et al., 1998). These included neurofibrillary tangles of hyperphosphorylated microtubule-associated protein Tau, as well as senile plaques composed of extracellular deposits of amyloids in the gray matter of the brain (Smith et al., 1998). Proteolysis of amyloid precursor protein (APP) generates  $\beta$ -amyloid, the principal component of the senile plaques (Sinha et al., 1999). APP has been shown to work as a ferroxidase and mediate neuronal iron export in conjunction with FPN (Duce et al., 2010). Inhibition of APP ferroxidase activity results in neuronal iron loading, as observed in AD (Duce et al., 2010). Furthermore, Tau ablation in mice is associated with mislocalization of APP, as well as neuronal iron retention, which is consistent with disruption of FPN-mediated iron export (Lei et al., 2012). Intriguingly, APP has been recently recognized as an IRP-target gene (Rogers et al., 2002).

Increasing the body of evidences linking dysregulation of the IRP/IRE system to neurodegenerative diseases, abnormally high IRP1 activity has been found in patients suffering from Parkinson's disease (PD) (Faucheux et al., 2002). In PD, the degeneration of dopaminergic neurons of the substantia nigra is characterized by local iron accumulation. The iron loading was found to be associated with a lack of up-regulation of the iron storage protein ferritin, which may contribute to increased oxidative stress in this region. Consistent with abnormally low levels of ferritin, IRP1 activity was not decreased in spite of the iron loading (Faucheux et al., 2002).

While the primary cause of iron accumulation in dopaminergic neurons of PD patients is not clear, aberrant IRP1 activity might contribute to neuronal oxidative stress and death by decreasing safe storage of excess iron into ferritin.

Along the line of neurodegenerative diseases, Friedreich's ataxia (FA) has also been correlated with aberrant IRP activity. FA is a neurodegenerative condition caused by silencing of the *FXN* gene due to unstable expansion of a GAA repeat in its coding sequence (Campuzano et al., 1996). *FXN* has been proposed to function as iron chaperone for the synthesis of Fe-S clusters in the mitochondria (Bulteau et al., 2004) (see 1.3.2) and its deficiency impairs Fe-S cluster assembly (Mühlenhoff et al., 2002). Typically, defects that lead to disruption of Fe-S cluster biogenesis result in decreased activity of mitochondrial Fe-S proteins (due to reduced Fe-S cluster availability) and mitochondrial iron accumulation (consequent to decreased iron utilization) (Sheftel et al., 2010). As a consequence, this leads to IRP1 activation (due to limited Fe-S cluster availability to form the cytosolic aconitase) and, in cases of cytosolic iron depletion, also to increased IRP2 stabilisation (Ye and Rouault, 2010). In FA, increased IRP1 activity along with mitochondrial iron loading are observed both in cardiac myocytes and neurons, as part of the tissues that are specifically affected by the disease (Pandolfo, 2003). A mouse model of FA that was generated by targeted deletion of *FXN* shows the same abnormalities observed in patients suffering from FA (Puccio et al., 2001).

FA is not the only disorder associated with disrupted Fe-S cluster machinery and associated with aberrant IRP activation. Human patients carrying a mutation that results in a drastic reduction of the Fe-S cluster scaffold protein ISCU suffer from a form of hereditary myopathy with exercise intolerance (Mochel et al., 2008; Olsson et al., 2008). An intronic substitution leads to a splicing error that includes a premature stop-codon in the ISCU transcript. ISCU deficiency impairs Fe-S cluster synthesis and leads to abnormal IRPs activation in the skeletal muscle of the affected patients (Crooks et al., 2012).

A single nucleotide substitution interfering with correct splicing is also the leading cause of *GLRX5* deficiency (Camaschella et al., 2007). Despite the dramatic reduction of *GLRX5* in all tissues, only the erythron seems to be significantly affected. The only disease manifestation is an anemia characterized by erythroblasts with iron-overloaded mitochondria (also known as sideroblasts). The sideroblastic anemia linked to *GLRX5* deficiency is also featured by IRP1 activation, which was shown to be responsible for *eALAS* repression (via its 5'IRE) and

consequent impairment of hemoglobin synthesis (Camaschella et al., 2007). Study of the corresponding animal model of the disease, the mutant zebrafish shiraz, has revealed the centrality of abnormal IRP1 activation in the etiology of the disorder (Wingert et al., 2005). In fact, either the overexpression of a version of the eALAS mRNA lacking the 5'IRE or the use of an antisense oligo to knockdown IRP1 was sufficient to restore hemoglobin synthesis in the GLRX5 mutant fish (Wingert et al., 2005).

To summarize, mouse models with loss of IRP function have extended our understanding on the importance of the IRP/IRE system in body physiology. Both systemic and conditional, as well as single and double, IRP deletions have provided information on the physiological role of the IRP/IRE system in vivo as well as the pathological consequences of its deregulation (see 1.5.3). A handful of human conditions with alterations of the IRP/IRE system have been reported, either with mutations in the IRE sequence of IRP target genes or polymorphisms of the IRP2 promoter. Intriguingly, abnormally high IRP activity, secondary to impairment of the Fe-S cluster biogenetic machinery, has also been observed in human patients. Of note, the aforescribed diseases caused by primary defects in the Fe-S cluster biogenesis machinery display a strong tissue-specificity. Their manifestation appears to be limited either to the neurons (FXN deficiency), the muscles (ISCU deficiency) or the erythron (GLRX5 deficiency). Conceivably, this may account for tissue-specific roles of the respective defective genes (FXN, ISCU and GLRX5) and/or for the special requirement for efficient production of heme- and Fe-S- proteins in the relevant tissues. Alternatively, or in addition, the tissue-specific manifestations of these disorders could be due to the unique effects of aberrant IRP activation in a given tissue, as it has been clearly demonstrated in the case of GLRX5 deficiency. A model with primary overexpression of IRP activity could help dissect these different hypotheses and show the direct consequences of aberrant IRP activity on body physiology. Attempts to generate such an in vivo experimental model system have been made, although the apparent toxicity of IRP overexpression has posed a great challenge (DeRusso et al., 1995; Lind et al., 2006; Surdej et al., 2008). A mammalian model of gain of IRP function has not yet been described.

## 1.6 AIM OF THE THESIS

Deregulation of iron metabolism is a key feature and frequent cause of some of the most common human diseases worldwide. Hepcidin is the systemic regulator of iron homeostasis and mutations affecting the genes involved in its expression, i.e. *HAMP*, *HFE*, *HJV*, *TfR2* (Feder et al., 1996; Camaschella et al., 2000; Roetto et al., 2002; Papanikolaou et al., 2003), as well as its direct molecular target ferroportin (*FPN*) (Montosi et al., 2001; Njajou et al., 2001), are well known causes of hereditary iron overload disease. Iron regulation at the cellular level is secured by the IRP/IRE system. The importance of the IRP/IRE system for life was revealed by the embryonic lethality of mice with constitutive combined ablation of both IRPs (Smith et al., 2006; Galy et al., 2008). While the regulation of systemic iron balance is certainly essential, an integrated view of the implications of deregulated cellular iron homeostasis for body physiology is still missing. Mouse models with loss of IRP function have provided insights to the detrimental consequences of altered cellular iron deregulation (Cooperman et al., 2005; Galy et al., 2005b, 2008, 2010). In humans, various reports exist connecting defects of the IRP/IRE system to diseases (Beaumont et al., 1995; Girelli et al., 1995; Kato et al., 2001; Coon et al., 2006; DeMeo et al., 2009). In particular, abnormally high IRP activity has been observed in disorders including sideroblastic anemia linked to *Glrx5* deficiency (Camaschella et al., 2007), Friedreich's ataxia (Lobmayr et al., 2005) and Parkinson's disease (Faucheux et al., 2002). However, until now a suitable animal model system to specifically investigate the pathological consequences of IRP1 hyperactivity was not available.

To gain a deeper understanding of the significance of appropriate IRP activity in vivo, our laboratory generated a new mouse model with gain of IRP1 function. The aim of this PhD project was to:

1. analyze the impact of abnormally high IRP1 activity on iron homeostasis in vivo;
2. explore the consequences of IRP dysregulation on general body physiology under standard laboratory conditions;
3. characterize the adaptive response of mice with gain of IRP1 function to acute and chronic iron challenges.



## 2. MATERIALS AND METHODS

### 2.1 MATERIALS

#### 2.1.1 Chemicals and reagents

All chemicals used in this study were purchased from Gibco BRL, Merck or Sigma-Aldrich with the following exceptions:

<b>Chemical</b>	<b>Company</b>
100bp DNA ladder	New England Biolabs
1kb DNA ladder	New England Biolabs
40% Acrylamide/Bis Solution 19:1	BioRad
30% Acrylamide/Bis Solution 37.5:1	BioRad
$\alpha$ [ <sup>32</sup> P]UTP, 800 Ci/mmol	Hartmann Analytic
Amino acid mixture, complete	Promega
ATP, CTP, GTP, UTP	Roche
Agar	Serva
Agarose	Invitrogen
Apoprotin	Roche
Complete EDTA-free Protease Inhibitor Cocktail	Roche
Dextran	Chemos GmbH
Deoxynucleotides (dNTPs)	PeqLab
Ethidium bromide	MP Biomedicals
E-64	Roche
EDTA	Roche
Fetal Bovine Serum (low endotoxin)	Invitrogen
G418	Invitrogen
Hemin	Normosang
Iron atomic spectroscopy standard solution	Fluka
Leupeptin	Roche
Milk powder	Frema Reform

## 2. MATERIALS AND METHODS

---

N,N,N',N'-tetramethylethylenediamine (TEMED)	Fluka
Pefabloc	Roche
Penicillin-streptomycin	Invitrogen
Pepstatin	Roche
Phenol/chloroform/isoamylalcohol, 25:24:1	AppliChem
Random hexamer primers	Invitrogen
RPMI 1640 plus Glutamax	Invitrogen
Tungsten Carbide Bead, 3mm	QIAGEN
TRIzol®	Invitrogen

### 2.1.2 Antibodies and enzymes

**Table 2.1 Enzymes used for western blot.** All secondary antibodies were coupled to horseradish peroxidase.

Primary	Source	Dilution	Secondary	Company	Dilution
<b>IRP1</b>	<b>“home-made”*</b>	<b>1:1000</b>	<b>α-rabbit</b>	<b>GE Healthcare</b>	<b>1:10000</b>
<b>FLAG-tag</b>	<b>BioLegend</b>	<b>1:2000</b>	<b>α-rat</b>	<b>GE Healthcare</b>	<b>1:10000</b>
<b>FPN</b>	<b>Alpha Diagnostic</b>	<b>1:1000</b>	<b>α-rabbit</b>	<b>GE Healthcare</b>	<b>1:10000</b>
<b>α-TfR1</b>	<b>Zymed</b>	<b>1:1000</b>	<b>α-mouse</b>	<b>GE Healthcare</b>	<b>1:10000</b>
<b>α-FTL</b>	<b>Santa Cruz</b>	<b>1:500</b>	<b>α-goat</b>	<b>Invitrogen</b>	<b>1:5000</b>
<b>α-β-actin</b>	<b>Sigma</b>	<b>1:10000</b>	<b>α-mouse</b>	<b>GE Healthcare</b>	<b>1:10000</b>

\* immunoprecipitated rabbit antibody raised against full length mouse IRP1

**Table 2.2 Enzymes used for flow cytometry.**

Antigen	Conjugated fluorophore	Company	Dilution
<b>Ter119</b>	<b>PeCy5</b>	<b>eBiosciences</b>	<b>1:200</b>
<b>CD44</b>	<b>FITC</b>	<b>eBiosciences</b>	<b>1:400</b>
<b>CD71</b>	<b>PE</b>	<b>eBiosciences</b>	<b>1:800</b>

Other enzymes used in this study were:

<b>Enzyme</b>	<b>Company</b>
FastStart PCR master	Roche
Platinum taq DNA polymerase	Invitrogen
Proteinase K	Sigma
Restriction enzymes	New England Biolabs
RNaseA	Sigma
RNasin® RNase inhibitor	Promega
RQ1 DNase	Promega
Spermidin	Sigma
Superscript II reverse transcriptase	Invitrogen
SYBR Green PCR master mix	Applied Biosystems
T7-RNA polymerase	Promega

### 2.1.3 Buffers and solutions

All solutions were prepared with double deionized water (ddH<sub>2</sub>O).

<b>Buffer</b>	<b>Composition</b>
Depurination solution (for Southern Blot)	0.25M HCl
Denaturizing solution (for Southern Blot)	0.5M NaOH 1.5M NaCl
DNA loading buffer (6x)	0.25% (w/v) Bromphenol blue 0.25% (w/v) Xylene cyanol FF 40% (w/v) Sucrose
HotSHOT Alkaline Lysis Reagent	25 mM NaOH 0.2 mM EDTA pH 12
HotSHOT neutralizing reagent	40 mM Tris-HCl pH 5

## 2. MATERIALS AND METHODS

---

Lysis buffer (for DNA extraction)	50mM Tris pH8 100mM EDTA 100mM NaCl 1% SDS)
Monroe buffer	10 mM Hepes 3mM MgCl <sub>2</sub> 40 mM KCl 5% Glycerol 0.2% Nonidet P-40
Neutralizing solution (for Southern Blot)	1M Tris pH 7.6 1.5M NaCl
RIPA buffer	10mM TrisHCl pH8 150mM NaCl 1mM EDTA 1% NP-40 0.1% SDS
RNA elution buffer	0.1% SDS 0.3 M ammonium acetate 0.02 M Tris PH 7.5 0.01 M EDTA
RNA loading buffer (2x)	95% Formamide 0.025% SDS 18 mM EDTA 0.0012% Bromophenol blue
SDS Protein loading buffer (4x)	350mM Tris pH 6.8 30% Glycerin 1% SDS

	0.5 M DTT
	0.0012% Bromophenol blue
TBARS reaction buffer	0.005 $\mu$ M butylated hydroxytoluene
	0.4% SDS
	7.5% acetic acid pH 3.5
	0.3% thiobarbituric acid
TBE buffer (10x)	0.89 M Tris, pH 8.0
	0.9 M boric acid
	10 mM EDTA
TBST	25 mM Tris
	150 mM NaCl
	2 mM KCl pH 7.4
	0.1% Tween 20
Transfer buffer (10x)	250 mM Tris
	2M Glycin
RIPA buffer	10mM TrisHCl pH8
	150mM NaCl
	1mM EDTA
	1% NP-40
	0.1% SDS

#### 2.1.4 Laboratory materials and kits

The following section lists laboratory materials used in this study as well as their suppliers.

<b>Material</b>	<b>Company</b>
0.2 ml reaction tubes (Thermo Tube™)	PeqLab
1.5 ml reaction tubes	Eppendorf
80 $\mu$ m cell strainer	BD Biosciences

## 2. MATERIALS AND METHODS

---

Biomax films	Kodak
Bottle top filters, 0.22 µm pore size	Millipore
Cell culture plates	Nunc
CHROMA SPIN 30 and 100 columns	Clontech
DC Protein Assay	Biorad
General glass ware	Schott
General plastic ware	Nunc
Glass potters Duall 20	Kontes Glass, Co
Gloves (Latex or Nitrile)	Kimberley-Clark
Iron (SFBC) Bathophenanthroline	BIOLABO
Parafilm	Pechiney Plastic Packaging
Plastic cuvettes	Nunc
PVDF membrane	Millipore
QIAquick Gel Extraction Kit	QIAGEN
Syringes	Becton Dickinson
Supersignal West Femto Chemiluminescent Substrate	ThermoScientific
U.I.B.C. Unsaturated Binding Capacity	BIOLABO
Western Lightning-PLUS ECL kit	ThermoScientific

### 2.1.5 Instruments

The following section lists laboratory instruments used in this study as well as their suppliers.

<b><u>Instrument</u></b>	<b><u>Company</u></b>
ABC Animal Blood Analyzer	Scil Vet
ABI PRISM 7500 instrument	Applied Biosystems
Cooled tabletop microcentrifuge	Eppendorf
Electrophoresis power supply	Pharmacia
FLA2000 phosphorimager	Fuji film
MOFLO high-speed cell sorter	Beckman-Coulter
Nanodrop 1000	Peqlab
RC-5B/C Centrifuge and appropriate rotors	Sorvall
Scintillation counter	PerkinElmer

Spectrophotometer (Ultrospec 2100 pro)	Amersham Biosciences
T-100 Thermal Cycler	Biorad
TissueLyser II	QIAGEN
Western Blot wet transfer cell	Biorad

### 2.1.6 PCR primers

**Table 2.3 Primer sequences.** All primers were purchased from Eurofins MWG. They were obtained in desalted, lyophilized form and were diluted in H<sub>2</sub>O to a 100 pmol/μl working solution.

Gene/Locus	Sequence (5'-3')	Code	Use
<i>Rosa26</i>	AGTCGCTCTGAGTTGTTATCA G	P1	PCR - genotyping
<i>Splicing Acceptor</i>	GCGAAGAGTTTGTCTCAACC	P2	
<i>Rosa26</i>	CCCAGATGACTACCTATCCTC	P3	
<i>Rosa26</i>	TCCTCAGAGAGCCTCGGCTAGG	P4	RT-PCR
<i>Splicing Acceptor</i>	GTTTGTCTCAACCGCGAGC	P5	
<i>Rosa26</i>	TGGAGCCGTTCTGTGAGACAG	P6	RT-PCR
<i>Irf1</i>	CTCAGCAAGGTGTGCAAATGGG	P7	
<i>Rosa26</i>	AAGGATACTGGGGCATACGCCACAGG	PB1-F	PCR (probe pb1)
<i>Rosa26</i>	CGTTGGGCCTAACTCGAGTCTCGCTGC	PB1-R	
<i>Neo</i> (β-geo stop cassette)	TCAGAAGAACTCGTCAAGAAGGCG	PB2-F	PCR (probe pb2)
<i>Neo</i> (β-geo stop cassette)	GCTTACATAAACAGTAATACAAGGGG	PB2-R	
<i>Cre</i>	CGCAGAACCTGAAGATGTTTCG		PCR - genotyping

<i>Cre</i>	<b>GTCGAAATCAGTGCGTTCGAAC</b>	
<i>Hepcidin</i>	<b>AACAGATAACCACACTGGGAA</b>	<b>qPCR</b>
<i>Hepcidin</i>	<b>ATACCAATGCAGAAGAGAAGG</b>	
<i>Fpn</i>	<b>GGGTGGATAAGAATGCCAGACTT</b>	<b>qPCR</b>
<i>Fpn</i>	<b>GTCAGGAGCTCATTCTTGTGTAGGA</b>	
<i>TfR1</i>	<b>CCCATGACGTTGAATTGAACCT</b>	<b>qPCR</b>
<i>TfR1</i>	<b>GTAGTCTCCACGAGCGGAATA</b>	
<i>Ftl</i>	<b>CGTGGATCTGTGTCTTGCTTC</b>	<b>qPCR</b>
<i>Ftl</i>	<b>GCGAAGAGACGGTGCAGACT</b>	
<i>Tubulin</i>	<b>GGGAAATCGTGCACATCCA</b>	<b>qPCR</b>
<i>Tubulin</i>	<b>ATGCCATGTTTCATCGCTTATCA</b>	
<i><math>\beta</math>-Actin</i>	<b>GCTTCTTTGCAGCTCCTTCGT</b>	<b>qPCR</b>
<i><math>\beta</math>-Actin</i>	<b>ACCAGCGCAGCGATATCG</b>	

### Mouse transgenesis

The plasmids pBigT and pROSA26PA were obtained from S. Srinivas (Srinivas et al., 2001). The PGK-Neo cassette from pBigT was modified to an IRESbgeo (Galy et al., 2004). The KpnI linearization site of pROSA26PA was replaced by a SfiI/FseI/PmeI multi-cloning site. Irp1 cDNA was cloned from mouse Sv129 ES cells. By step PCR, three cysteine residues required for Fe-S cluster assembly, C437, C503, C506, were mutated to serine and a fourth one, C118, to alanine, resulting in stabilization of the apoprotein in the presence of heme (A. Vasanthakumar and R. Eisenstein, unpublished findings). The resulting mutant Irp1 cDNA was fused to a DYKDDDDK (FLAG) tag (designated Irp1\*) and inserted into pBigTIRESbgeo to produce the pBigTIRESbgeoIRP1\* plasmid. PacI-AscI digested pBigTIRESIRP1\* was inserted into the modified pROSA26PA plasmid.

E14 ES cells were electroporated with the XhoI-linearized targeting construct and cultivated in the presence of G418 (Invitrogen). Resistant ES cell clones were analysed using RT-PCR and

Southern blotting. Targeted ES cell clones were injected into C57BL6/J embryos to obtain chimeras that were backcrossed to C57BL6/J to check for germ-line transmission of the knock-in *Rosa26* locus. Animals carrying the targeted allele have been crossed with a Hprt-Cre deleter strain (Tang et al., 2002). Mice bearing the recombined *Rosa26* locus were backcrossed to C57BL6/J for 5 generations and heterozygotes were then intercrossed to obtain wild-type, heterozygous and homozygous littermates.

## **2.2 METHODS**

### **2.2.1 Standard conditions and treatments of laboratory animals**

#### **Mouse husbandry and sample collection**

Animals were kept on constant light/dark cycle and food was supplied ad libitum. Mice were normally sacrificed at 8-10 weeks of age by CO<sub>2</sub> inhalation. Heparinized blood was collected by cardiac puncture and pieces of tissues were flash-frozen. For molecular analyses of duodenal samples, mice were euthanized by cervical dislocation to avoid sample degradation. Animal handling was in accordance with EMBL guidelines.

#### **Pharmacological iron overload**

30 weeks old males received one single intravenous dose of 1 mg of iron-dextran (Sigma-Aldrich) versus dextran alone (Chemos GmbH). Both chemicals were diluted in NaCl 150 mM and filtered through 0.22 µm filters before use. Animals were euthanized 24 hours after injection.

#### **Chronic iron overload**

HFE KO mice (Herrmann et al., 2004) were kindly provided by Muckenthaler laboratory. Mice bearing the recombined *Rosa26* locus (IRP1\*) in homozygosis were crossed with homozygous HFE KO mice, as a model of chronic iron overload. Double heterozygous mice were then intercrossed and, among the littermates, four experimental groups were selected, including double homozygous (IRP1\*/HFE KO), double wildtype as well as single homozygous mice. Animals were analysed at the age of 20 weeks.

### **Determination of $^{59}\text{Fe}$ distribution in mouse tissues**

To determine body iron distribution, mice were administered intravenously with  $^{59}\text{Fe}$  in isotonic HEPES-buffered saline ( $\text{Fe}(\text{NO}_3)_3$ -complexed with nitrotriacetic acid (NTA) (1:2); labeled with  $\sim 2\mu\text{Ci } ^{59}\text{Fe}/\text{animal}$ ;  $0.2\mu\text{mol Fe}/\text{kg}$  body weight).  $^{59}\text{Fe}$  activity in tissues was measured 2 weeks after injection using a well-type  $\gamma$ -counter (1282 Compugamma CS, LKB, Wallac, Finland). Results were normalized by subtraction of the amount of  $^{59}\text{Fe}$  calculated to be in the residual blood of each organ (Schümann et al., 2007).

### **2.2.2 Standard mouse phenotyping**

The standard phenotypic analysis was performed at the Mouse Clinic Institute (ICS - Strasbourg) in accordance with the European Council Directive of 24 November 1986. Here is described only a short selection of the standard tests performed at the ICS and whose corresponding results are shown in the main body of this thesis (see 3.3). A more comprehensive list of the assays carried out is included in the Appendix.

#### **Rotarod test**

The rotarod test measures the ability of the animal to maintain balance on a rotating rod with a diameter of 4.5 cm (Bioseb, Chaville, France). Mice were submitted to 3 repeated trials, separated by 15 min intervals, during which the rotation speed accelerated from 4 to 40 rpm in 5 min. The latency before falling was recorded and used as index of motor coordination/motor endurance performance.

#### **Exercise test**

Exercise performance was assessed using a treadmill system, which comprises a belt enclosed in a plexiglass chamber and a stimulus device consisting of a metal shock grid attached to a rear of the belt. The speed and the slope of the belt are electronically adjusted. Mice were first subjected to an incremental protocol, whereby they began with a 20 min acclimatization period at 25 cm/s and a slope of 5 degrees. The following day, a defined protocol was applied with increase in speed and slope until exhaustion of the animal. The duration of the running and the total distance covered were measured to evaluate the performance of the mice.

### **Grip test**

This test measures the muscle strength using an isometric dynamometer connected to a grid (Bioseb, Chaville, France). Once the animal was holding the grid with its forepaws, it was slowly moved backwards until it released it. The dynamometer recorded the maximal strength developed.

### **Electromyography**

Electromyographic recording allows neurophysiological measurement of sensory-motor function. Recordings were performed under Imalgen-Rompun anesthesia using a Key Point electromyograph (EMG) apparatus (Medtronic, France). The body temperature was maintained at 37 °C with an homeostatic blanket (Harvard, Paris, France).

To measure the sensitive nerve conduction velocity (SNCV), recording electrodes were inserted at the base of the tail, while stimulating electrodes were placed 20 mm away from the recording needles, towards the extremity of the tail. A ground needle electrode was inserted between the stimulating and recording electrodes. The caudal nerve was stimulated with a series of 20 pulses during 0.2 ms each at a supramaximal intensity. The average response of these 20 stimulations was included for statistical analysis.

To assess the stimulation-evoked activity, the compound muscle action potential (CMAP) was measured in gastrocnemius or plantar muscles after the sciatic nerve stimulation. For this purpose, stimulating electrodes were placed at the level of the sciatic nerve and recording electrodes in the gastrocnemius muscle. A ground needle was inserted in the contralateral paw. Sciatic nerve was stimulated with a single 0.2 ms pulse at a supramaximal intensity. The amplitude (mV) and the distal latency of the responses (ms) were measured.

### **2.2.3 Hematology and tissue biochemistry**

#### **Blood cell profiles and serum biochemistry**

Hematological parameters were determined from freshly collected and heparinized blood samples using a Scil Vet ABC Animal Blood Analyzer. Serum was obtained by centrifugation of the blood samples at 4500 rpm for 10 minutes at 4°C and collection of the supernatant. Serum iron and transferrin saturation were measured using BIOLABO reagent kits, i.e. Iron (SFBC) Bathophenanthroline and U.I.B.C. Unsaturated Binding Capacity (BIOLABO) according to the

manufacturer's instructions. Serum ferritin was measured by the Claude Bernard Institute Chemistry Laboratory (Paris, France) using an Olympus 400 analyser.

### **Determination of total non-heme iron content in mouse tissues**

Non-heme iron content was measured in whole tissue lysates using the bathophenanthroline chromogen method. Tissues were dried at 45°C for 3 days, weighted and digested for 48 hours at 65°C in 10% TCA/10% HCl (1 ml per 100 mg of dried liver material; 3 ml per 100 mg of splenic and duodenal material) to allow deproteinisation and mineralization of non-heme iron. 200 µl of diluted extracts (1:20 for spleen, 1:10 for liver and duodenum) were added to 1 ml of chromogen solution (bathophenanthroline-disulfonic acid 0.01% / thioglycolic acid 0.1% / 7M Na-acetate). The thioglycolic acid allows ferric iron to be reduced to its ferrous form that can then react with disulphonated bathophenanthroline and form a coloured complex. After 10 min of incubation, absorbance at 535 nm (Abs<sub>535</sub>) was read using a Ultrospec 2100 pro (Amersham Biosciences). The amount of non-heme iron was quantified using a standard curve made with iron atomic spectroscopy standard solution (Fluka).

### **Determination of lipid peroxides in mouse tissues**

Thiobarbituric acid reactive substances (TBARS) were measured according to Okawa et al, 1979 (Ohkawa et al., 1979). Tissue homogenates were prepared in 20mM sodium-phosphate buffer (pH 7.4) and 0.1% SDS. While an aliquot was used for the determination of protein concentration, a 200-µl aliquot of tissue homogenate was added to 0.005 µM butylated hydroxytoluene, 0.4% SDS, 7.5% acetic acid at pH 3.5, and 0.3% thiobarbituric acid in a final volume of 4 ml. Samples were incubated at 95°C for 60 min and then cooled at room temperature. Lipids were extracted using n-butanol:pyridin (15:1, v/v), centrifuged at 4,000×g for 10 min and the Abs<sub>532</sub> of the upper layer was estimated using a Ultrospec 2100 pro (Amersham Biosciences). The amount of TBARS was quantified using a standard curve of malonaldehyde bis- (dimethyl acetal) (Sigma-Aldrich).

### **2.2.4 Cell biology**

#### **Primary cultures of bone marrow-derived macrophages (BMDM)**

BMDM were obtained from femurs. Bones were disinfected in ethanol (EtOH) 70% and their heads removed with a scalpel. The marrow was flushed out using a syringe and ice-cold

Hank's Balanced Salt Solution (HBSS) 14185 (Gibco) and the cell suspension was filtered through a 80  $\mu\text{m}$  cell strainer (Falcon, BD Biosciences). Cells were seeded at a density of approximately  $5 \times 10^4$  cells/ $\text{cm}^2$  in RPMI 1640 plus Glutamax (Invitrogen) supplemented with 10% (v/v) heat-inactivated low endotoxin fetal bovine serum (FBS) (Invitrogen), 1% Penicillin + Streptomycin (Invitrogen) and 100 ng/ml macrophage colony-stimulating factor 1 (Sigma-Aldrich). Cells were grown at 37°C in a 5% CO<sub>2</sub> atmosphere. After 4 days, non-adherent cells were removed by washing with HBSS and the medium daily replaced until cells reached a 70-80% confluence (typically 6 to 7 days after seeding), when they were treated. Treatment consisted in a 10 hours exposure to hemin 100  $\mu\text{M}$  (Normosang), as an iron source, to the chelator deferoxamine (DFO) 100  $\mu\text{M}$  or to an equivalent amount of DMSO as a control. After incubation with the stimulus, cells were quickly harvested in ice-cold phosphate-buffered saline (PBS), centrifuged for 5 min at 5000 rpm and at 4°C. The supernatant was then removed and the dry cell pellet snap-frozen for subsequent molecular analysis.

### **Flow cytometry analysis of bone marrow-derived cells**

Bone marrow derived cells were obtained from femurs. Bones were quickly crushed in a mortar with ice cold RPMI 1640 plus Glutamax supplemented with 2% FBS and the cell suspension was then filtered through a 40  $\mu\text{m}$  cell strainer.  $2 \times 10^6$  cells were co-stained with PeCy5-labeled Ter119 (1:200), FITC-conjugated CD44 (1:400) and PE-conjugated CD71 (1:800) antibodies (eBiosciences) in 200  $\mu\text{l}$  of 50% 2.4G2 (BD Biosciences) / 50% (PBS 2% FBS) at 4°C for 20 minutes and in the dark. Flow cytometry was performed with a MOFLO high-speed cell sorter (Beckman-Coulter). Flow-Jo software (Tree Star, Ashland, OR) was used for analysis.

### **2.2.5 Molecular biology**

#### **DNA extraction**

When high quality genomic DNA was needed for Southern Blot analysis, the following procedure was applied. A piece of tissue was incubated in 500 $\mu\text{l}$  lysis buffer (50mM Tris pH8; 100mM EDTA; 100mM NaCl; 1% SDS) supplemented with 200 $\mu\text{g}$  proteinase K (Sigma), at 55°C shaking overnight. The DNA was then purified by phenol/chloroform/isoamylalcohol (25:24:1) extraction, performed twice, followed by chloroform and isopropanol precipitation. The precipitated DNA was washed once with EtOH 70%, air dried and re-dissolved in water. The concentration of the DNA samples was determined by reading of the Abs<sub>260</sub> using a Nanodrop

1000 (Peqlab). When genomic DNA was required for genotyping, a fast “HotSHOT” (Hot Sodium Hydroxide and Tris) method of DNA extraction was performed as described (Truett et al., 2000). Briefly, a small piece of tissue (typically the tip of the tail) was boiled at 95°C and for 40 min in 100 µl of alkaline lysis reagent (25 mM NaOH, 0.2 mM EDTA – pH 12). The sample was then briefly cooled on ice and 100 µl of neutralizing reagent (40 mM Tris-HCl in water – pH 5) were added. DNA samples were stored at -20°C.

### **RNA extraction**

Total RNA was extracted with Trizol reagent (Invitrogen) according to the manufacturer’s instructions. Briefly, a small piece of tissue was added to an eppendorf tube containing one Tungsten Carbide Bead of 3mm (QIAGEN) and 1 ml of cold TRIzol reagent. For RNA extraction from BMDM pellets, the amount of TRIzol reagent (as well as of the subsequent reagents) was halved. The sample was homogenised for 2 min at maximum speed using a TissueLyser II (QIAGEN). To completely dissociate nucleoprotein complexes, the homogenates were incubated at room temperature for 5 min. 200 µl of chloroform was added, and the tubes were vigorously shaken and incubated at room temperature for a further 3 min. The samples were centrifuged at 12,000 x g for 15 min at 4°C. RNA was obtained by removal of the aqueous phase, and precipitated by addition of 500 µl of isopropanol at room temperature. After 10 min, precipitated RNA was collected by centrifugation at 12,000 x g for 15 min at 4°C. The supernatant was removed and the RNA precipitate was washed with 75% ethanol, air dried and re-dissolved in water at 60°C. The RNA concentration was determined by measuring the Abs<sub>260</sub> using a Nanodrop 1000 (Peqlab) and the samples stored at -80°C.

### **Protein extraction**

Total protein extracts from pieces of tissue (or BMDM pellet) were obtained by homogenization of the sample in ice-cold RIPA buffer (10mM TrisHCl pH8, 150mM NaCl, 1mM EDTA, 1% NP-40, 0,1% SDS) supplemented with a cocktail of protease inhibitors (Pefabloc 4 ml/ml, Apoprotin 0.1 mg/ml, Leupeptin 0.02 mg/ml, E-64 0.04 mg/ml, Pepstatin 0.004 ml/ml, EDTA 2 mg/ml) (Roche) using glass potters Duall 20 (Kontes). To obtain cytosolic protein extracts, Monroe buffer (10 mM Hepes pH 7.6, 3 mM MgCl<sub>2</sub>, 40 mM KCl, 5% glycerol, 0.2% nonided P-40) supplemented with an EDTA-free proteinase inhibitor cocktail (Roche) was used instead. Homogenates were incubated on ice for 30 min, clarified by centrifugation at 10,000 rpm for 15 min in a cooled tabletop microcentrifuge (Eppendorf) and supernatants collected. Protein

concentration was measured using a Lowry-based DC Protein Assay (Biorad). Protein samples were snap-frozen and stored at -80°C.

### **cDNA synthesis**

Total RNA was treated with RQ1 DNase (Promega) and 1 µg was reverse-transcribed with random primers and Superscript II (Invitrogen) following the manufacturer's instructions. When the cDNA was generated for subsequent qPCR analysis, 2 independent reverse-transcription reactions were performed on each sample, to control the degree of technical variability. In addition, mock reactions (without the reverse-transcriptase) of a selection of the samples were also included, to control the RNA dependence of the synthesized cDNA. Newly generated cDNA was then stored at -20°C.

### **Polymerase Chain Reaction (PCR)**

Duplex PCR was routinely performed for genotyping of the mice. For discrimination of the wildtype and targeted/recombined *Rosa26* alleles primers P1, P2 and P3 were used. The Cre transgene was detected using primers Cre\_fwd and Cre\_rev. Cre-mediated removal of the stop cassette was assessed by RT-PCR using primer pairs P4/P5 and P6/P7. FastStart PCR master (Roche) was used for all PCR reactions, which included 2 µl of genomic DNA, primers at a concentration of 1.75 µM in a total reaction volume of 20 µl. PCR conditions were as following: 95°C for 5 minutes, (95°C for 30 seconds, 55°C for 30 seconds, 72°C for 30 seconds) for 35 cycles, 72°C for 5 minutes. The same PCR conditions, but scaled up to a reaction volume of 50 to 100 µl, were used to generate, with the appropriate primer pairs, DNA fragments to be subsequently used as standard for absolute quantification of the qPCR data. By contrast, genotyping of the HFE allele required different PCR conditions, including the use of a platinum taq DNA polymerase (Invitrogen) and of a different amplification cycle. The latter consisted of: 95°C for 5 minutes, (95°C for 30 seconds, 63°C for 30 seconds, 72°C for 1 minute) for 30 cycles, 72°C for 5 minutes. All primers used for PCR are listed in table 2.3.

### **Quantitative real-time PCR (qPCR)**

As template for the qPCR reaction, duplicate cDNA, produced by 2 independent reverse-transcription reactions, were used for each sample. When the reverse-transcription was performed using 1 µg of RNA as starting material, the generated cDNA was diluted 1:100 before use for qPCR. The reaction mix contained 10 µl of SYBR Green PCR Master Mix (Applied Biosystems), 0.3 µM of the forward and reverse primers and 5 µl of cDNA in a total volume of 20 µl. The

qPCR reaction was run on ABI Prism 7500 sequence-detection system and software (Applied Biosystems) according to the following thermocycle protocol: 50°C 2 min, 95°C 10 min, (95°C 15 s, 60°C 1 min) × 40 cycles. An ABI Prism 7500 sequence-detection software was used for analysis of the qPCR data. A method of absolute quantification was adopted and required the use of appropriate standard curve produced with PCR-generated fragment of the gene of interest. For each target gene, the level of expression was calculated as average of the duplicates and then calibrated to  $\beta$ -tubulin mRNA levels. Similar results were obtained when using  $\beta$ -actin as reference gene (not shown). All primers are listed in table 2.3.

### **Agarose gel electrophoresis.**

Typically, a 2% agarose gel was used for electrophoretic separation of PCR-generated fragments, e.g. for genotyping analysis. A 0.8% agarose gel was instead used for analysis of intact genomic DNA, i.e. for Southern Blot. The desired amount of agarose was boiled in 1x TBE buffer (45 mM Tris-borate, 1 mM EDTA – pH 8) until it was completely dissolved. After it cooled down, ethidium bromide (EtBr) solution (0.5  $\mu$ g/ml final concentration) was added to the liquid agar, which was then poured in a flat-bed tray with combs. When the agarose solidified, the DNA in the loading buffer was loaded into the wells and separated electrophoretically. Ethidium bromide intercalates with the DNA's GC base pairs resulting in DNA-EtBr-complex that could be detected on a UV-light tray at 265 nm or using a gel documentation system. For preparative gels, a weaker UV-light source was used (365 nm) to avoid irradiation damage of DNA.

### **Purification of DNA fragments**

PCR-generated DNA fragments of a gene of interest were purified from agarose gels, to be subsequently quantitated and used as standard for absolute quantification of qPCR data. DNA fragments were purified using a Gel Extraction Kit (Qiagen) according to the manufacturer's instructions. Briefly, slices containing the fragment of interest were excised from the gel and dissolved at 50°C in an appropriate amount of buffer QG and applied to the silica-based purification column. The DNA selectively adsorbs to the silica membrane in the presence of high-salt, while contaminants pass through the column during a centrifugation step. After washing the column with EtOH-containing buffer PE, the pure DNA was eluted with 30-50  $\mu$ l water.

### **Restriction digest of DNA**

Restriction digests were performed either for Southern Blot analysis of genomic DNA or for linearization of a plasmidic template to be used for in vitro transcription of RNA probes for EMSA. For Southern Blot, about 4 µg of genomic DNA were digested in a 20 µl reaction, overnight at 37°C. 30000 units of either EcoRV or MfeI restriction enzymes (NEB) were used, together with the buffer suggested by the supplier and supplemented with Spermidine 0.4 M and 2 µg of RNaseA (Sigma). To generate the template for in vitro transcription, a I12CAT plasmid, containing the FTH1-IRE sequence was linearized with XbaI restriction enzyme (NEB) following the manufacturer's recommendations, overnight at 37°C. The linearized plasmid was then purified by phenol/chloroform extraction and the concentration determined by measuring the Abs<sub>260</sub> with the Nanodrop.

### **Southern Blot**

Proper targeting of the *Rosa26* locus was verified by Southern blotting. Digested genomic DNA was run on 0,8% agarose-TBE gel, with no EtBr. When the size marker was sufficiently separated, the gel was depurinated with in 0,25 M HCl for 20min, rinsed with water for 20 min, denaturized with 0,5M NaOH/1,5M NaCl twice for 20 min, neutralized with 1M Tris pH 7,6; 1,5M NaCl twice for 20 min, washed with water twice for 10min and equilibrated in 10x SSC (NaCl 1,5 M, Na-citrate 150 mM - pH 7) for 10min. The genomic DNA in the gel was then blotted overnight onto a Hybond N+ nylon membrane and subsequently crosslinked to it with a Stratalinker (autocrosslink program: 254 nm and 1200 µJoules). For hybridization, PCR probes, obtained with primers PB1-F/PB1-R and PB2-F/ PB2-R (table 2.3), were radio-labeled using αP32-dCTP labeling beads (Amersham), according to the manufacturer's instruction, for 30 min at 37°C. Radiolabeled probes were then purified over Chromaspin P100 column (Clontech). Hybridization was performed following the protocol from Church and Gilbert (Church and Gilbert, 1984). The hybridized probe was detected by exposure of the treated membrane to x-ray Biomax film (Kodak).

### **In vitro transcription**

In vitro transcription was performed to synthesize RNA probes for EMSA. For synthesis of "hot" P32-labeled IRE-probes, 1µg of XbaI-linearized I12CAT plasmid, containing the FTH1-IRE sequence downstream to T7 promoter, was used as template for the in vitro transcription reaction. 4 µl of α-P32-UTP (800 Ci/mmol) (Hartman) were used as only source of UTPs and the transcription was carried out with T7 polymerase (Promega) following the manufacturer's

instructions. After the synthesis of radiolabeled transcripts, the RNA was loaded onto Chromaspin P30 columns (Clontech) to remove the excess of unincorporated radio-nucleotides. 1 volume of formamide blue loading dye was then added to the RNA sample, which was boiled at 95°C for 3 min and quickly chilled on ice. Samples were electrophoretically separated on denaturing 7.5% acrylamide gel (20:1 acrylamide:bis/ urea 7M) in order to purify the correct band from potential side-products of the reaction. After electrophoretic run, the gel was exposed to x-ray Biomax film (Kodak). The correct RNA band was cut out and eluted from the gel in 800 µl of RNA elution buffer (0.1% SDS/ 0.3 M ammonia acetate/ 0.02 M Tris PH 7.5/ 0.01 M EDTA, in H<sub>2</sub>O), overnight at 37°C. The eluted RNA probe was then purified by phenol/chloroform/isoamyl alcohol extraction. The concentration in cpm/µl of the final resuspension was determined with a scintillation counter (Perkin Elmer). Aliquots were stored at -20°C and used within 2 weeks. “Cold” trace-labeled IRE-probes were in vitro transcribed using the Megascript T7 kit (Ambion) following the manufacture’s protocol. The newly synthesized probes were purified by phenol/chloroform/isoamyl alcohol extraction and additionally loaded onto Chromaspin P30 columns (Clontech) to remove the unincorporated radio-nucleotides. After quantification of the cpm/µl of the final resuspension, aliquots were stored at -80°C.

### **Electrophoretic Mobility Shift Assay (EMSA)**

EMSAs were performed using 8 µg of cytoplasmic extracts and in vitro-transcribed <sup>32</sup>P-labeled human ferritin-H1 IRE probe (40.000 cpm per reaction). Probes were pre-boiled at 95°C for 2 min and chilled on ice. The binding reaction was performed as following: cytoplasmic protein extracts were incubated with probes and 4 units of RNasin (Promega) for 15 min at room temperature and for additional 10 min upon addition of heparin (50 µg). For supershift experiments, antibodies (0.5 and 1.5 µg) against either IRP1 and FLAG or the appropriate rabbit and rat IgG controls were added to the reaction during the 10 min incubation with heparin. Competitive EMSAs were performed using an increasing molar excess (i.e 0.25x, 1x, 4x, 16x, 64x) of unlabeled wildtype FTH1-IRE probe or a mutant version bearing a C deletion in the IRE loop, which impairs the IRP-IRE interaction (Gray et al., 1996). The competitor was normally pre-mixed with the “hot” probe before addition to the reaction. At the end of the 25 min of binding-reaction, loading buffer (50% glycerol/H<sub>2</sub>O) was added and the reaction immediately loaded on 5% native acrylamide (60:1 acrylamide:bis) gel. Electrophoretic separation of the RNA-protein complexes was carried out at 5V/cm<sup>2</sup> for about 5 hours. Gel was then dried and exposed to Biomax film (Kodak). The bands corresponding to IRP-IRE complexes were quantified using a FLA2000 phosphorimager (Fuji film, Tokyo, Japan).

**Western Blot**

Equal amounts of total protein extracts were prepared and loading buffer (350mM Tris, pH 6.8, 30% Glycerin, 1% SDS, 0.5 M DTT, 0.0012% Bromophenol blue) was added to them. Proteins were denatured at 95°C for 5 min (except when FPN needed to be detected) and separated by 8% or 12% SDS-PAGE. Proteins were subsequently transferred onto a PVDF membrane pre-activated by a short incubation in methanol. A BioRad wet-blot chamber was used and blotting occurred in 1x Transfer buffer (25 mM Tris, 0.2M Glycin) at 400mA for two hours, or at 200 mA overnight. The membrane was subsequently blocked with 5% dry fat-free milk in TBST (25 mM Tris, 150 mM NaCl, 2 mM KCl, pH 7.4, 0,1% Tween 20) for 1 hour at room temperature. Incubation with primary antibody in 1x TBST/5% milk was performed for 2 hours at room temperature. Primary antibodies used and the relative dilutions were:  $\alpha$ -IRP1 (1:1000),  $\alpha$ -FLAG-tag (1:2000) (BioLegend),  $\alpha$ -FPN (Alpha Diagnostic) (1:1000),  $\alpha$ -TfR1 (Zymed) (1:1000),  $\alpha$ -FTL (1:500) (Santa Cruz) (1:500),  $\alpha$ - $\beta$ -actin (Sigma) (1:10000). After washes with 1x TBST, the membrane was incubated for 1 hour at room temperature with appropriate secondary antibody coupled to horseradish peroxidase (1:10000) in 1x TBST/5% milk. After washing, the secondary antibody was detected using ECL-Plus (Thermoscientific) and by exposure to Biomax film (Kodak). A Femto-ECL (ThermoScientific) was employed when the  $\alpha$ -flag primary antibody was used. Relative protein expression was assessed by densitometric analysis of immunoblot staining intensity using the ImageJ software (National Institutes of Health, Bethesda, Maryland, US).

**2.2.6 Statistical Analyses**

Data are shown as mean values  $\pm$  SEM. Statistical analysis was performed using two-tailed Student's t test. For the phenotypical analysis, data were analysed using one-way or two-way analysis of variance (ANOVA) with one between-subjects factor (genotype) and one within-subjects factor (time). Qualitative parameters were analysed using  $\chi^2$  test. P values  $<$  0.05 were considered statistically significant.



### 3. RESULTS

Due to the great similarities between mouse and human iron metabolism, murine models have proven to be very useful in providing important insights into the regulation of human iron homeostasis as well as disorders of iron metabolism. In particular, such models provide an integrated picture of the dynamics and complexities of iron metabolism in the whole animal, which is not possible in the simpler cell culture systems. Following the advent of the Cre/Lox technology, the number of available mouse lines with floxed iron-related genes, together with the broad availability of tissue-specific and ligand-induced Cre-deletor strains, has allowed elegant studies on the *in vivo* consequences of cell- and temporal-selective deletion of these genes (Fleming et al., 2011).

In particular, to explore the *in vivo* functions of the IRP/IRE regulatory system, mouse lines with constitutive and tissue-specific IRP ablation have been analyzed during the last decade (LaVaute et al., 2001; Galy et al., 2004, 2005a; Meyron-Holtz et al., 2004a). Using a complementary approach, but still exploiting the advantages of the Cre/Lox technology, a new mouse line with conditional gain of IRP1 function has been recently generated in our laboratory. When I joined the project, chimeras had just been derived from blastocysts injected with transgenic ES clones. My initial task was to validate the proper insertion of the targeting cassette into the genomic locus. Next, in order to systemically activate the gain-of-function IRP1 transgene, the targeted mice were crossed with a pan-Cre-deletor strain. The molecular characteristics of the resulting mouse line expressing a constitutive gain of IRP function are described, including the extent of gain of IRP function achieved in different tissues. The line has been investigated to reveal the impact of abnormally high IRP1 activity on iron homeostasis and general body physiology, under standard laboratory conditions as well as in response to experimental challenges.

### 3.1 Generation of a mouse model with gain of IRP1 function

#### 3.1.1 Targeted expression of a conditional gain of IRP1 function allele from the mouse *Rosa26* locus

Normally, IRP1 is present mostly in its cytosolic aconitase form, but is able to switch to IRE-binding upon Fe-S cluster disassembly (Rouault, 2006). To generate a gain of IRP1 function expression construct, three cysteine residues required for Fe-S cluster assembly (C437, C503, C506) (Clarke et al., 2006) and one contributing to heme-targeted degradation (C118) (A. Vasanthakumar and R. Eisenstein, unpublished results) were substituted by serine or alanine residues, respectively. The resulting mutant IRP1, referred to as IRP1\*, is stabilized and escapes Fe-S cluster-mediated regulation (Clarke et al., 2006), being constitutively active in its IRE-binding form (Fig. 3.1). IRP1\* was also C-terminally FLAG-tagged, in order to be able to distinguish it from the endogenous IRP1.

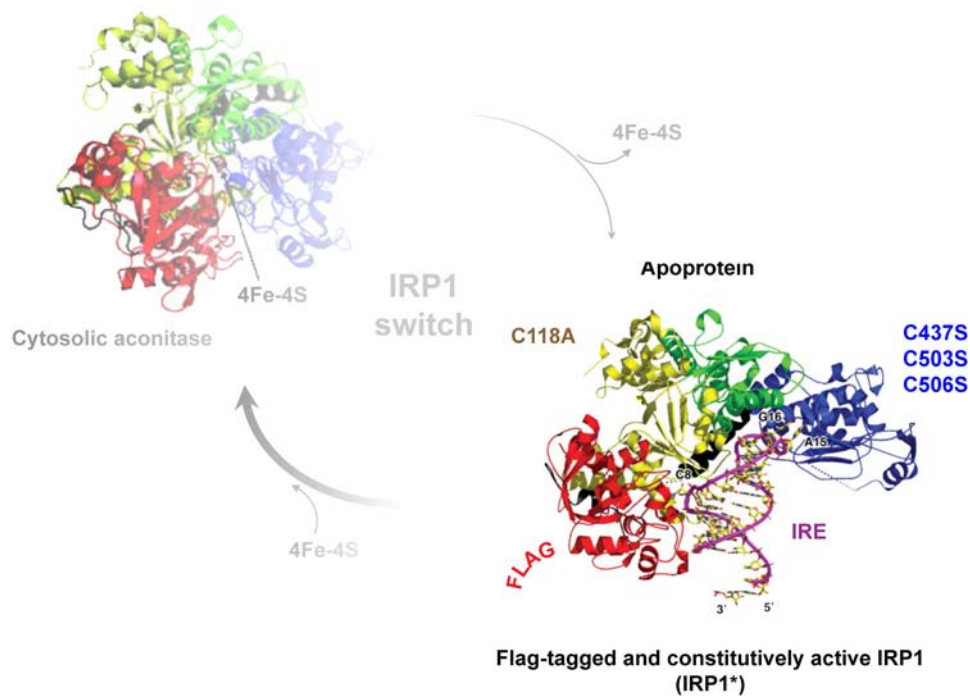


**Figure 3.1. The gain-of-function IRP1\* protein is a constitutive IRE-binder.**

Schematic representation of the aminoacidic substitutions to prevent the Fe-S switch and heme-targeted degradation of IRP1\*. The C-terminally-fused flag-tag is also displayed. Shown are the crystal structures of both cytosolic aconitase (Dupuy et al., 2006) and IRP1-IRE (Walden et al., 2006).

To avoid the potential toxicity of high level IRP1 expression, we generated a conditional mutant using Cre/Lox technology. To express the transgene at a moderate level, we targeted the permissive and ubiquitously expressed *Rosa26* locus (Zambrowicz et al., 1997) with a promoterless construct. In addition, the IRP1\* cDNA was placed downstream of a floxed  $\beta$ -geo stop cassette to prevent IRP1\* transcription from the endogenous promoter. The targeted allele is normally silent (hence mice carrying it are phenotypically identical to wildtype) until activated by Cre-mediated removal of the stop cassette, which enables IRP1\* expression in a conditional manner (Fig. 3.2).

Proper targeting of the *Rosa26* locus and subsequent successful Cre-mediated activation of the knock-in allele were first tested on targeted ES clones transfected with a plasmid encoding the Cre transgene (experiments performed by post-doc Lydie Viatte prior to my arrival and not shown in this thesis).

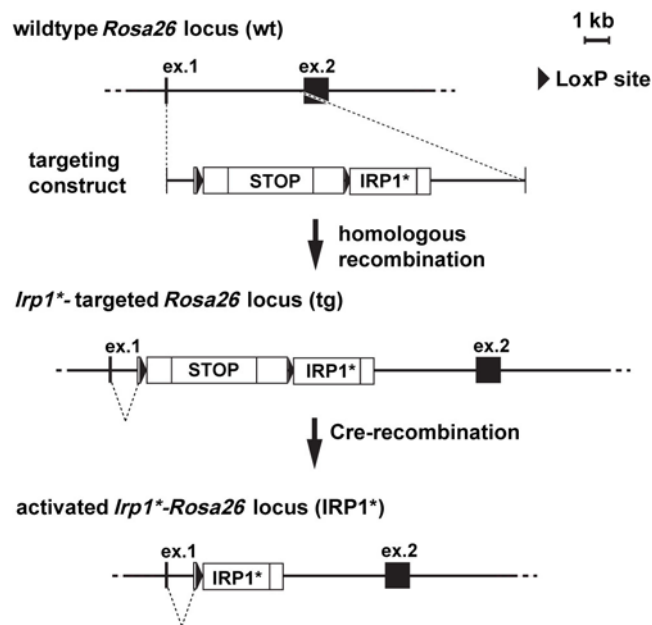


**Figure 3.2. Targeting of the *Rosa26* locus with a Cre/Lox inducible IRP1\* expression construct.**

Schematic representation of the wildtype, IRP1\*-targeted and -activated *Rosa26* locus and of the targeting construct. The targeting construct contains arms homologous to the *Rosa26* locus to allow targeted insertion by homologous recombination. The cDNA encoding IRP1\* is engineered downstream to a floxed  $\beta$ -geo stop cassette to allow conditional expression of IRP1\* by Cre-mediated recombination.

Correct insertion of the targeting cassette was also confirmed by Southern-blot on chimeras derived from embryos injected with targeted ES clones (Fig. 3.3); routine genotyping was performed by PCR analysis (Fig. 3.4).

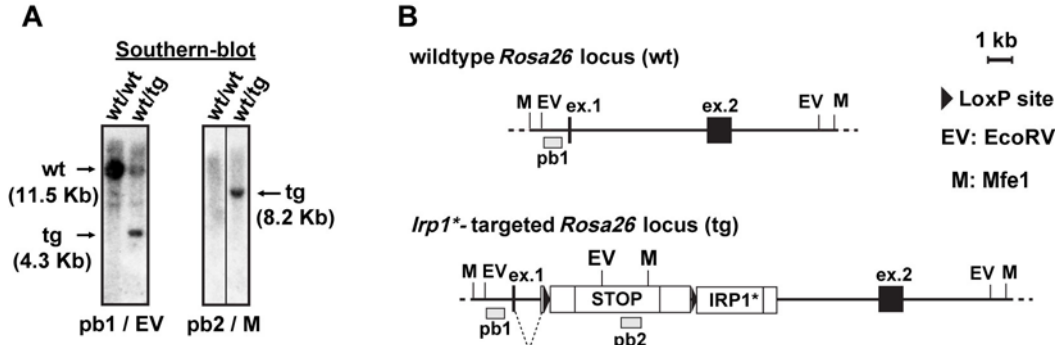


**Figure 3.3. Southern-blot showing bona fide targeting of the *Rosa26* locus.**

(A) Restriction enzymes used for digestion of genomic DNA and <sup>32</sup>P-labeled DNA probes are specified below the panels; genotypes are indicated above each lane. (B) Scheme showing the localization of the restriction sites for EcoRV (EV) and Mfe1 (M) on the wildtype and targeted *Rosa26* locus. The external probe, pb1, (recognizing the 1<sup>st</sup> exon of the *Rosa26* locus) and the internal one, pb2, (recognizing the stop cassette) are also shown.

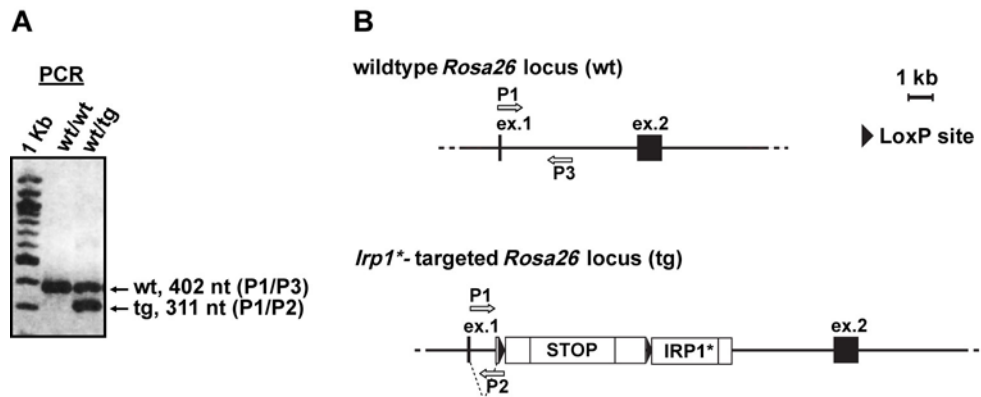


**Figure 3.4. Detection of the targeted *Rosa26* locus by multiplex-PCR.**

(A) Representative PCR analysis of genomic DNA. Genotypes are indicated above each lane. (B) Scheme indicating the localization of the primer pairs used on the wildtype and targeted *Rosa26* locus.

To achieve systemic expression of IRP1\*, we crossed mice bearing the IRP1\*-targeted *Rosa26* allele with a Cre deleter strain expressing the Cre transgene under the control of the ubiquitously active murine *Hprt* promoter (Tang et al., 2002). The latter allows removal of the stop cassette early at the zygote stage and consequent IRP1\* expression in the whole body. Figure 3.5 depicts the RT-PCR analysis to confirm Cre-mediated excision of the stop cassette.

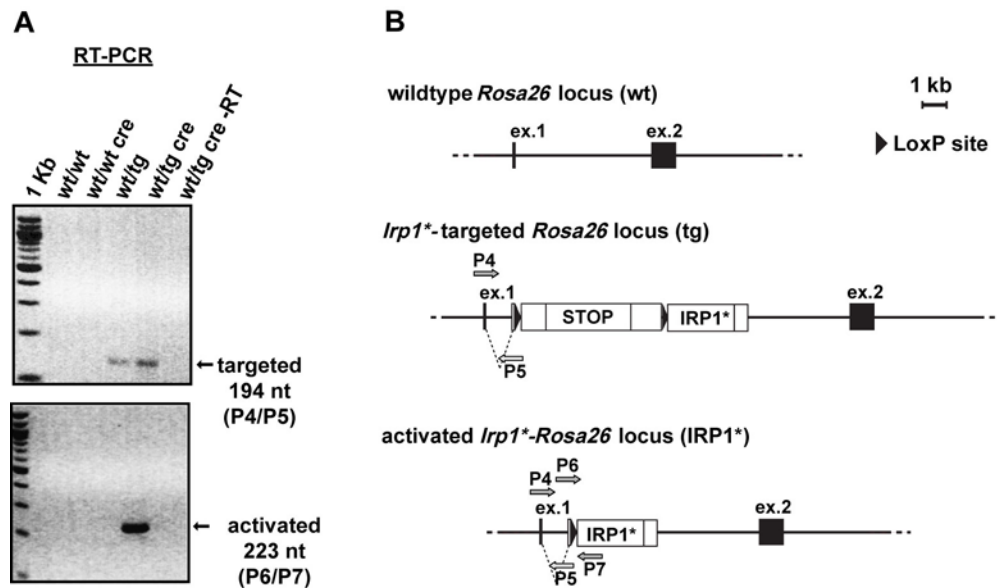


**Figure 3.5. RT-PCR analysis confirms Cre-mediated recombination of the targeted *Rosa26* locus.**

(A) Representative RT-PCR performed on cDNA derived from duodenal samples. Genotypes are indicated above each lane. Primer pair P4/P5 is specific for the targeted locus, but does not discriminate the recombination event (top panel). P6/P7 is specifically designed to detect the activated allele (bottom panel). (B) Scheme showing the primer pairs used to distinguish the targeted and recombined *Rosa26* locus.

Mice homozygous for the systemically activated IRP1\**-Rosa26* locus have been obtained in Mendelian ratio (Table 3.11); they are viable, fertile and reach adulthood without overt abnormalities.

	males			females		
	wt/wt	wt/IRP1*	IRP1*/IRP1*	wt/wt	wt/IRP1*	IRP1*/IRP1*
number	34	67	28	28	56	39
% over tot	13.5	26.6	11.1	11.1	22.2	15.5

**Table 3.1 IRP1\* mice are obtained in Mendelian ratios.**

Ratios (%) of each genotype are calculated over a total number of 252 animals. % do not significantly differ from what is expected according to mendelian distribution, i.e. 12.5 % of each homozygous and 25% of heterozygous, for each gender.

Immunoblot with an anti-FLAG antibody shows IRP1\* expression in different organs, including spleen, duodenum, kidney and liver. Consistently, IRP1\* expression is higher in homozygotes compared to heterozygous mice (Fig. 3.6). The use of an anti-IRP1 antibody, reactive with IRP1\* as well as endogenous IRP1, indicates that IRP1\* protein is not highly overexpressed compared to the endogenous protein (Fig. 3.6).

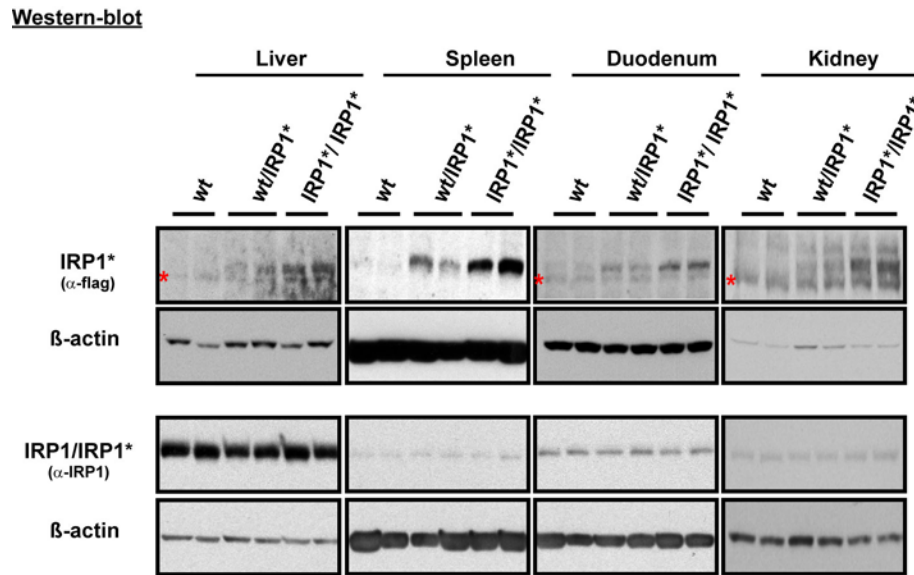


**Figure 3.6. IRP1\* protein expression is detected by Western-blot in tissues from IRP1\* mice.**

Representative Western-blot showing IRP1\* or IRP1+IRP1\* (IRP1/IRP1\*) expression in spleen, duodenum, kidney and liver extracts. An anti-FLAG-tag antibody is used to detect IRP1\*, an antibody raised against IRP1 recognizes both IRP1 and IRP1\*. In liver, duodenum and kidney samples, a cross-reacting band is marked with an asterisk. β-actin is used as protein loading control.

Overall, systemic expression of IRP1\* from the *Rosa26* locus is well tolerated in the mouse, which allows for the first time to study the consequences of in vivo gain of IRP1 function in a mammalian organism.

### 3.1.2 Mice expressing IRP1\* display increased IRE-binding activity

First, the functionality of IRP1\* as a specific IRE-binding protein was tested. To this end, we performed electrophoretic mobility shift assays (EMSAs) using cytoplasmic protein extracts from selected tissues. Typically, when samples from wildtype animals are incubated with a <sup>32</sup>P-labeled FTH1-IRE probe, two RNA-protein complexes, representing IRP1- and IRP2-IRE respectively, are electrophoretically separated from the free IRE probe (Fig. 3.7). When samples from IRP1\* mice were analysed, a third RNA-protein complex appeared with intermediate mobility between the two endogenous complexes. The intermediate band was specifically supershifted by an anti-FLAG antibody and also, together with IRP1-IRE, by an anti-IRP1 antibody recognizing both IRP1 and IRP1\* (Fig. 3.7). Addition of control immunoglobulins does not produce similar effects. This experiment shows that IRP1\* is able to bind IRE sequences.

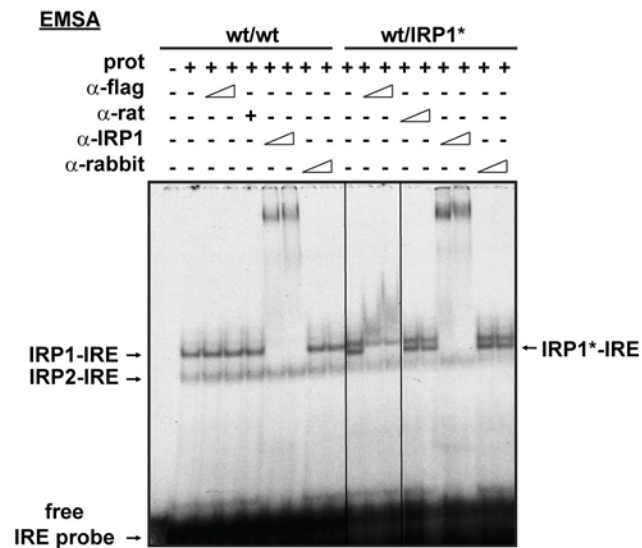


**Figure 3.7. IRP1\* shows IRE-binding activity.**

EMSA analysis to assess the IRE-binding activity of IRP1\*. Cytoplasmic extracts from ileum are incubated with a  $^{32}\text{P}$ -labeled FTH1 IRE probe. An anti-FLAG antibody is used to identify the IRP1\*-IRE complex by supershift. An antibody recognizing both IRP1 and IRP1\* is used to supershift both IRP1- and IRP1\*-IRE complexes. Normal rat and rabbit IgGs, respectively, are used as a negative controls.

Competitive EMSA experiments also demonstrated the specificity of the IRP1\*-IRE interaction (Fig. 3.8). IRP1\* binding to the radiolabeled IRE probe was progressively competed by increasing molar excess of unlabeled wildtype IRE sequence but not by a mutant version bearing a C deletion in the IRE loop which impairs the IRP-IRE interaction (Gray et al., 1996).

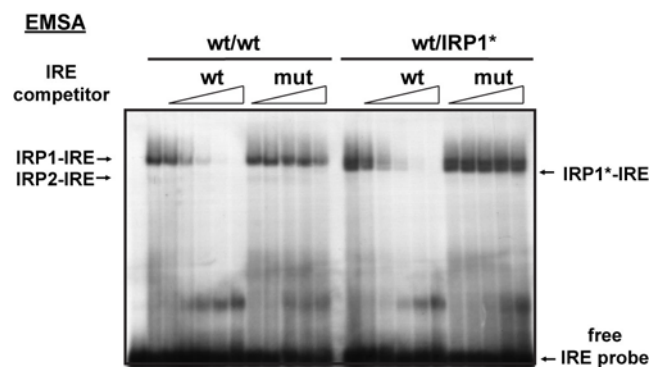


**Figure 3.8. The IRE-binding activity of IRP1\* is specific.**

Competitive EMSA using cytoplasmic extracts from ileum. Molar excess of an unlabeled wildtype or mutant FTH1 IRE competitor RNAs over the radiolabeled FTH1 IRE probe is used.

### 3. RESULTS

To quantify the degree of gain of IRP1 activity, we systematically analysed extracts from different organs, namely brain, spleen, kidney, liver, heart, lung and duodenum, by EMSA. Figure 3.9 depicts a representative result from brain, spleen and kidney samples, showing the increase in IRE-binding activity in organs expressing IRP1\*.

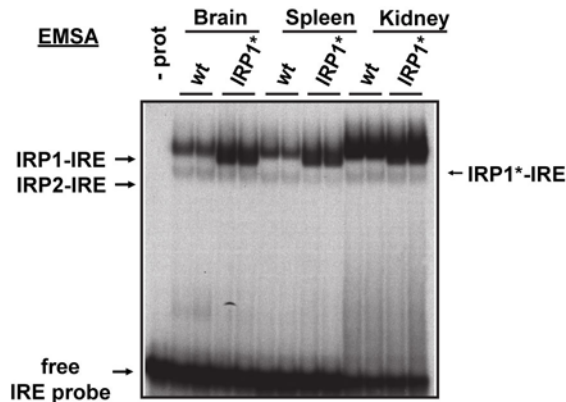


**Figure 3.9. Expression of IRP1\* yields a detectable gain of IRP activity in mouse tissues.**

Representative EMSA showing the degree of gain of IRP1 activity in cytoplasmic extracts from brain, spleen and kidney. Wildtype and IRP1\* homozygous animals are analysed; genotypes are indicated above each lane.

Quantification of the assays performed on a larger number of animals (Fig. 3.10) revealed that, while IRP2 binding activity remains largely unchanged, the sum of IRP1 and IRP1\* activity is significantly higher in IRP1\* samples compared to wildtype. This increase in IRE-binding activity displays tissue-dependent differences, ranging from a mild gain (10-30%) in kidney and liver, to a 2- to 3-fold increase in the brain, spleen, heart, lung and duodenum.

These data document that IRP1\* exerts specific IRE-binding activity and that its presence results in a significant gain of total IRP1 activity in all organs analysed.

Overall, the engineering of a constitutively active IRP1 protein, as well as its targeting and expression from the *Rosa26* locus via Cre/Lox technology, proved to be a successful strategy. Indeed, it allowed the generation of a viable mouse model with detectable gain of IRP function that can be explored to gain valuable insights into the relevance of adequate IRP regulation in vivo.

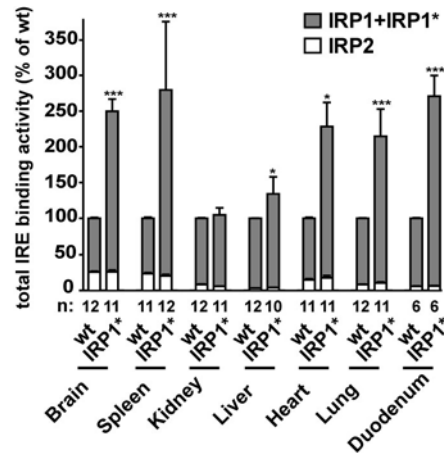


**Figure 3.10. Quantification of IRP activity in IRP1\* mouse tissues reveals tissue-specific differences in the degree of gain of IRP function.**

The histogram represents the relative quantification of a series of EMSAs performed on a larger number of animals using cytoplasmic extracts from brain, spleen, kidney, liver, heart, lung and duodenum. Sample size is indicated (n). \* is  $p < 0.05$ , \*\*\* is  $p < 0.001$ .

### 3.2 Impact of gain of IRP1 function on iron metabolism

To study the importance of adequate IRP activity in vivo, we first looked at a series of parameters directly related to iron metabolism. At the molecular level, we analysed the effect of abnormally high IRP1 activity on the pattern of expression of direct IRP target genes. At the systemic level, we explored the consequences of gain of IRP function on body iron distribution as well as on blood values and erythropoiesis.

#### **3.2.1 Increased IRE-binding activity alters the expression of IRP targets in vivo**

Increased IRE-binding activity is predicted to translationally repress 5'IRE-targets, such as FPN and FTL, and to stabilize mRNAs bearing an IRE in their 3'UTR, such as TfR1. To assess the in vivo effects of gain of IRP1 function on the post-transcriptional regulation of IRP target genes, we determined RNA and protein levels of FPN, TfR1 and FTL in key tissues of iron metabolism, including liver, spleen and duodenum (Fig. 3.11).

In the liver, FPN protein levels are mostly unchanged, while FPN mRNA levels tend to be diminished. In splenic samples, we observe a tendency towards decreased FPN protein levels without corresponding changes in mRNA levels. Duodenal FPN mRNA also appears unchanged, while the corresponding protein expression is slightly increased. TfR1 protein and mRNA levels tend to be upregulated in the spleen. In the duodenum, TfR1 protein levels are also elevated, while its mRNA is mostly unchanged. In the liver, TfR1 mRNA and protein levels are largely normal. Surprisingly, the expected decrease of FTL expression could not be observed in any of the three tissues. In the spleen, both FTL protein and mRNA are unchanged. FTL protein appears upregulated in the liver, while its mRNA is decreased. In the duodenum, we detected a marked and statistically significant increase of FTL protein without change of the corresponding mRNA. (Fig. 3.11)

Despite the apparent tissue-specific and inter-individual variability observed, the gain of IRP1 function has a detectable impact on the expression of IRP target genes, resulting in a predicted tendency towards FPN repression and TfR1 upregulation. However, an unexpected sustained FTL protein expression was observed in IRP1\* mice. This last point will be further discussed in the next chapter, section 4.2.1.

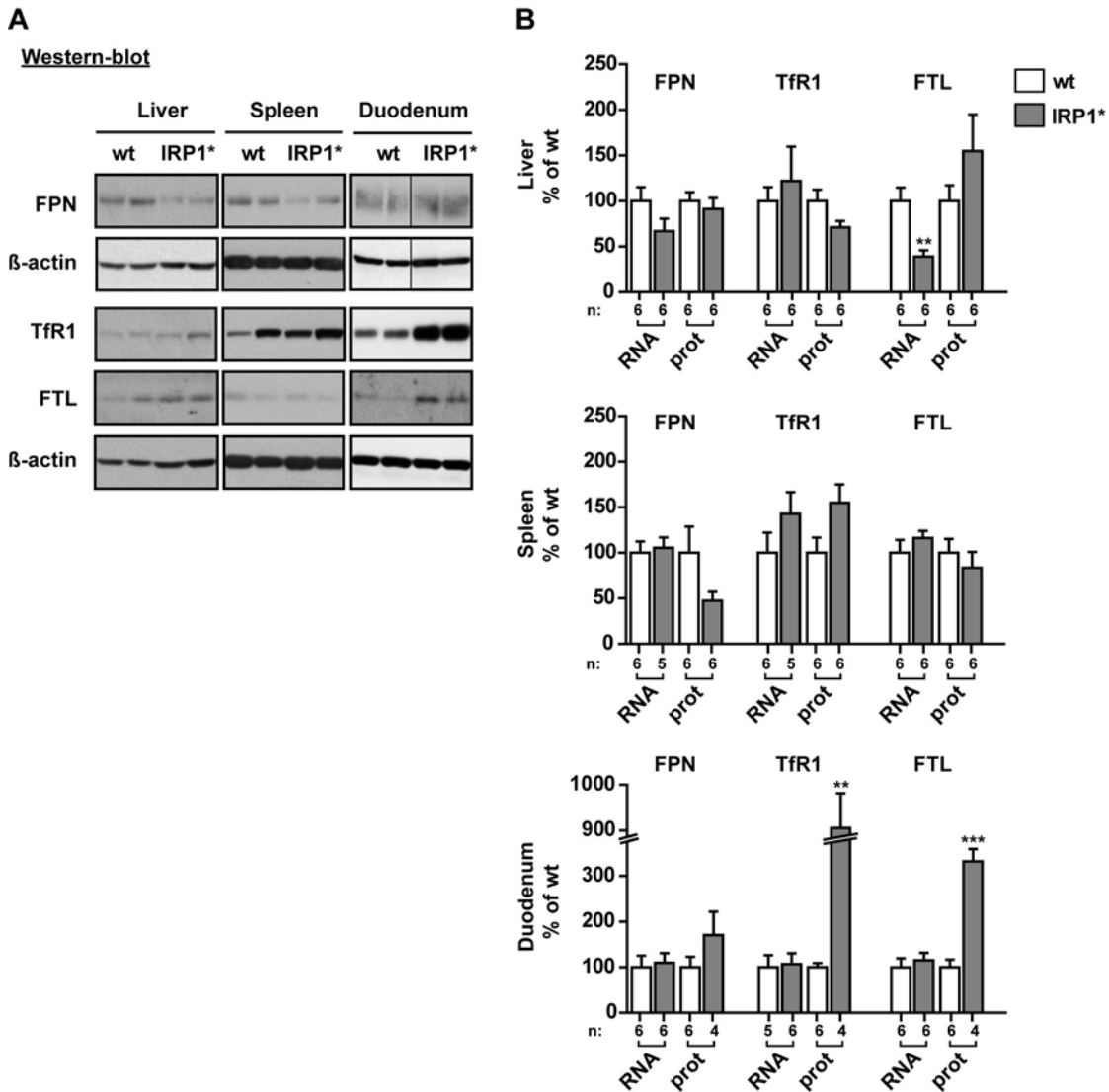


**Figure 3.11. Impact of gain of IRP1 function on the expression of IRP target genes.**

(A) Representative Western-blot of ferroportin (FPN), transferrin receptor 1 (TfR1) and ferritin L (FTL) using protein extracts from liver, spleen and duodenum.  $\beta$ -actin is used as protein loading control. Homozygous males are analysed; genotypes are indicated above each lane. (B) The histograms represent relative quantification of protein and RNA levels (obtained by qPCR) of each IRP target in the three organs. Protein levels are normalized to  $\beta$ -actin, RNA levels to  $\alpha$ -tubulin mRNA. Wildtype and IRP1\* homozygous animals are analysed; sample size is indicated (n). \*\* is  $p < 0.01$ .

#### **3.2.2 Gain of IRP1 function promotes iron loading in liver, spleen and duodenum**

IRE-binding activity is normally increased in conditions of cellular iron depletion. An artificially generated state of IRP activation, such as IRP1\* expression, would thus be expected to trigger an increase in cellular iron content. To assess whether gain of IRP1 function affects iron levels in mouse tissues, we performed spectrophotometric measurements of the total non-heme iron content of liver, spleen and duodenum. This analysis revealed increased iron levels in all three organs, between 1.7-fold in the liver, 1.5-fold in the duodenum and 1.3-fold in the spleen, respectively (Fig. 3.12A).

To determine whether gain of IRP1 function affects body iron distribution more broadly, in collaboration with Prof. Klaus Schümann (Technische Universität München, Germany), we injected  $^{59}\text{Fe}$  intravenously and monitored its deposition in several tissues two weeks after administration (Fig. 3.12B). In agreement with the spectrophotometric measurements described above, this experiment shows preferential accumulation of  $^{59}\text{Fe}$  in the liver and spleen of mice expressing IRP1\* (Fig. 3.12C). There was no detectable accumulation of  $^{59}\text{Fe}$  in the duodenum, which could reflect the consequences of sloughing of duodenal enterocytes during the two weeks following the  $^{59}\text{Fe}$  injection.

To test whether the increased non-heme iron content observed in the duodenum might result from higher dietary iron intake, rather than increased serum iron uptake, we measured the levels of the apical iron importer DMT1. Currently, four DMT1 transcript variants have been described, which are generated by the use of alternative exons, 1A or 1B, and alternative 3' splicing giving rise to IRE- or non-IRE-containing transcripts (Gunshin et al., 2001; Hubert and Hentze, 2002). Knowing that DMT1A is the predominant 5' isoform expressed in the duodenum (Hubert and Hentze, 2002), we used primer pairs specific for either of the two 3' variants and measured the mRNA levels of the IRE- and non-IRE-containing isoforms. Similar to TfR1, the 3'IRE isoform of DMT1 was predicted to be increased by gain of IRP function. We found that the levels of DMT1-no-IRE were unchanged, while DMT1-IRE was unexpectedly diminished in IRP1\* mice (Fig. 3.13). This correlated with a slight decrease of DcytB, the reductase coupled to DMT1 to allow cellular ferric intake. These results indicate that the elevated duodenal non-heme iron in IRP1\* mice is not associated with increased levels of DMT1 and thus unlikely due to increased dietary iron uptake.

Overall, these data show that gain of IRP1 function alters body iron distribution with preferential iron loading in liver, spleen and duodenum, associated with changed expression of at least some of the IRE-containing target mRNAs.

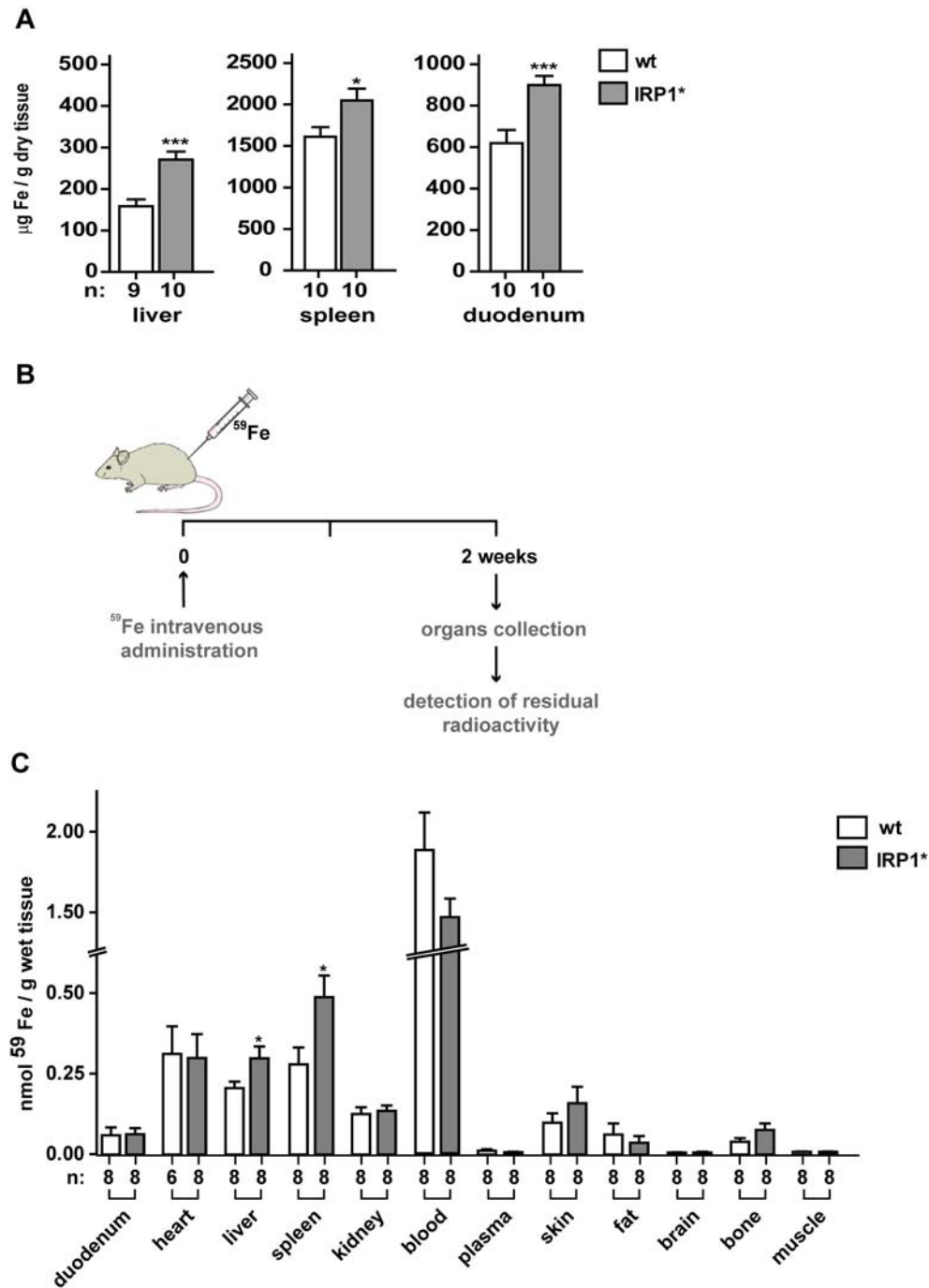


**Figure 3.12. Gain of IRP1 function causes iron loading in liver, spleen and duodenum.**

(A) Spectrophotometric determination of non-heme iron content in total extracts from liver, spleen and duodenum. (B) Schematic representation of the experimental setup to determine the kinetics of body iron distribution. (C) Histogram showing the <sup>59</sup>Fe content determined in different tissues. Homozygous males are analysed; sample size is indicated (n). \* is  $p < 0.05$ , \*\*\* is  $p < 0.001$ .

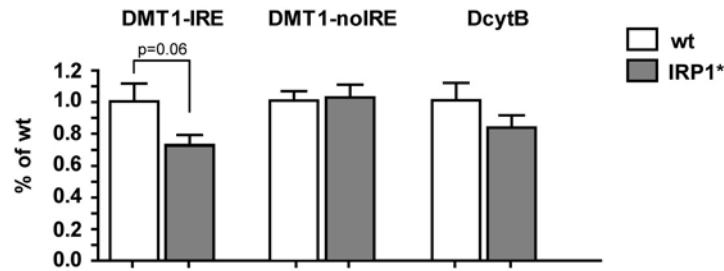


**Figure 3.13. DMT1 levels are not increased in the duodenum of IRP1\* mice.**

Relative quantification of DMT1-IRE, DMT1-noIRE and DcytB mRNAs (by qPCR) from the duodenum of IRP1\* mice. mRNA levels are calibrated to  $\alpha$ -tubulin. 6 homozygous animals per genotype are analysed.

### 3.2.3 Abnormally high IRP1 activity causes macrocytic anemia

In the body iron is mainly used for the hemoglobinization of red blood cells. To evaluate whether gain of IRP1 function affects hematological parameters, we analysed blood cell profiles as well as plasma iron values. IRP1\* mice are erythropenic (decreased red blood cell count - RBC) and have a lower hemoglobin content, lower hematocrit and increased mean cell volume (MCV) with some differences between genders (IRP1\* females display a bigger increase in MCV and mean cell hematocrit (MCH) compared to males of the same genotype) (Table 3.2).

	males		females	
	wt	IRP1*	wt	IRP1*
RBC ( $\times 10^6/\mu\text{L}$ )	11.0 $\pm$ 0.2	*** 9.7 $\pm$ 0.2	11.2 $\pm$ 0.2	*** 10.1 $\pm$ 0.1
Hemoglobin (g/dL)	15.7 $\pm$ 1.0	*** 14.1 $\pm$ 0.3	16.4 $\pm$ 0.2	15.6 $\pm$ 0.4
Hematocrit (%)	58.9 $\pm$ 0.4	** 51.8 $\pm$ 1.1	60.3 $\pm$ 1.2	** 55.3 $\pm$ 0.8
MCV (fL)	53.2 $\pm$ 0.1	53.8 $\pm$ 0.3	52.9 $\pm$ 0.2	*** 54.9 $\pm$ 0.1
MCH (pg)	14.3 $\pm$ 0.2	14.6 $\pm$ 0.1	14.6 $\pm$ 0.1	* 15.1 $\pm$ 0.2

**Table 3.2. IRP1\* mice display moderate macrocytic erythropenia.**

Table of blood cell profiles. Results are shown as mean  $\pm$  SEM. 10 homozygous animals per gender and per group are analysed. RBC, red blood cell; MCV, mean corpuscular volume; MCH, mean corpuscular hemoglobin. \* is  $p < 0.05$ , \*\* is  $p < 0.01$  and \*\*\* is  $p < 0.001$ .

Serum iron and ferritin levels are unchanged, although transferrin saturation is decreased in males as a result of increased total iron binding capacity (TIBC) (Table 3.3).

	males		females	
	wt	IRP1*	wt	IRP1*
Serum Fe (mg/dL)	122.4 ± 9.6	104.3 ± 13.4	149.5 ± 10.1	146.7 ± 1.6
TIBC (mg/dL)	373.6 ± 35.7	500.5 ± 38.8	346.6 ± 29.1	358.3 ± 30.5
Tf saturation (%)	36.0 ± 4.4	** 20.6 ± 1.9	46.8 ± 6.3	44.0 ± 4.2
Ferritin (ng/L)	136.8 ± 11.9	142.0 ± 13.4	153.9 ± 12.4	139.1 ± 6.4

**Table 3.3. Serum iron parameters in IRP1\* mice.**

Blood biochemistry values. TIBC (total iron-binding capacity) = serum Fe + UIBC (unbound iron binding capacity); Tf: transferrin; Tf saturation = serum Fe/TIBC x 100. Results are shown as mean ± SEM. \*\* is p<0.01.

To assess potential responses of the systemic regulator of iron homeostasis, we measured hepcidin mRNA levels in the liver and found it to be largely unchanged (Fig. 3.14). This result shows that systemic gain of IRP1 function and the ensuing changes in body iron distribution and hematological parameters do not trigger changes in hepcidin expression.

Altogether, increased IRP1 activity causes a mild macrocytic anemia, without altered systemic iron availability.

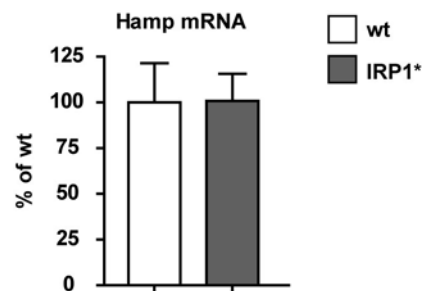


**Figure 3.14. IRP1\* expression does not alter hepcidin mRNA levels.**

Relative quantification of hepcidin (Hamp) mRNA from the liver of IRP1\* mice, obtained by qPCR. Hepcidin mRNA levels are calibrated to  $\alpha$ -tubulin. 6 homozygous animals per genotype are analysed.

### 3.2.4 IRP1 hyper-activity impairs erythroid maturation

To assess whether the macrocytic anemia affecting IRP1\* mice results from impaired erythropoiesis, we analysed the maturation state of bone marrow-derived erythroid progenitors by flow cytometry. Co-staining for Ter119 (erythroid lineage marker) and CD71 (corresponding to TfR1) allows separation of erythroblasts into immature (Ter119+, CD71 high) and more mature (Ter119+, CD71 low) erythroid cells (Fig. 3.15A). Quantification of erythroid cells isolated from a larger number of animals revealed a ~1.3 fold increase in the frequency of immature progenitors

### 3. RESULTS

accompanied by a ~30% decrease of the more mature erythroid cells in IRP1\* mice (Fig. 3.15B). As a matter of fact, this analysis holds a contextual bias as it relies on TfR1 levels to define the maturation stage of erythroid cells. TfR1 is an IRP target and has been shown to be upregulated in other tissues from IRP1\* mice and the same could apply to erythroblasts. The cumulative cell frequency distribution of Ter119+ cells according to TfR1 intensity (Fig. 3.15C, left panel) shows that the majority of IRP1\* erythroblasts (lying in the 3<sup>rd</sup> quartile, including the 50-75% of the total cells) are indeed characterized by profoundly higher TfR1 intensities compared to erythroblasts from wildtype mice. This prompted us to use an alternative marker of erythroid differentiation that would not be affected by IRP activity, such as CD44 (adhesion receptor). Distribution of Ter119+ cells according to CD44 intensity (Fig. 3.16C, right panel) shows similar CD44 levels in erythroblasts from both wildtype and mutant mice.

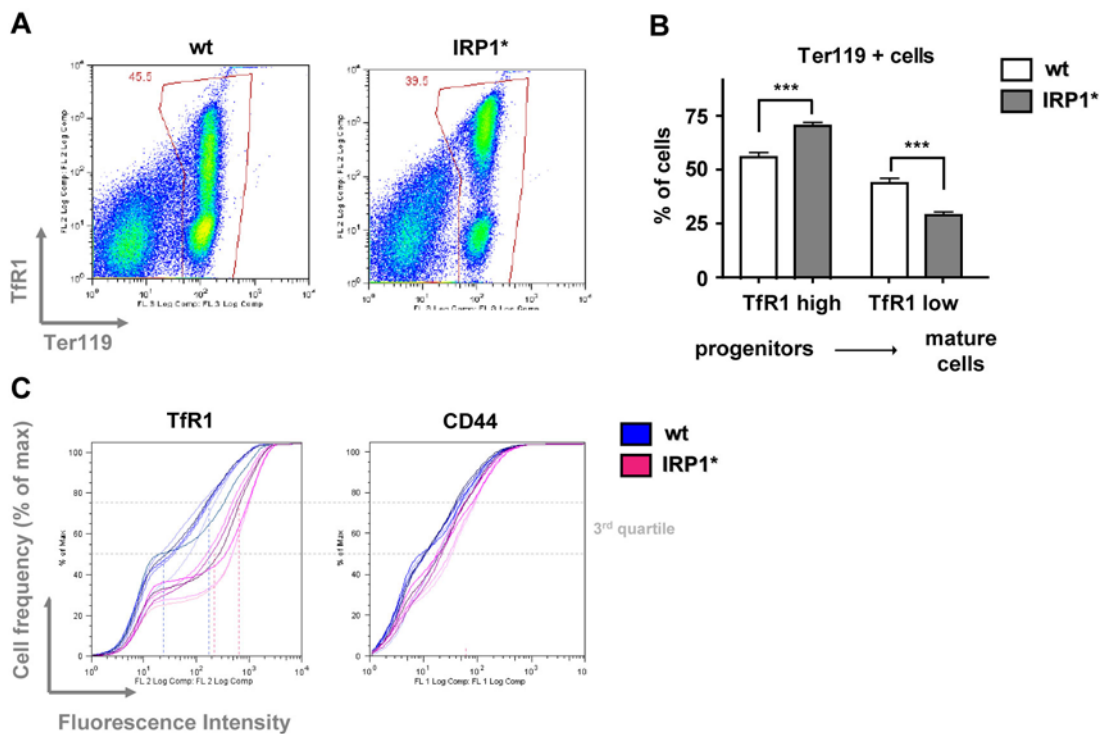


**Figure 3.15. IRP1\* expression impairs normal erythropoiesis.**

(A) Representative FACS profiles of bone marrow-derived erythroid progenitor cells co-stained with Ter119 and CD71. For each genotype, indicated on top of each panel, the panels show the classical Ter119/CD71 profiles allowing for separation of immature (Ter119+, CD71 high) and more mature (Ter119+, CD71 low) cells. (B) Relative quantification of the frequencies of the two populations (defined by TfR1 levels) of Ter119+ cells. 6 homozygous females per each genotype are analysed. (C) Cumulative

cell frequency distribution of Ter119<sup>+</sup> cells according to Tfr1 (left panel) and CD44 levels (right panel). \*\*\* is  $p < 0.001$ .

Co-staining for Ter119 and CD44 has recently shown (Chen et al., 2009) to allow a finer separation of erythroblasts into five different subpopulations according to FSC (forward scatter) and CD44 levels (Fig. 3.16A-B). We found a significant increase (1.4- to 1.6- fold) in the relative abundance of the three earliest precursors, i.e. proerythroblasts, basophilic and polychromatophilic erythroblasts (Fig. 3.16C). Also, we detected a significant decrease of the mature erythrocytes (~30%) (Fig. 3.16C), which is consistent with the decrease in RBC observed in peripheral blood.

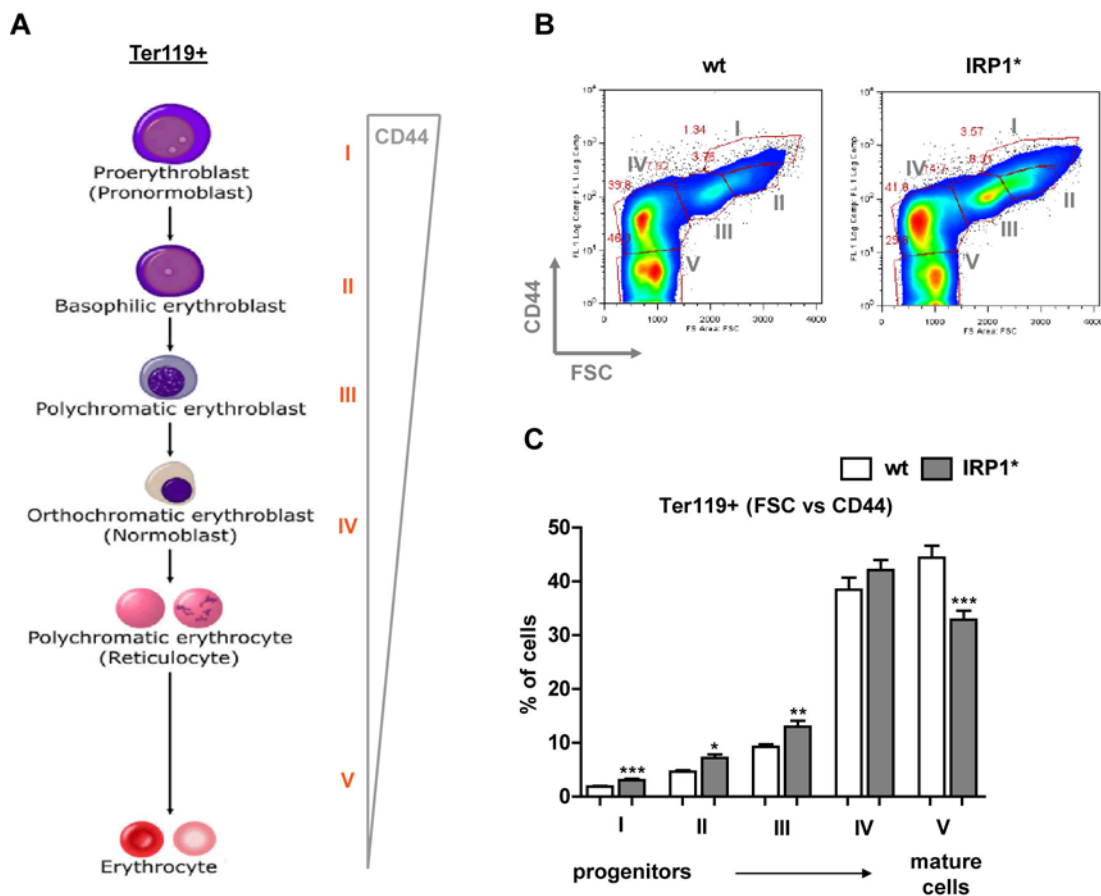


**Figure 3.16. IRP1\* expression impairs erythroblastic maturation.**

(A) Schematic representation of erythroid cells differentiation. Ter119 is expressed in all cells from the erythroid lineage, while CD44 shows a defined and discrete pattern of expression, with higher levels in immature erythroblasts and sequentially lower levels following the maturation steps. Figure modified from Porayette P., Phd thesis 2008. (B) Representative FACS profiles of bone marrow-derived erythroid progenitor cells co-stained with Ter-119 and CD44. For each genotype, indicated above each panel, the panels represent CD44 vs FSC (forward scatter) distribution of cells in the erythroid gate established in the

### 3. RESULTS

Ter119/CD71 profile. I, II, III, IV and V represent distinct and progressively more mature erythroid populations (Chen et al., 2009). (C) Relative quantification of the frequencies of each erythroid population. 6 homozygous females per each genotype are analysed. \* is  $p < 0.05$ , \*\* is  $p < 0.01$  and \*\*\* is  $p < 0.001$ .

Co-staining for TfR1 also revealed increased levels of the iron importer in all five subpopulations of bone marrow-derived erythroid precursors (Fig. 3.17A). We observed a significant increase of TfR1 intensity, corresponding to increases of ~1.7-fold in subpopulation I, ~2-fold in II, ~2.8-fold in III, ~3.2-fold in IV and ~1.3-fold in V (the latter not being apparent in the graph due to TfR1 approaching background levels in mature erythrocytes from both wildtype and IRP1\* mice) (Fig. 3.17B). These data suggest that excessive iron import via TfR1 may interfere with normal erythropoiesis.

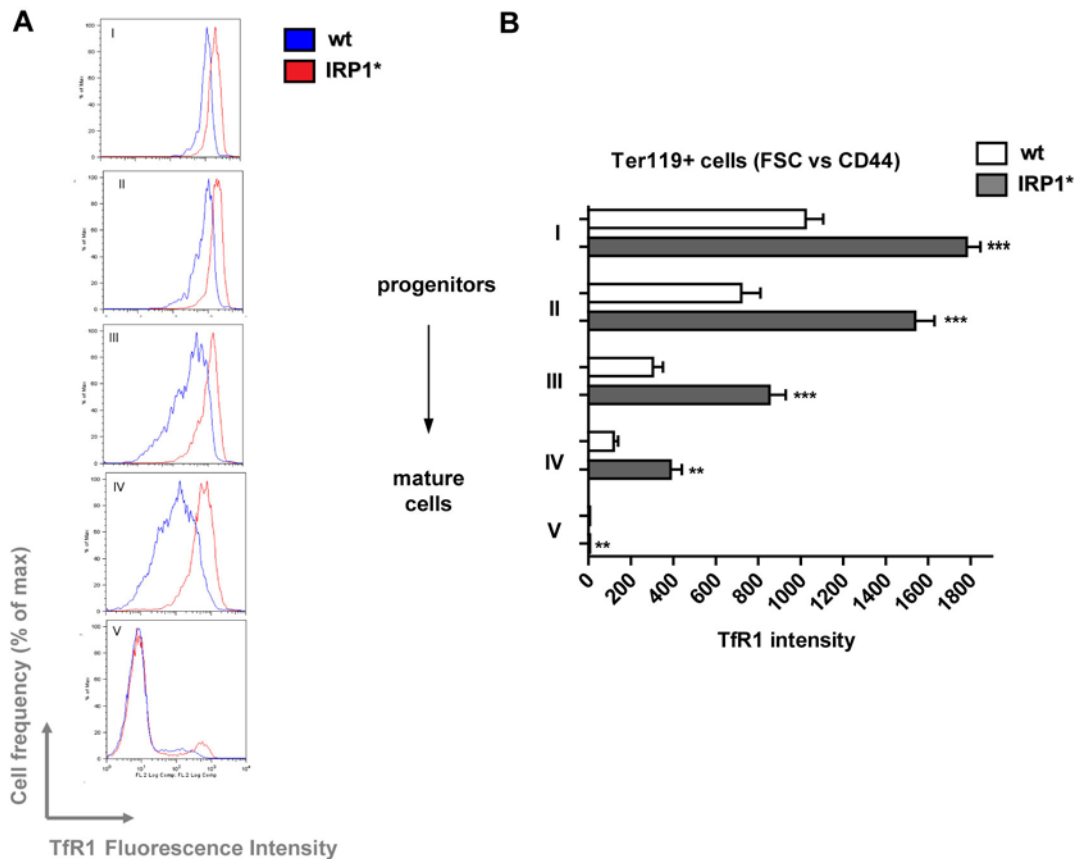


**Figure 3.17. TfR1 levels are increased in erythroblast progenitors of IRP1\* mice.**

(A) Histograms showing the peaks of cell frequency distribution as a function of TfR1 intensity in the distinct five subpopulations of erythroid progenitors. (B) Relative quantification of TfR1 intensity in each erythroid subpopulation. 6 homozygous females per each genotype are analysed. \*\* is  $p < 0.01$ , \*\*\* is  $p < 0.001$ .

These observations indicate that IRP1 activity critically influences erythroid maturation. The mechanisms underlying this phenotype are not entirely resolved yet (discussed in 4.2.2).

Overall, we showed that gain of IRP1 function has a detectable impact on IRP target genes, resulting in an altered pattern of expression in different organs. Moreover, analysis of IRP1\* mice revealed an important role of physiological IRP regulation for maintenance of appropriate body iron distribution as well as for securing normal erythropoiesis.

### **3.3 Standard phenotyping of mice with gain of IRP1 function**

Our study was focused so far on the examination of parameters directly related to iron metabolism. However, the current emergence of the IRP regulon beyond the circle of well-known iron handling molecules (see 1.4.4), together with the involvement of iron in many different biological pathways, encouraged us to broaden our focus of research. To explore additional aspects of mouse physiology that could be affected by the gain of IRP1 function, IRP1\* mice have been subjected to a broad standard phenotyping protocol. This has been done in collaboration with the mouse clinic Institut (ICS, Strasbourg, France). The standard phenotyping program included a large panel of tests ranging between hematology and clinical chemistry, metabolism, cardiology, neurobiology and behaviour. The homogenization of the procedures to the EMPReSS (European Mouse Phenotyping Resource of Standardised Screens) standards also offers the possibility to directly compare the phenotype of IRP1\* mice with other mouse models that have been subjected to the same protocols. The following section covers experiments where IRP1\* mice have shown differences compared with wildtype mice. Data not shown in this chapter are documented in the Appendix.

#### **3.3.1 Gain of IRP1 activity does not affect the general health status of IRP1\* mice**

Animals were not found to have gross abnormalities by inspection. While confirming the hematological data obtained in our laboratory describing a moderate macrocytic erythropenia (see Appendix), analysis of body weight and temperature, fat/lean ratio, blood biochemistry, energy metabolism, and glucose homeostasis did not identify any significant anomalies (see Appendix).

This indicates that the gain of IRP1 activity does not affect the general health status of IRP1\* mice under standard laboratory condition.

### 3.3.2 IRP1\* mice display altered motor coordination and reduced endurance

Gross neurobehavioral examination revealed that the physical appearance, including body posture, tremor and locomotion, together with neurological reflexes and sensory abilities (vision, audition, touch and vestibular function) were normal in IRP1\* mice (see Appendix). Interestingly, while not showing abnormalities in spontaneous locomotory activity or anxiety behavior, as assessed by the open field test (see Appendix), IRP1\* mice displayed decreased performance in the rotarod test. In this test, the time (latency) before the mouse falls off a rod rotating under continuous acceleration is considered as measure to maintain balance; performance over repeated trials is quantitated as a measure of motor learning. The histogram (Fig. 3.18) shows that mice with gain of IRP1 function fall off the accelerated rotating drum earlier than wildtype littermates. The difference is further enhanced over repeated trials as a result of the improved performance of wildtype mice. This test indicates that IRP1\* mice have altered motor coordination and slightly reduced motor learning capacity.

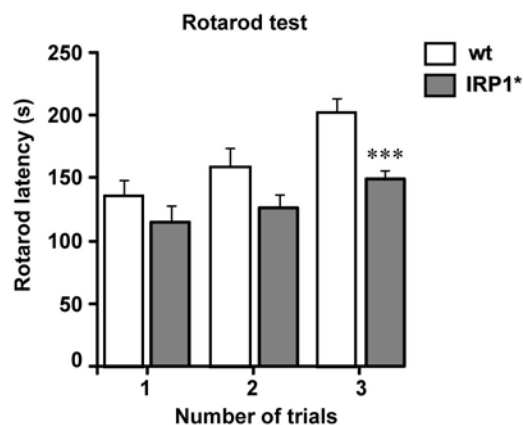


**Figure 3.18. IRP1\* mice display altered motor coordination.**

The time (latency) before mice fall off the accelerated (4-40rpm) reel is measured over 3 trials separated by 15 minutes interval. 12 homozygous males per each genotype are analysed. \*\*\* is  $p < 0.001$ .

Moreover, when forced to run on a treadmill, mice with gain of IRP1 function displayed lower latency to exhaustion and travelled for shorter distances (Fig. 3.19). This shows that IRP1\* mice also have reduced motor endurance. These motor alterations cannot be explained by a general decrease in muscle strength, as assessed by the grip strength test when calibrated over weight (Fig. 3.20).

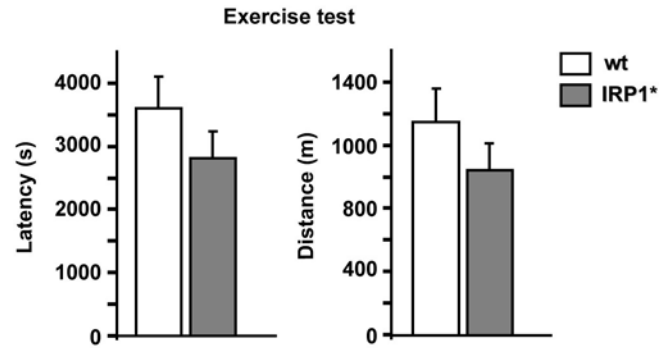


**Figure 3.19. IRP1\* expression decreases motor endurance.**

The duration (latency) of the running and the distance covered by mice forced to run on an electronically controlled treadmill are measured. 12 homozygous males per each genotype are analysed.

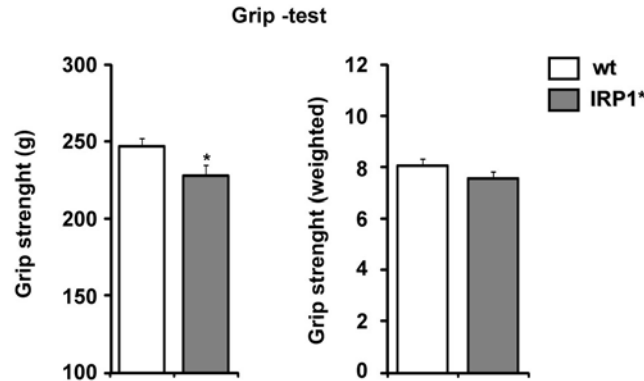


**Figure 3.20. IRP1\* mice display normal muscle strength calibrated over weight.**

Grip strength developed by mice pulled away from a grid connected to a dynamometer is measured. 12 homozygous males per each genotype are analysed. \* is  $p < 0.05$ .

Overall, these data demonstrate that basic sensory functions, spontaneous locomotory activity and behaviour appeared to be normal in IRP1\* mice. However, IRP1\* expression has a negative impact on motor coordination and endurance, which is not correlated to decreased muscle strength.

### 3.3.3 Abnormally high IRP1 activity impairs neuromuscular transmission

To investigate whether the altered motor functions of IRP1\* mice correlated to defects in nerve conduction or neuromuscular transmission, mice were subjected to electromyographic examination. Nerve conduction was assessed by measuring the speed of an electrical impulse

### 3. RESULTS

travelling along the caudal nerve, which is one of the most accessible nerves in the mouse (together with the sciatic nerve) for investigation. While nerve conduction was not affected, IRP1\* mice displayed a delayed motor response of the gastrocnemius muscle after sciatic nerve stimulation (Fig. 3.21). This suggests that the altered motor functions in mice with gain of IRP1 function may be associated with a neuromuscular defect.

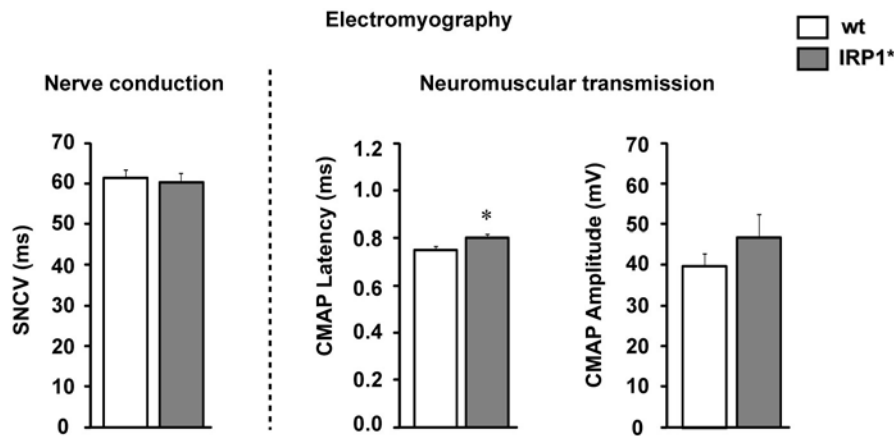


**Figure 3.21. IRP1\* expression impairs neuromuscular transmission.**

The left panel shows the sensitive nerve conduction velocity (SNVC) after the caudal nerve stimulation. The right panels display the compound muscle action potential (CMAP) of gastrocnemius muscle after sciatic nerve stimulation. The time (latency) before contraction and the intensity (amplitude) of the muscle response are measured. 12 homozygous males per each genotype are analysed. \* is  $p < 0.05$ .

To explore this aspect further, muscle biopsies were subjected to histological and ultrastructural analyses. Sections of both fast-twitch (i.e. gastrocnemius and tibialis) and slow-twitch (i.e. soleus) leg muscles, stained with hematoxylin-eosin, did not show any signs of altered fiber structure or organization (see Appendix). This ruled out the possibility that the observed defects could be linked to a gross structural problem of the muscular fibers.

These data show that IRP1\* expression has an impact on neuromuscular function, with effects on motor coordination and endurance. Since the impaired neuromuscular transmission of IRP1\* mice could potentially derive from alterations of the neuromuscular junction and/or of mitochondria (discussed in 4.3), muscle samples have been submitted for investigation by electron microscopy.

Phenotypic analysis of IRP1\* mice under standard laboratory conditions did not reveal a significant impact of inappropriate IRP1 regulation on general health. In fact, IRP1\* mice do not display any gross abnormalities when subjected to a large battery of analyses of their health status

(see Appendix). However, appropriate IRP1 expression appears to be important to secure proper body iron distribution and normal erythropoiesis. Also, adequate IRP activity seems to be a requirement for normal neuromuscular transmission, although further investigation is needed to understand the underlying mechanism (discussed in 4.2.2).

### **3.4 Impact of IRP1\* expression on the response to iron loading**

In addition to the analysis of the effect of abnormally high IRP activity on body physiology under standard laboratory conditions, we also intended to assess whether IRP1\* expression affects the response to iron loading, a condition when IRPs are normally switched off. In a wildtype cell, iron loading typically leads to IRP inhibition, which helps preventing potential cellular iron toxicity by reducing further iron entry and increasing iron export and storage (see 1.4.1). In a cell expressing IRP1\*, while endogenous IRPs will be switched off, IRP1\* will still be active, thus preventing the physiological response to iron loading, potentially leading to oxidative stress.

In a first *ex vivo* experiment, we looked for a proof of principle that gain of IRP1 activity impairs cellular iron sensitivity. Subsequently, we examined how mice with abnormally high IRP1 activity handle either acute or chronic iron overload.

#### **3.4.1 IRP1\* expression alters the response of bone marrow-derived macrophages to fluctuations of iron levels *ex vivo***

To assess whether IRP1\* expression affects the cellular response to iron loading, we performed a pilot experiment on an *ex vivo* system. We chose to analyse bone marrow-derived macrophages (BMDM), because they are relatively easy to obtain from the mouse, they express the IRP target genes and their response to iron exposure has been well characterized in our laboratory. BMDM were isolated from femurs of wildtype and IRP1\* mice and exposed to an external iron source (to deactivate endogenous IRPs) or an iron chelator (to activate endogenous IRPs). The pattern of expression of some IRP target genes was then analysed, both at the protein and mRNA level (Fig. 3.23).

Iron chelation caused an increase in TfR1 mRNA level, consistent with IRP-mediated stabilization. Besides that, treatment with the iron chelator desferrioxamine (DFO) was not detectable on the pattern of expression of the other IRP targets. In contrast, BMDM from wildtype mice showed the expected response to hemin treatment. That included an increase in

### 3. RESULTS

FPN and FTL protein levels, consistent with a reduced IRP-mediated translational repression. In addition, the mRNA of both targets was also increased, in agreement with hemin-mediated transcriptional activation, as already described (Coccia et al., 1992; Delaby et al., 2008). On the other hand, TfR1 mRNA and protein levels were decreased, consistent with loss of IRP-mediated mRNA stabilization. Compared to wildtype, BMDM from IRP1\* mice showed an altered expression pattern of IRP target genes already under control condition. FPN protein levels were increased along with elevated TfR1 protein levels, with no change of the corresponding mRNAs. This is in agreement with what is expected from a state of higher IRP activity. In addition, upon hemin treatment, IRP1\* BMDM showed an impaired response to iron loading. Both FPN and FTL were not upregulated to the same extent as in wildtype BMDM, at the protein and mRNA levels. Also, TfR1 protein was not downregulated as strongly as in wildtype, while the corresponding mRNA was similarly decreased. This altered expression pattern of FPN, FTL and TfR1 could be explained by persistence of post-transcriptional regulation by IRP1\*, which, in contrast to endogenous IRPs, is still active even in iron-replete conditions.

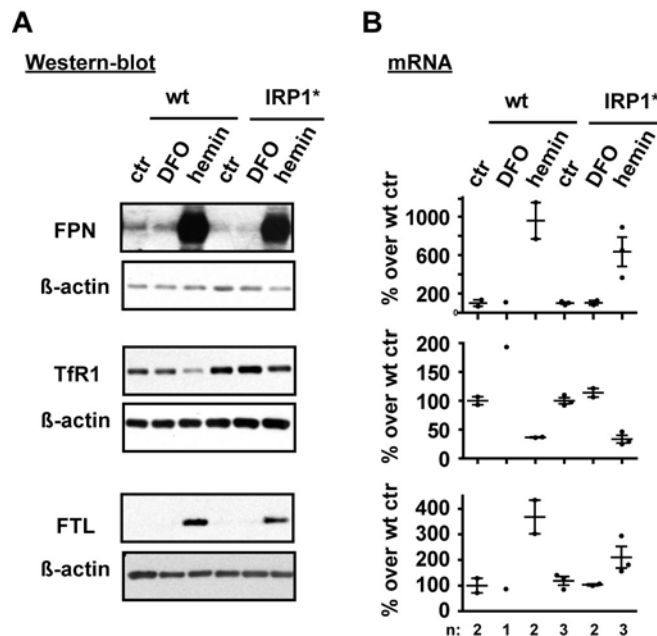


**Figure 3.23. IRP1\* expression alters the pattern of expression of IRP target genes in BMDM exposed to changes in iron levels ex vivo.**

(A) Representative Western-blots of FPN, TfR1 and FTL, using protein extracts from BMDM isolated from wildtype or IRP1\* homozygous mice. β-actin is used as protein loading control. Genotypes and corresponding conditions are indicated above each lane. Ctr: untreated BMDM; DFO and hemin: BMDM exposed ex vivo to DFO or hemin (100 μM for 10 hours). (B) Relative quantification of mRNA of each IRP target (normalized to α-tubulin) by qPCR. Genotypes and corresponding conditions are displayed

above the histograms. Sample size (n) is indicated. Biological replicates displayed similar response in an independent experiment (not shown).

To assess the actual degree of IRE binding activity under iron-replete conditions, we performed EMSA analysis (Fig. 3.24). As expected, due to IRP1\* expression, the total IRE binding activity in IRP1\* BMDM is higher than in wildtype cells, already under control conditions (and, to a greater extent upon iron chelation). This is accompanied by partial downregulation of IRP2. The latter could be due to elevated intracellular iron levels following IRP1\*-driven increase of TfR1-mediated iron intake and/or decrease of FPN-mediated iron export. As expected, IRP1\*-IRE binding activity persists upon hemin treatment, although diminished to some extent.

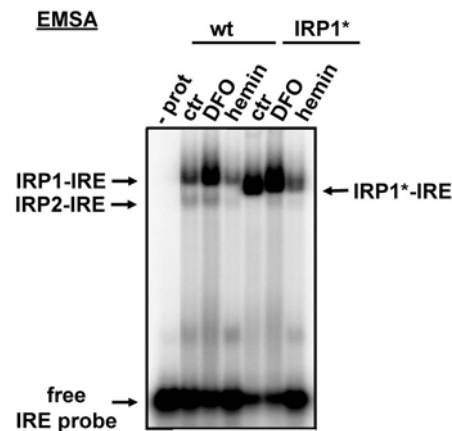


**Figure 3.24. Total IRP activity remains high in IRP1\* BMDM upon ex vivo iron loading.**

Representative EMSA experiment on cytoplasmic extracts from BMDM isolated from wildtype or IRP1\* homozygous mice. Genotypes and corresponding conditions are indicated above each lane. Ctr: untreated BMDM; DFO and hemin: BMDM exposed ex vivo to DFO or hemin (100  $\mu$ M for 10 hours).

To address whether the *Rosa26* locus is sensitive to iron levels, we measured IRP1\* mRNA levels and found them to be largely unchanged compared to controls (Fig. 3.25). This indicates that the promoter activity of the *Rosa26* locus is unlikely to be affected by iron.

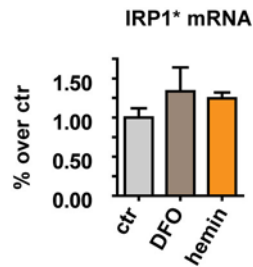


**Figure 3.25. IRP1\* mRNA levels from the *Rosa26* promoter are not affected by changes in iron levels.**

Relative quantification of IRP1\* mRNA (normalized to  $\alpha$ -tubulin), by qPCR, in BMDM isolated from 3 IRP1\* homozygous mice. Ctr: untreated BMDM; DFO and hemin: BMDM exposed ex vivo to DFO or hemin (100  $\mu$ M for 10 hours).

When measuring IRP1\* protein levels, we found a significant reduction of IRP1\* expression upon hemin treatment (Fig. 3.26). This could be explained by hemin-induced IRP1\* protein degradation and would suggest that mutation of C118 diminishes but not completely abolishes heme-mediated degradation.

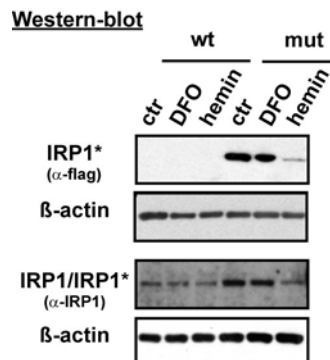


**Figure 3.26. IRP1\* protein levels are diminished upon hemin treatment ex vivo.**

Representative Western-blots of IRP1\* and IRP1, using protein extracts from BMDM isolated from wildtype or IRP1\* homozygous mice.  $\beta$ -actin is used as protein loading control. An anti-FLAG-tag antibody is used to detect IRP1\*. The anti-IRP1 antibody recognizes both IRP1 and IRP1\*. Genotypes and corresponding conditions are indicated above each lane. Ctr: untreated BMDM; DFO and hemin: BMDM exposed ex vivo to DFO or hemin (100  $\mu$ M for 10 hours).

These data on primary BMDM demonstrate that expression of IRP1\* alters the set point of IRP/IRE-mediated responses to iron loading. Having shown that in a simplified ex vivo setting, we next wanted to assess the organismal response to iron loading using two approaches, i.e. acute and chronic iron overload in vivo.

### 3.4.2 IRP1\* does not detectably aggravate liver iron accumulation and ensuing oxidative injury in acutely iron overloaded mice

The adaptive response to pharmacological administration of colloidal iron has been well studied both in animals and humans. A well established *in vivo* model of experimental acute iron overload is generated by iron-dextran injection. Once in circulation, iron-dextran is readily cleared by the reticuloendothelial system (Muir and Golberg, 1961). There, the iron-dextran complex dissociates and iron is released into the circulation bound to plasma transferrin. Excess iron is then absorbed primarily by the liver where it accumulates (Theurl et al., 2005). Being a well-known catalyst for the formation of highly toxic radicals, tissue iron overload can lead to damage and organ dysfunction (Halliwell and Gutteridge, 1992).

Based on a pilot dose-/time-response experiment on wildtype mice, we decided to administer a dose of Fe-dextran equal to 1 mg, which triggered substantial iron loading without major adverse effects (not shown). We also decided to sacrifice mice one day after injection, corresponding to the peak in hepatic iron accumulation (not shown). Wildtype and IRP1\* mice were intravenously injected with Fe-dextran, or dextran alone (vehicle), and analysed for hepatic iron accumulation and potential signs of oxidative injury. Compared to vehicle-injected wildtype mice, we found that pharmacological iron treatment determined, both in wildtype and IRP1\* mice, a ~5 fold increase of hepatic iron (Fig. 3.27A). Hepatic iron loading was accompanied by a ~1.6 fold and ~1.8 fold increase in lipid peroxides (measured as sign of oxidative injury) in wildtype and IRP1\* mice, respectively (Fig. 3.27B).

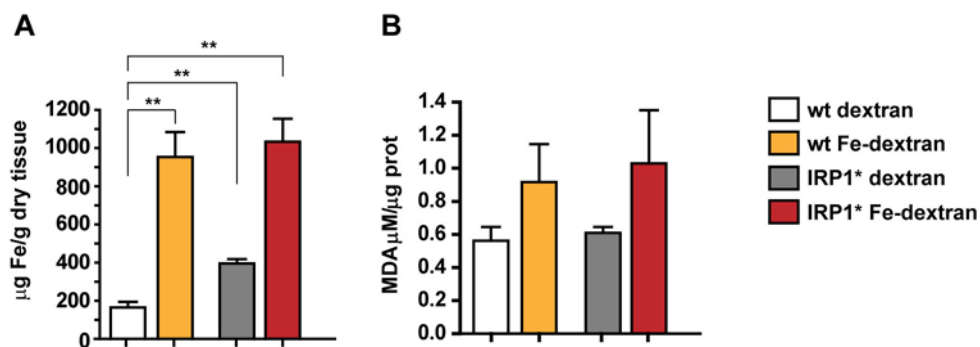


**Figure 3.27. IRP1\* expression does not aggravate liver iron accumulation and lipid peroxides levels in response to acute iron loading.**

(A) Non-heme iron content in total extracts from liver of mice intravenously injected with 1 mg of Fe-dextran or dextran alone. 6 homozygous males per group are analysed. (B) Corresponding malondialdehyde

(MDA) levels measured in total liver extracts (with the TBARS assay) as index of lipid peroxidation. \*\* is  $p < 0.01$ .

These data indicate that the response to acute iron loading, under the above mentioned experimental conditions, is not detectably altered in the liver of IRP1\* mice. However, it is possible that other organs may be more sensitive than the liver to acute iron overload.

#### **3.4.3 Consequences of IRP1\* expression in chronic iron overloaded mice**

HFE is part of sensory complex present on the surface of hepatocytes and that stimulates the expression of the hepatic hormone hepcidin to avoid/combat inappropriate increase of plasma iron levels. HFE deficiency diminishes hepcidin expression and ensuing systemic iron overload (see 1.2.2). To study the effect of IRP1\* expression on the adaptive response to chronic iron overload, we crossed IRP1\* mice with HFE KO mice, a mouse model of primary iron overload.

Mice carrying both IRP1\* and the HFE null allele in homozygosity (referred to as IRP1\*/HFE) have been generated. Animals are viable, fertile and reach adulthood with no overt abnormalities. IRP1\*/HFE KO mice were compared to control groups, namely wildtype mice and single mutants (IRP1\* and HFE KO). Since the yield of double mutant males was initially poorer compared to the other experimental groups of the same gender, this thesis focuses on the analysis of female mice.

HFE ablation normally results in high serum iron, ferritin and transferrin saturation, together with hepatic iron loading. Indeed, when compared to wildtype animals, HFE KO mice showed a ~ 1.2 and ~ 1.4 fold increase in serum iron and ferritin respectively (Table 3.4). This was accompanied by a ~1.4 fold increase in transferrin saturation (Table 3.4) as well as a ~ 4.2 fold elevated liver iron content (Fig. 3.28). Despite the systemic iron loading, hepcidin levels were unchanged and therefore inappropriately low (Fig. 3.29). Having confirmed the hallmarks of HFE ablation in our experimental setting, we next measured the same parameters in IRP1\*/HFE KO mice to confirm the chronic iron overload. Compared to IRP1\* mice, IRP1\*/HFE KO animals showed a ~1.4 fold increase in serum iron, a ~ 2.2 fold higher transferrin saturation as well as a ~ 1.6 fold increase in serum ferritin (Table 3.4). In addition, IRP1\*/HFE KO mice displayed a ~ 2.7 fold elevated hepatic iron (Fig. 3.28). This shows that IRP1\*/HFE KO mice are significantly iron overloaded compared to IRP1\*. In spite of that, hepcidin expression was found not to be detectably increased (Fig. 3.29). Next, we examined whether gain of IRP1 function potentially aggravated the iron loading driven by HFE ablation. We found that the increase in serum iron, transferrin saturation, ferritin (Table 3.4) as well as liver iron (Fig. 3.28), when

compared to wildtype animals, was similar in IRP1\*/HFE KO and HFE KO mice. Also, despite the general iron loading, hepcidin was unchanged in both IRP1\*/HFE KO and HFE KO animals (Fig. 3.29).

Overall, these data suggest that higher IRP1 activity does not have a strong impact on the chronic iron loading driven by HFE ablation. However, the consequences of gain of IRP1 function on the response to chronic iron challenge remain to be examined in detail, including measure of oxidative injury in different tissues as well as serum markers of organ dysfunction.

	wt	IRP1*	HFE KO	IRP1*/HFE KO
Serum Fe (mg/dL)	109.7 ± 17.7	98.9 ± 10.9	136.2 ± 13.2	* 135.4 ± 12.7
TIBC (mg/dL)	335.5 ± 31.4	401.6 ± 30.6	280.5 ± 18.2	** 266.9 ± 31.1
Tf saturation (%)	33.9 ± 3.3	25.5 ± 2.7	45.8 ± 6.9	** 57.0 ± 6.1
Ferritin (ng/L)	287.0 ± 34.6	242.2 ± 25.7	424.7 ± 52.5	385.6 ± 57.2

**Table 3.4. Serum iron, ferritin and transferrin saturation are elevated in primary iron loaded mice with gain of IRP1 function.**

Blood biochemistry values. TIBC (total iron-binding capacity) = serum Fe + UIBC (unbound iron binding capacity); Tf: transferrin; Tf saturation = serum Fe/TIBC x 100. Results are shown as mean ± SEM. \* is p<0.05, \*\* is p<0.01, compared to IRP1\* mice.

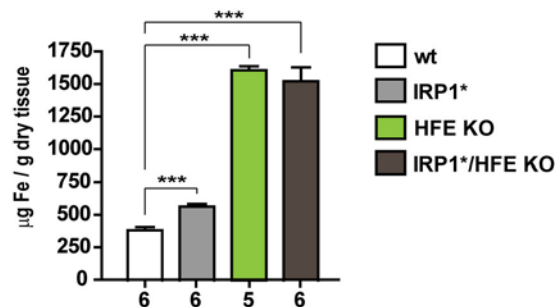


**Figure 3.28. Primary iron loaded mice with high IRP1 activity show strong hepatic iron accumulation, similarly to HFE KO animals.**

Non-heme iron content in total extracts from liver. Homozygous females are analysed. Sample size is indicated (n). \*\*\* is p<0.001.

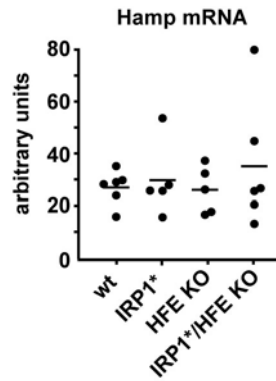


**Figure 3.29. Hepcidin levels are unchanged in primary iron loaded mice with hyper-active IRP1.**

Relative quantification of hepcidin (Hamp) mRNA from the liver, obtained by qPCR. Hepcidin mRNA levels are calibrated to  $\alpha$ -tubulin. 6 homozygous females per genotype are analysed. Genotypes are indicated below the histogram.

Taken together, IRP1\* expression alters the sensitivity to iron and the response to iron loading ex vivo. However, acute or chronic iron overload in vivo does not yield clear alterations in IRP1\* compared to wildtype mice. This will be discussed in the next chapter (section 4.4).

---



## 4. DISCUSSION

Since its initial discovery 25 years ago, enormous progress has been made towards the understanding of the IRP/IRE system as an elegant posttranscriptional regulatory machinery that maintains intracellular iron homeostasis. Extensive studies in cultured cells have formed the basis for the molecular understanding of how the IRP/IRE system acts on its molecular targets and how the IRPs themselves are in turn regulated by iron-dependent and -independent mechanisms (Anderson et al., 2012). The generation of murine models with loss of IRP function has provided insights into the importance of the IRP/IRE system for viability (Smith et al., 2006; Galy et al., 2008, 2010) and for the functionality of central organs of iron metabolism (LaVaute et al., 2001; Cooperman et al., 2005; Galy et al., 2005b, 2008, 2010; Ferring-Appel et al., 2009). Recently, transcriptome-wide studies have revealed novel IREs in mRNAs encoding proteins involved in diverse cellular pathways (Sanchez et al., 2011), thus expanding the IRP/IRE network (or regulon) beyond iron homeostasis. Furthermore, diverse human diseases have been linked to alterations of the IRP/IRE system, including mutations of the ferritin-IRE (Beaumont et al., 1995; Girelli et al., 1995; Kato et al., 2001), polymorphisms of the IRP2 promoter (Coon et al., 2006; DeMeo et al., 2009), or abnormally high IRP activity (Faucheux et al., 2002; Lobmayr et al., 2005; Camaschella et al., 2007; Crooks et al., 2012).

To complement published studies of IRP KO models and to expand our understanding on the involvement of dysregulated IRP activity in disease progression, we generated a mouse model of gain of IRP1 function.

### 4.1 First mammalian model with primary gain of IRP1 function

At physiological tissue oxygen and iron concentrations, IRP1 is present mostly in its cytosolic aconitase form, but is able to switch to IRE-binding upon Fe-S cluster disassembly (Meyron-Holtz et al., 2004a, 2004b). To generate a constitutively active form of IRP1, we replaced the three cysteines that are required for Fe-S cluster coordination by serines, blocking the iron-dependent molecular switch to its cytosolic-aconitase form and locking it into its IRE-binding conformation (Fig. 3.1). IRP1 overexpression has previously been reported to be toxic in

cells (DeRusso et al., 1995). In flies, ubiquitous and muscle-specific overexpression of IRP1A, the only IRP homolog possessing IRE-binding activity of the two cytosolic aconitases, has been shown to cause pre-adult lethality (Lind et al., 2006; Surdej et al., 2008). To minimize the risk of potential lethality associated with expression of a constitutively active IRP1 (IRP1\*), we generated a conditional allele by Cre/Lox technology. For moderate rather than excessive levels of IRP1\* expression, we targeted the ubiquitously active *Rosa26* locus (Zambrowicz et al., 1997) with a promoterless construct, which allows IRP1\* transcription at the endogenous *Rosa26* promoter rates. The engineering of a silent targeted cassette, together with the permissivity of the *Rosa26* locus (Zambrowicz et al., 1997), made possible the generation of animals bearing an inactive IRP1\* transgene. The latter can be subsequently activated, either in a constitutive- or a tissue-specific manner, by breeding with relevant Cre-deletor strains (Fig. 3.2). In this thesis, the effects of the ubiquitous gain of IRP1 function have been explored in a mouse line where the IRP1\* transgene has been activated in the whole body. Future work could focus on the consequences of activation of IRP1\* in specific tissues, which would allow a finer dissection of local anomalies caused by gain of IRP1 function. This would also enable the discrimination between systemic and cell-autonomous effects among the alterations observed in mice expressing IRP1\* systemically. Among others, the use of an erythroid-specific Cre-line would be of particular interest to further characterize the macrocytic anemia of IRP1\* mice. If the blood defect was phenocopied upon erythroid-restricted IRP1\* expression, this would prove an erythroid-autonomous nature of the macrocytic anemia in IRP1\* mice. Conceivably, the organism may also, over time, adapt to a certain degree of gain of IRP function by adopting appropriate counterbalancing mechanisms. Hence, an inducible activation of IRP1\* expression at a specific stage of mouse development might allow acute effects of gain of IRP1 function to emerge.

In general, the conditional targeting strategy applied proved to be successful in obtaining, for the first time, live animals expressing a gain of IRP1 function protein (IRP1\*). Moreover, it holds promise for further studies on the effect of abnormally high IRP1 activity in specific tissues or at specific stages of the mouse life.

Increased IRP1 activity is achieved in all tissues analysed (Fig. 3.10), with a tissue-specific increment of total IRE-binding activity that is partially derived from the strength of the *Rosa26* promoter and the basal activity of endogenous IRP1 in each tissue. The kidney and, to a lower extent, the liver are among the organs where IRP1 is normally expressed at the highest levels (Meyron-Holtz et al., 2004a). This most probably explains why the contribution of IRP1\* in those 2 organs is relatively smaller when compared to the gain of IRP1 function achieved in the other tissues with lower basal IRP1 activity, such as brain, spleen, heart, lung and duodenum.

IRP1\* mice are viable and fertile, suggesting that IRP1\* expression is well tolerated and does not dramatically interfere with overall mouse physiology. Yet, we cannot conclude that appropriate IRP1 regulation is not important for health. Conceivably, the rather moderate level of gain of IRP1 function that we used to avoid potential lethality of IRP1 overexpression may be below a hypothetical pathological threshold. Upregulating IRP1\* expression in the mouse may result in increasingly prominent pathological effects, potentially affecting multiple biological processes and organs and eventually leading to animal death.

## **4.2 Appropriate IRP1 regulation is necessary for body iron homeostasis**

### **4.2.1 IRP1\* expression affects the expression of IRP targets and alters body iron distribution**

IRP1\* alters the expression of IRP target genes (Fig. 3.11), although we noticed inter-individual and tissue-dependent variability. Tissue-specific responses to high IRP1 activity as well as the different degree of gain of IRP1 function in different organs may account for the inter-tissue variability of the expression of IRP targets.

Expression of IRP1\* causes iron accumulation in liver, spleen and duodenum (Fig. 3.12A). While the molecular mechanisms underlying iron deposition in IRP1\* mice remain to be understood in detail, forced cellular iron accumulation entirely meets the predicted phenotype. Indeed, IRE-binding activity is normally increased to combat cellular iron depletion, thus artificial IRP activation is expected to elevate intracellular iron levels. Contrary to the IRP2 KO mouse phenotype where the spleen is iron-depleted, the splenic iron content of IRP1\* mice is elevated, which correlates with a decreased expression of the iron exporter FPN. The latter is likely explained by stronger translational repression of the FPN mRNA, which is in agreement with high IRP activity and unchanged hepcidin expression. When IRP2 is ablated, liver and duodenum are iron-loaded and this is associated with higher ferritin levels (Galy et al., 2005b, 2008). In mice with gain of IRP1 function, hepatic and duodenal iron accumulation is also associated with FTL upregulation. Sustained FTL expression in a context of high IRP1 activity is somewhat counterintuitive considering the IRP/IRE regulatory paradigm, which would instead predict repression of 5'IRE targets, such as FTL. While future work will have to dissect the molecular mechanisms underlying this unexpected response, lack of FTL repression concomitant with elevated IRP1 activity has already been reported in other experimental settings (Cairo et al., 1997, 1998; Wang and Pantopoulos, 2002; Chen et al., 2007). IRPs translationally repress 5'IRE

targets by inhibiting the cap-dependent recruitment of the small ribosomal subunit (Muckenthaler et al., 1998). Sustained FTL expression in the liver and duodenum from IRP1\* mice could possibly be explained by an alternative mechanism of cap-independent translation via the internal ribosomal entry site (IRES) recently found in the 5'UTR of FTL mRNA (Daba et al., 2012). Otherwise, ferritin turnover has previously been shown to be directly affected by iron levels, as ferritin protein levels linearly increase with iron influx, as a consequence of its reduced degradation (Truty et al., 2001). Conversely, ferritin is destabilized and degraded upon cellular iron depletion (De Domenico et al., 2006; Kidane et al., 2006). Hence, increased FTL protein levels in IRP1\* mice could also be a consequence of reduced FTL degradation due to iron excess, both in the liver and duodenum.

The exact molecular mechanisms underlying iron accumulation in the duodenum of IRP1\* mice remain to be elucidated. Yet, several hypotheses can be entertained. For instance, duodenal iron loading could result from elevated TfR1-mediated serum transferrin-bound iron transport across the baso-lateral surface of enterocytes. This would be in agreement with increased levels of TfR1 found in the duodenum of IRP1\* mice. However, intravenously administered <sup>59</sup>Fe did not preferentially accumulate in the duodenum (Fig. 3.12C), which might show that duodenal iron loading is not associated with increased baso-lateral serum iron uptake. Perhaps more likely, the lack of radioactive iron accumulation in the duodenum might be a consequence of sloughing of duodenal mucosa during the two weeks following the <sup>59</sup>Fe injection. In IRP2 KO mice, duodenal iron accumulation also seemed to be independent from TfR1 mediated serum iron uptake. Iron deposits were indeed restricted to the duodenal villi rather than the crypts (Galy et al., 2005b), where TfR1 is preferentially expressed (Roy and Enns, 2000). Alternatively, duodenal iron accumulation in IRP1\* mice might also originate from elevated dietary iron absorption. This could in principle be explained by increased DMT1-mediated apical iron transport, which was an expected consequence of IRP1\*-mediated stabilization of the DMT1 3'IRE-containing isoform. However, duodenal DMT1 was found not to be upregulated in IRP1\* mice (Fig. 3.13). This might be explained by a superimposition of HIF2 $\alpha$  mediated regulation. HIF2 $\alpha$  is at the same time a transcriptional activator of DMT1 (Mastrogiannaki et al., 2009) and a target of IRP translational regulation (Sanchez et al., 2007b) (see 1.5.2). Conceivably, IRP1\*-mediated repression of HIF2 $\alpha$  via its 5'IRE may account for a decrease of HIF2 $\alpha$ -mediated activation of DMT1, which might in turn predominate over the DMT1 mRNA stabilization by IRP1\*. Ribosome profiling on sucrose density gradient analysis would be a good way to assess if HIF2 $\alpha$  mRNA is repressed in duodenal extracts from IRP1\* mice. The latter would predict that HIF2 $\alpha$  mRNA is predominantly

localized in the subpolysome fraction of translational inactive mRNAs as opposed to the heavier ribosome-associated mRNAs.

#### **4.2.2 High IRP1 activity impairs normal erythropoiesis**

Mice with gain of IRP1 function display macrocytic anemia (Table 3.2) associated with impaired erythroid maturation (Fig. 3.16). Thus, an abnormally high IRP1 activity compromises normal erythropoiesis, which can in turn explain the macrocytosis by a release of abnormally differentiated erythrocytes into the circulation. The detailed mechanism underlying the hematological phenotype observed in IRP1\* mice remains to be elucidated but it could be due to systemic and/or cell-autonomous defects, as following described.

Example of a systemic defect that could potentially be involved in the etiology of macrocytosis is dietary malabsorption of either folate or vitamin B12. These are two important cofactors required for the maturation of red blood cells and their deficiency is commonly associated with macrocytic anemia (Koury and Ponka, 2004). To examine whether IRP1\* mice appropriately acquire these two vitamins from the diet, folate and vitamin B12 serum levels could be measured. Alternatively, macrocytic anemia can also be associated with kidney failure (Suega et al., 2005), which results in the decreased production of erythropoietin (EPO) and the ensuing reduced stimulation of erythropoiesis. EPO expression in the kidney is under the positive transcriptional control of HIF2 $\alpha$  (Scortegagna et al., 2003a, 2003b), being part of a loop that activates erythropoiesis in response to low tissue-oxygenation. HIF2 $\alpha$  is in turn a target of IRP-mediated translational regulation and its repression via 5'IRE is conceivable in a setting of high IRP1 activity (see 1.5.1). If IRP1\* expression results in HIF2 $\alpha$  downregulation, this may in turn impair HIF2 $\alpha$ -mediated induction of EPO expression in the kidney, resulting in reduced erythropoietic stimulus. EPO levels in the serum would need to be tested to further explore this hypothesis.

However, an alternative hypothesis is that the macrocytic anemia of IRP1\* mice is a cell-autonomous defect. Indeed, the anemia seems to be independent of changes in systemic iron availability, as, under standard laboratory conditions, IRP1\* mice show unchanged serum iron and ferritin level (Table 3.3) as well as normal hepcidin expression (Fig. 3.14). Generation of mice with erythroid-specific IRP1\* expression would be a good way to test this hypothesis, as IRP1\* expression limited to red blood cells might phenocopy the macrocytosis of IRP1\* pan-expressing mice. Otherwise, bone marrow transplantation could be used to demonstrate the cell-autonomous nature of the blood defect. In that case, wildtype mice transplanted with IRP1\* bone

marrow would be expected to recapitulate the macrocytic anemia. Alternatively, the anemia of IRP1\* mice should be reverted following wildtype bone marrow transplantation.

Assuming that the macrocytic anemia of IRP1\* mice is a cell-autonomous defect, different hypotheses could explain the underlying molecular mechanism. In IRP2 KO mice, the microcytic anemia is associated with lower TfR1 levels (Galy et al., 2005b) and iron depletion in bone marrow iron (Cooperman et al., 2005). Conversely, we have shown that TfR1 expression on the cell membrane of erythroid progenitors from IRP1\* mice is increased (Fig. 3.17). This finding points towards the possibility that the erythropoietic defect in the IRP1\* mouse model is a consequence of increased iron uptake by erythroid precursors and ensuing iron toxicity. The opposite pattern of TfR1 expression could also account for the microcytosis of IRP2 KO mice and the macrocytic red blood cells in IRP1\* mice. While alternative or additional explanations are possible, iron toxicity represents one of the potential causes of the defective erythropoiesis in IRP1\* mice. FPN has recently been hypothesized to export iron also from erythroid cells (Zhang et al., 2011) and our data suggest that FPN tends to be diminished in IRP1\* expressing tissues. If reduced FPN expression also applies to erythroid precursors, diminished iron export could contribute to intracellular iron toxicity. Erythroid 5-aminolevulinate synthase (eALAS), the enzyme catalyzing the rate-limiting step in heme biosynthesis, could also be implicated in the anemia of IRP1\* mice (see 1.5.1). eALAS mRNA is translationally regulated by the IRP/IRE system and has previously been shown to be upregulated in erythroid precursors from IRP2 KO mice (Cooperman et al., 2005). If eALAS was translationally repressed via its 5'IRE in erythroblasts from IRP1\* mice, an ensuing block of heme synthesis could contribute to toxic iron accumulation. This would also be consistent with the zebrafish shiraz model, where IRP1 over-activation (secondary to GLRX5 deficiency) is demonstrated to cause anemia due to eALAS repression (Wingert et al., 2005). Furthermore, the 5'IRE target mitochondrial aconitase (mACO), an enzyme involved in the TCA cycle, could possibly also be downregulated by a gain of IRP1 activity. Interestingly, when mACO is pharmacologically inhibited by fluoroacetate, mice develop a hematological phenotype reminiscent of that of IRP1\* mice (Talbot et al., 2011). Although the heme exporter FLCVR does not appear to be an IRP target, the hematological phenotype of IRP1\* mice somewhat recalls the FLCVR KO model. There, heme toxicity has been hypothesized to cause the early erythropoietic blockade and ensuing macrocytosis (Keel et al., 2008). In principle, all these factors, involving different IRP targets, could act either in isolation or in combination to cause the macrocytic anemia of IRP1\* mice. Prussian blue staining of bone marrow-derived cells could reveal the presence of iron accumulation, while isolated

erythroblasts could also be assessed for the level of the expression of each of the aforementioned IRP targets as well as for the presence of oxidative stress.

### **4.3 The IRP1\* model reveals a potential involvement of the IRP/IRE system in neuromuscular function**

Mice with gain of IRP1 function show altered motor coordination (Fig. 3.18) and endurance (Fig. 3.19), together with a defect in neuromuscular transmission (Fig. 3.21). Together, this potentially reveals a novel and intriguing role of the IRP/IRE system in neuromuscular function. While an understanding of the underlying mechanisms determining this phenotype require further in depth investigation, the neuromuscular defect of IRP1\* mice could reflect a problem with structure/organization of the muscular fibers, mitochondria/energy metabolism or alterations at the neuromuscular junction.

Regarding the possibility of a morphological defect, histological analysis of muscle fibers of IRP1\* mice did not reveal any sign of structural alterations (see Appendix). This indicates that the neuromuscular defect of IRP1\* mice cannot, at least, be attributed to gross dysmorphology of the muscles.

IRPs strongly respond to iron fluctuation in skeletal muscle following dietary iron manipulation (Liew and Shaw, 2005), thus showing that the IRP/IRE system plays a role in this tissue. Additionally, IRP activation correlates with human myopathies due to defects in iron-sulfur cluster assembly/disassembly and ensuing problems with energy metabolism or oxidative stress (Crooks et al., 2012) (see 1.5.4). In flies, muscle-specific overexpression of the homolog IRP1A is lethal (Lind et al., 2006). When human IRP1 was heterologously overexpressed in flies, it was coupled to 5'IRE-mediated translational repression of succinate dehydrogenase B (SDHb), which is part of the mitochondrial respiratory chain (Surdej et al., 2008). Given the importance of SDHb for mitochondrial energy metabolism, the authors speculated that IRP1A-mediated repression of SDHb in muscles was the main cause of flies' lethality (Surdej et al., 2008). In humans, deficiency of SDH, together with decreased mACO, has been linked to lifelong exercise intolerance marked by premature muscle fatigue (Haller et al., 1991), which was later recognized as a myopathy due to iron-sulfur cluster assembly protein (ISCU) deficiency (Mochel et al., 2008; Olsson et al., 2008). This disorder shows that there is a correlation between severely impaired muscle oxidative phosphorylation and an abnormal response to physical exercise. However, nothing resembling an IRE sequence has been identified in the 5'UTR of mouse or human SDH

mRNAs, thus preventing any direct connection between IRP1\* and SDH to explain the neuromuscular phenotype of IRP1\* mice. Nevertheless, a direct connection with mACO could instead be drawn. In iron-deficient muscles, increased IRPs activity correlates with decreased levels of mACO function (Liew and Shaw, 2005), thus fitting with the paradigm of IRP-mediated translational repression of mACO via its 5'IRE (Gray et al., 1996). Furthermore, aberrant IRP activation has been recently shown in muscles from patients affected by myopathy with ISCU deficiency (Crooks et al., 2012). This pathology of exercise intolerance is also characterized by deficiency of mACO, as well as of several other Fe-S cluster containing proteins in the respiratory chain (Haller et al., 1991; Hall et al., 1993). IRP1\*-mediated translational repression of mACO is conceivable in skeletal muscles from IRP1\* mice and might directly interfere with muscular energy metabolism.

The defect in neuromuscular transmission in IRP1\* mice may also be explained by potential alterations at the neuromuscular junction, which is reminiscent of a mouse model with complete loss of superoxide dismutase (SOD1) (Missirlis et al., 2003; Clarke et al., 2006). SOD1 catalyzes the conversion of  $O_2^-$  to  $H_2O_2$  and  $O_2$ , thus preventing oxygen toxicity. Mutations of SOD1 in mice cause marked denervation of the muscles, with distinct alterations of synaptic vesicles and mitochondria within the neuromuscular junctions (Cappello et al., 2012). SOD1 mutant mice are largely used as models to study the inherited amyotrophic lateral sclerosis (ALS). In humans, ALS is a fatal adult-onset neurodegenerative disease characterized by loss of motor neurons and progressive muscle atrophy and paralysis (Dupuis and Loeffler, 2009). Of note, SOD1 deficiency in mice promotes cytosolic oxidative stress, damaging Fe-S clusters, including the one of cytosolic aconitase. Hence, the consequent increase in IRP1 activity might potentially play a role in some of the neuromuscular defects observed in SOD1 mutant mice.

Both ALS and ISCU deficiency, among other disorders of Fe-S cluster biogenesis, have shown a connection between dysfunction of the mitochondrial Fe-S cluster assembly machinery and abnormal IRP activation (see 1.5.4). In addition, mouse models with IRP deficiency have revealed a crucial role of the IRP/IRE system in securing mitochondrial function (see 1.5.3). In that context, it would be interesting to further investigate the IRP1\* mouse model for the expression and activity of heme- and Fe-S cluster- enzymes involved in the TCA cycle and the mitochondrial respiratory chain. This could help to better define the apparent relationship between the mitochondrion and the IRP/IRE system and whether an adequate level of IRP activity is also important to secure mitochondrial function. Further exploration of the IRP1\* mouse model, including electron microscopic analysis of muscles, has been initiated to assess

whether any alterations of the neuromuscular junctions and/or of mitochondria morphology could be revealed.

#### **4.4 Impact of IRP1\* expression on acute or chronic iron loading**

During iron overload, downregulation of IRPs is a physiological response that cells activate to combat iron toxicity. We have shown that expression of IRP1\* impairs the adaptive response to iron loading *ex vivo*. In iron overloaded cells from IRP1\* mice, sustained IRP activity correlated with an altered expression pattern of IRP target genes (Fig. 3.23). The impact of IRP1\* on the adaptation to iron loading *ex vivo*, prompted us to examine the response of IRP1\* mice to *in vivo* challenges, such as acute and chronic iron loading.

Pharmacological iron overload triggered a similar hepatic iron accumulation in wildtype and IRP1\* mice (Fig. 3.27A). Lack of a cumulative effect of IRP1\* on the degree of hepatic iron loading was expected due to the intrinsic characteristics of the experimental setting. The iron injected intravenously is indeed quickly absorbed by the liver, where it rapidly reaches a virtual plateau. However, due to increased IRP1 activity, we investigated the possibility that IRP1\* mice would show an impaired capability to manage iron loading, potentially resulting in a higher oxidative insult. Our data show that while elevated levels of oxidative stress could be detected in the liver of iron-challenged wildtype and IRP1\* mice, there was no detectable differential increase in the oxidative injury due to IRP1\* expression (Fig. 3.27B).

There are multiple factors that could explain the apparent lack of differential response to iron loading of IRP1\* mice. First, the dose of iron injected could be a critical parameter if we assume that a possible effect of IRP1\* could only be detectable over a certain range. For instance, the amount of iron injected could have been excessive and lead to saturation of the system, hence masking any possible contribution of IRP1\*. Conversely, the dose used could have been too low to trigger a differential response in IRP1\* mice. A possible way to discern between these two options would be analysing the response of IRP1\* mice to a range of different doses of iron. Furthermore, the increase in complexity that is added when moving from the *ex vivo* to the *in vivo* setting is not neglectable. *In vivo*, the significant gain in systemic networks and buffer mechanisms, which are lost in the *ex vivo* culture, may be responsible for counterbalancing any potential effect triggered by IRP1\*. For instance, the increase in FTL observed in the liver of IRP1\* mice kept under standard laboratory conditions was not reproduced on *ex vivo* cultures of BMDM isolated from IRP1\* mice. *In vivo*, a potential mechanism of cap-independent translation

of FTL, via its recently discovered IRES (Daba et al., 2012), could compensate for an increased tendency of FTL translational repression driven by IRP1\*. This would eventually result in a net increase of safe iron storage into ferritin shells, thus protecting the hepatocytes from iron-mediated oxidative stress. The levels of FTL could be measured to verify a possible differential increase of FTL in the liver of iron-loaded IRP1\*. Besides, the liver, as an iron-storage organ, is specialized to handle a sudden burst of iron, which might mask any possible IRP1\* contribution. Moreover, together with the kidney, the liver of IRP1\* mice is the organ that displays the mildest gain of IRP function under steady state condition. In addition, IRP1\* contains a mutation of a cysteine shown to be important for iron-mediated degradation of IRP1 (R.S. Eisenstein, unpublished findings). However, ex vivo iron loaded BMDM from IRP1\* mice revealed that IRP1\* expression was partially impaired upon hemin-treatment (Fig. 3.24), indicating that the mutant IRP1\* protein may not be fully resistant to iron-mediated degradation. Therefore, we cannot exclude a potential further decrease in the degree of hepatic gain of IRP function following IRP1\* partial degradation upon acute iron loading. Potentially, analysis of other organs that are more sensitive to iron overload, as well as displaying a higher gain of IRP1 function, could still reveal a role for proper IRP1 regulation in response to iron loading in vivo.

As in the acute iron challenge, the exploration of the response of IRP1\* mice to chronic iron loading will benefit from further investigation. Secondary iron overload was generated in IRP1\* mice by concurrent HFE ablation. HFE is part of a sensory complex responsible for activation of hepcidin negative response to systemic iron loading (Vujić Spasić et al., 2008). IRP1\* mice have shown, under standard conditions, elevated TfR1 expression in the liver (as result of increased IRP-mediated TfR1 mRNA stabilization). Despite the basal tendency of hepatic TfR1 levels to be elevated, the liver of chronically-iron overloaded IRP1\* (or IRP1\*/HFE KO) mice does not accumulate more iron than single HFE KO mice (Fig. 3.28). The lack of aggravated hepatic iron loading in IRP1\*/HFE KO mice might relate to the nature of iron that is normally accumulated in the hepatocytes from HFE KO mice. In fact, iron overload in HFE KO mice leads to an over-saturation of serum transferrin, with a consequent accumulation of non-transferrin-bound-iron (NTBI). NTBI is then taken up by the liver via, yet to be determined, TfR1-independent mechanisms (Chua et al., 2004). Despite an apparently non-aggravated iron overload as compared to the single HFE KO mouse, further analyses need to be carried out to address whether IRP1\*/HFE KO mice are more sensitive to the pathological consequences of chronic iron loading. This will include assessment of oxidative stress markers in different organs, such as liver and heart, which are the organs that most typically suffer failure due to chronic iron loading

(Camaschella, 2005). Related to that, serum markers of organ dysfunction could also be measured.

Importantly, the HFE KO is a mouse model of hereditary hemochromatosis (HH), which is a frequent human disorder of systemic iron overload in the Caucasian population (see 1.2.2). The most common HFE-related HH occurs in approximately 1 in 400 individuals and has an estimated carrier frequency of 1 in 10 individuals of Northern European descent (Feder et al., 1996). The HFE mutant allele has typically low penetrance, which implies that other genetic and/or environmental factors can influence the development of the disease (Deugnier and Mosser, 2008). Given the prevalence of the disease, an increasing field of research is directed to finding possible “modifier genes” that, if co-occurring in combination with the HH mutations, could trigger the manifestation of the disease. In this context, we analyzed whether gain of IRP1 function could be able to modify the HFE phenotype. The results showed that compound mutant IRP1\*/HFE KO mice have a similar increase in serum iron and ferritin levels (Table 3.4), transferrin saturation, as well as hepatic iron loading (Fig. 3.28) (which are the distinctive characteristics of the single HFE KO model).

Overall, our current data show that IRP1\*/HFE KO mice largely phenocopy the hallmarks of HFE-driven systemic iron overload, thus suggesting that gain of IRP1 function does not influence the typical alterations caused by HFE ablation per se.

#### **4.5 Concluding remarks**

The IRP/IRE system has fascinated researchers in the iron metabolism field since its discovery over 20 years ago for its sophisticated mode of securing proper cellular iron balance by post-translational regulation of iron metabolism genes. During the last decade, the IRP/IRE system has increasingly emerged as complex homeostatic machinery whose action extends to pathways beyond iron metabolism and the cellular boundaries. The generation of genetically modified mice carrying single or double deletions of the IRP genes has been pivotal for the understanding of the critical influence of the IRP/IRE system in the function of key organs of iron metabolism (LaVaute et al., 2001; Galy et al., 2004, 2005a, 2008, 2010; Meyron-Holtz et al., 2004a; Smith et al., 2006; Ferring-Appel et al., 2009). However, fundamental questions about the relevance of adequate IRP1 regulation and activity have remained unanswered mainly because of the lack of a suitable model system. The work described in this thesis presents the IRP1\* mouse,

which embodies the first model of primary and inducible gain of IRP1 function in a mammalian organism. Complementing the findings obtained from the mouse lines with loss of IRP function, the IRP1\* model provides the perfect ground for better understanding the significance of adequate IRP regulation in vivo. The results have shown that appropriate IRP1 activity is important for the maintenance of physiological body iron distribution and for normal erythropoiesis. Intriguingly, deeper phenotypic exploration of IRP1\* mice uncovered a novel role of the IRP/IRE system in neuromuscular function. This is particularly captivating as IRP1 overactivation, concurrent with mitochondrial dysfunction, is a common denominator of a number of human neurodegenerative disorders. Deeper exploration of the IRP1\* model may thus have profound implications on our understanding of the molecular etiology of human diseases such as sideroblastic anemia linked to GLRX5 deficiency (Camaschella et al., 2007) or Friedreich's ataxia (Lobmayr et al., 2005).

---



## 5. BIBLIOGRAPHY

Abboud, S., and Haile, D.J. (2000). A Novel Mammalian Iron-regulated Protein Involved in Intracellular Iron Metabolism. *Journal of Biological Chemistry* 275, 19906–19912.

Address, K.J., Basilion, J.P., Klausner, R.D., Rouault, T.A., and Pardi, A. (1997). Structure and dynamics of the iron responsive element RNA: implications for binding of the RNA by iron regulatory binding proteins. *Journal of Molecular Biology* 274, 72–83.

Agar, J.N., Krebs, C., Frazzon, J., Huynh, B.H., Dean, D.R., and Johnson, M.K. (2000). IscU as a Scaffold for Iron–Sulfur Cluster Biosynthesis: Sequential Assembly of [2Fe-2S] and [4Fe-4S] Clusters in IscU. *Biochemistry* 39, 7856–7862.

Anderson, C.P., Shen, M., Eisenstein, R.S., and Leibold, E.A. (2012). Mammalian iron metabolism and its control by iron regulatory proteins. *Biochimica Et Biophysica Acta (BBA) - Molecular Cell Research* 1823, 1468–1483.

Andrews, N.C. (2008). Forging a field: the golden age of iron biology. *Blood* 112, 219–230.

Arosio, P., and Levi, S. (2010). Cytosolic and mitochondrial ferritins in the regulation of cellular iron homeostasis and oxidative damage. *Biochimica Et Biophysica Acta (BBA) - General Subjects* 1800, 783–792.

Arosio, P., Yokota, M., and Drysdale, J.W. (1976). Structural and immunological relationships of iso-ferritins in normal and malignant cells. *Cancer Research* 36, 1735–1739.

Bartnikas, T.B. (2012). Known and potential roles of transferrin in iron biology. *Biometals: An International Journal on the Role of Metal Ions in Biology, Biochemistry and Medicine* 25, 677–686.

Basilion, J.P., Rouault, T.A., Massinople, C.M., Klausner, R.D., and Burgess, W.H. (1994). The iron-responsive element-binding protein: localization of the RNA-binding site to the aconitase active-site cleft. *Proceedings of the National Academy of Sciences* 91, 574–578.

- Batista-Nascimento, L., Pimentel, C., Andrade Menezes, R., and Rodrigues-Pousada, C. (2012). Iron and Neurodegeneration: From Cellular Homeostasis to Disease. *Oxidative Medicine and Cellular Longevity* 2012:128647.
- Beaumont, C., Leneuve, P., Devaux, I., Scoazec, J.-Y., Berthier, M., Loiseau, M.-N., Grandchamp, B., and Bonneau, D. (1995). Mutation in the iron responsive element of the L ferritin mRNA in a family with dominant hyperferritinaemia and cataract. *Nature Genetics* 11, 444–446.
- Bekri, S., Kispal, G., Lange, H., Fitzsimons, E., Tolmie, J., Lill, R., Bishop, F., and Bishop, D.F. (2009). Human ABC7 transporter: gene structure and mutation causing X-linked sideroblastic anemia with ataxia with disruption of cytosolic iron-sulfur protein maturation. *Blood* 96, 3256–3264.
- Bettany, A.J., Eisenstein, R.S., and Munro, H.N. (1992). Mutagenesis of the iron-regulatory element further defines a role for RNA secondary structure in the regulation of ferritin and transferrin receptor expression. *Journal of Biological Chemistry* 267, 16531–16537.
- Breuer, W., Shvartsman, M., and Cabantchik, Z.I. (2008). Intracellular labile iron. *The International Journal of Biochemistry & Cell Biology* 40, 350–354.
- Brissot, P., Ropert, M., Le Lan, C., and Loréal, O. (2012). Non-transferrin bound iron: a key role in iron overload and iron toxicity. *Biochimica Et Biophysica Acta* 1820, 403–410.
- Bulteau, A.-L., O'Neill, H.A., Kennedy, M.C., Ikeda-Saito, M., Isaya, G., and Szweda, L.I. (2004). Frataxin Acts as an Iron Chaperone Protein to Modulate Mitochondrial Aconitase Activity. *Science* 305, 242–245.
- Butt, J., Kim, H.Y., Basilion, J.P., Cohen, S., Iwai, K., Philpott, C.C., Altschul, S., Klausner, R.D., and Rouault, T.A. (1996). Differences in the RNA binding sites of iron regulatory proteins and potential target diversity. *Proceedings of the National Academy of Sciences* 93, 4345–4349.
- Cairo, G., Recalcati, S., Montosi, G., Castrusini, E., Conte, D., and Pietrangelo, A. (1997). Inappropriately High Iron Regulatory Protein Activity in Monocytes of Patients With Genetic Hemochromatosis. *Blood* 89, 2546–2553.

Cairo, G., Tacchini, L., and Pietrangelo, A. (1998). Lack of coordinate control of ferritin and transferrin receptor expression during rat liver regeneration. *Hepatology (Baltimore, Md.)* 28, 173–178.

Camaschella, C. (2005). Understanding iron homeostasis through genetic analysis of hemochromatosis and related disorders. *Blood* 106, 3710–3717.

Camaschella, C., Campanella, A., De Falco, L., Boschetto, L., Merlini, R., Silvestri, L., Levi, S., and Iolascon, A. (2007). The human counterpart of zebrafish shiraz shows sideroblastic-like microcytic anemia and iron overload. *Blood* 110, 1353–1358.

Camaschella, C., Roetto, A., Cali, A., Gobbi, M. De, Garozzo, G., Carella, M., Majorano, N., Totaro, A., and Gasparini, P. (2000). The gene TFR2 is mutated in a new type of haemochromatosis mapping to 7q22. *Nature Genetics* 25, 14–15.

Campillos, M., Cases, I., Hentze, M.W., and Sanchez, M. (2010). SIREs: searching for iron-responsive elements. *Nucleic Acids Research* 38, W360–7.

Campuzano, V., Montermini, L., Moltò, M.D., Pianese, L., Cossée, M., Cavalcanti, F., Monros, E., Rodius, F., Duclos, F., Monticelli, A., et al. (1996). Friedreich's Ataxia: Autosomal Recessive Disease Caused by an Intronic GAA Triplet Repeat Expansion. *Science* 271, 1423–1427.

Cappello, V., Vezzoli, E., Righi, M., Fossati, M., Mariotti, R., Crespi, A., Patruno, M., Bentivoglio, M., Pietrini, G., and Francolini, M. (2012). Analysis of neuromuscular junctions and effects of anabolic steroid administration in the SOD1G93A mouse model of ALS. *Molecular and Cellular Neuroscience* 51, 12–21.

Cazzola, M., Bergamaschi, G., Tonon, L., Arbustini, E., Grasso, M., Vercesi, E., Barosi, G., Bianchi, P.E., Cairo, G., and Arosio, P. (1997). Hereditary Hyperferritinemia-Cataract Syndrome: Relationship Between Phenotypes and Specific Mutations in the Iron-Responsive Element of Ferritin Light-Chain mRNA. *Blood* 90, 814–821.

Chen, C., and Paw, B.H. (2012). Cellular and mitochondrial iron homeostasis in vertebrates. *Biochimica Et Biophysica Acta (BBA) - Molecular Cell Research* 1823, 1459–1467.

## 5. BIBLIOGRAPHY

---

Chen, G., Fillebeen, C., Wang, J., and Pantopoulos, K. (2007). Overexpression of iron regulatory protein 1 suppresses growth of tumor xenografts. *Carcinogenesis* 28, 785–791.

Chen, H., Su, T., Attieh, Z.K., Fox, T.C., McKie, A.T., Anderson, G.J., and Vulpe, C.D. (2003). Systemic regulation of HephAestin and Ireg1 revealed in studies of genetic and nutritional iron deficiency. *Blood* 102, 1893–1899.

Chen, K., Liu, J., Heck, S., Chasis, J.A., An, X., and Mohandas, N. (2009). Resolving the distinct stages in erythroid differentiation based on dynamic changes in membrane protein expression during erythropoiesis. *Proceedings of the National Academy of Sciences of the United States of America* 106, 17413–17418.

Chen, O.S., Schalinske, K.L., and Eisenstein, R.S. (1997). Dietary Iron Intake Modulates the Activity of Iron Regulatory Proteins and the Abundance of Ferritin and Mitochondrial Aconitase in Rat Liver. *The Journal of Nutrition* 127, 238–248.

Cheng, Y., Zak, O., Aisen, P., Harrison, S.C., and Walz, T. (2004). Structure of the Human Transferrin Receptor-Transferrin Complex. *Cell* 116, 565–576.

Chollangi, S., Thompson, J.W., Ruiz, J.C., Gardner, K.H., and Bruick, R.K. (2012). Hemerythrin-like Domain within F-box and Leucine-rich Repeat Protein 5 (FBXL5) Communicates Cellular Iron and Oxygen Availability by Distinct Mechanisms. *The Journal of Biological Chemistry* 287, 23710–23717.

Chua, A.C.G., Olynyk, J.K., Leedman, P.J., and Trinder, D. (2004). Nontransferrin-Bound Iron Uptake by Hepatocytes Is Increased in the Hfe Knockout Mouse Model of Hereditary Hemochromatosis. *Blood* 104, 1519–1525.

Church, G.M., and Gilbert, W. (1984). Genomic sequencing. *Proceedings of the National Academy of Sciences of the United States of America* 81, 1991–1995.

Clarke, S.L., Vasanthakumar, A., Anderson, S.A., Pondarré, C., Koh, C.M., Deck, K.M., Pitula, J.S., Epstein, C.J., Fleming, M.D., and Eisenstein, R.S. (2006). Iron-responsive degradation of iron-regulatory protein 1 does not require the Fe-S cluster. *The EMBO Journal* 25, 544–553.

Cmejla, R., Petrak, J., and Cmejlova, J. (2006). A novel iron responsive element in the 3'UTR of human MRCK $\alpha$ . *Biochemical and Biophysical Research Communications* 341, 158–166.

Coccia, E., Profita, V., and Fiorucci, G. (1992). Modulation of ferritin H-chain expression in Friend erythroleukemia cells: transcriptional and translational regulation by hemin. *Molecular and Cellular Biology* 12, 3015–3022.

Cohen, L. a, Gutierrez, L., Weiss, A., Leichtmann-Bardoogo, Y., Zhang, D., Crooks, D.R., Sougrat, R., Morgenstern, A., Galy, B., Hentze, M.W., et al. (2010). Serum ferritin is derived primarily from macrophages through a nonclassical secretory pathway. *Blood* 116, 1574–1584.

Coon, K.D., Siegel, A.M., Yee, S.J., Dunckley, T.L., Mueller, C., Nagra, R.M., Tourtellotte, W.W., Reiman, E.M., Papassotiropoulos, A., Petersen, F.F., et al. (2006). Preliminary demonstration of an allelic association of the IREB2 gene with Alzheimer's disease. *Journal of Alzheimer's Disease: JAD* 9, 225–233.

Cooperman, S.S., Meyron-Holtz, E.G., Olivierre-Wilson, H., Ghosh, M.C., McConnell, J.P., and Rouault, T.A. (2005). Microcytic anemia, erythropoietic protoporphyria, and neurodegeneration in mice with targeted deletion of iron-regulatory protein 2. *Blood* 106, 1084–1091.

Cotter, P.D., Baumann, M., and Bishop, D.F. (1992). Enzymatic defect in “X-linked” sideroblastic anemia: molecular evidence for erythroid delta-aminolevulinate synthase deficiency. *Proceedings of the National Academy of Sciences* 89, 4028–4032.

Cox, T.C., Bawden, M.J., Martin, A., and May, B.K. (1991). Human erythroid 5-aminolevulinate synthase: promoter analysis and identification of an iron-responsive element in the mRNA. *The EMBO Journal* 10, 1891–1902.

Cremonesi, L., Foglieni, B., Fermo, I., Cozzi, A., Paroni, R., Ruggeri, G., Belloli, S., Levi, S., Fargion, S., Ferrari, M., et al. (2003a). Identification of two novel mutations in the 5'-untranslated region of H-ferritin using denaturing high performance liquid chromatography scanning. *Haematologica* 88, 1110–1116.

Cremonesi, L., Paroni, R., Foglieni, B., Galbiati, S., Fermo, I., Soriani, N., Belloli, S., Ruggeri, G., Biasiotto, G., Cazzola, M., et al. (2003b). Scanning mutations of the 5'UTR regulatory

sequence of L-ferritin by denaturing high-performance liquid chromatography: identification of new mutations. *British Journal of Haematology* *121*, 173–179.

Crooks, D.R., Jeong, S.-Y., Tong, W.-H., Ghosh, M.C., Olivierre, H., Haller, R.G., and Rouault, T.A. (2012). Tissue specificity of a human mitochondrial disease: differentiation-enhanced mis-splicing of the Fe-S scaffold ISCU renders patient cells more sensitive to oxidative stress in ISCU myopathy. *Journal of Biological Chemistry*.

Curtis, A.R.J., Fey, C., Morris, C.M., Bindoff, L.A., Ince, P.G., Chinnery, P.F., Coulthard, A., Jackson, M.J., Jackson, A.P., McHale, D.P., et al. (2001). Mutation in the gene encoding ferritin light polypeptide causes dominant adult-onset basal ganglia disease. *Nature Genetics* *28*, 350–354.

Daba, A., Koromilas, A.E., and Pantopoulos, K. (2012). Alternative Ferritin mRNA Translation Via Internal Initiation. *RNA* *18*, 547–556.

Dailey, H.A., Finnegan, M.G., and Johnson, M.K. (1994). Human ferrochelatase is an iron-sulfur protein. *Biochemistry* *33*, 403–407.

Dandekar, T., Beyer, K., Bork, P., Kenealy, M.R., Pantopoulos, K., Hentze, M., Sonntag-Buck, V., Flouriot, G., Gannon, F., and Schreiber, S. (1998). Systematic genomic screening and analysis of mRNA in untranslated regions and mRNA precursors: combining experimental and computational approaches. *Bioinformatics* *14*, 271–278.

Darshan, D., Vanoaica, L., Richman, L., Beermann, F., and Kühn, L.C. (2009). Conditional deletion of ferritin H in mice induces loss of iron storage and liver damage. *Hepatology (Baltimore, Md.)* *50*, 852–860.

Dautry-Varsat, A., Ciechanover, A., and Lodish, H.F. (1983). pH and the recycling of transferrin during receptor-mediated endocytosis. *Proceedings of the National Academy of Sciences* *80*, 2258–2262.

Delaby, C., Pilard, N., Puy, H., and Canonne-Hergaux, F. (2008). Sequential regulation of ferroportin expression after erythrophagocytosis in murine macrophages: early mRNA induction by haem, followed by iron-dependent protein expression. *The Biochemical Journal* *411*, 123–131.

DeMeo, D.L., Mariani, T., Bhattacharya, S., Srisuma, S., Lange, C., Litonjua, A., Bueno, R., Pillai, S.G., Lomas, D.A., Sparrow, D., et al. (2009). Integration of Genomic and Genetic Approaches Implicates IREB2 as a COPD Susceptibility Gene. *American Journal of Human Genetics* 85, 493–502.

DeRusso, P.A., Philpott, C.C., Iwai, K., Mostowski, H.S., Klausner, R.D., and Rouault, T.A. (1995). Expression of a Constitutive Mutant of Iron Regulatory Protein 1 Abolishes Iron Homeostasis in Mammalian Cells. *Journal of Biological Chemistry* 270, 15451–15454.

Deugnier, Y., and Mosser, J. (2008). Modifying factors of the HFE hemochromatosis phenotype. *Expert Review of Gastroenterology & Hepatology* 2, 531–540.

De Domenico, I., Vaughn, M.B., Li, L., Bagley, D., Musci, G., Ward, D.M., and Kaplan, J. (2006). Ferroportin-mediated mobilization of ferritin iron precedes ferritin degradation by the proteasome. *The EMBO Journal* 25, 5396–5404.

Donovan, A., Brownlie, A., Zhou, Y., Shepard, J., Pratt, S.J., Moynihan, J., Paw, B.H., Drejer, A., Barut, B., Zapata, A., et al. (2000). Positional cloning of zebrafish ferroportin1 identifies a conserved vertebrate iron exporter. *Nature* 403, 776–781.

Donovan, A., Lima, C.A., Pinkus, J.L., Pinkus, G.S., Zon, L.I., Robine, S., and Andrews, N.C. (2005). The iron exporter ferroportin/Slc40a1 is essential for iron homeostasis. *Cell Metabolism* 1, 191–200.

Drapier, J.C., Hirling, H., Wietzerbin, J., Kaldy, P., and Kühn, L.C. (1993). Biosynthesis of nitric oxide activates iron regulatory factor in macrophages. *The EMBO Journal* 12, 3643–3649.

Duce, J.A., Tsatsanis, A., Cater, M.A., James, S.A., Robb, E., Wikke, K., Leong, S.L., Perez, K., Johanssen, T., Greenough, M.A., et al. (2010). Iron-Export Ferroxidase Activity of  $\beta$ -Amyloid Precursor Protein Is Inhibited by Zinc in Alzheimer's Disease. *Cell* 142, 857–867.

Dupuis, L., and Loeffler, J.-P. (2009). Neuromuscular junction destruction during amyotrophic lateral sclerosis: insights from transgenic models. *Current Opinion in Pharmacology* 9, 341–346.

Dupuy, J., Volbeda, A., Carpentier, P., Darnault, C., Moulis, J.-M., and Fontecilla-Camps, J.C. (2006). Crystal Structure of Human Iron Regulatory Protein 1 as Cytosolic Aconitase. *Structure* *14*, 129–139.

Eisenstein, R.S., Tuazon, P.T., Schalinske, K.L., Anderson, S.A., and Traugh, J.A. (1993). Iron-responsive element-binding protein. Phosphorylation by protein kinase C. *Journal of Biological Chemistry* *268*, 27363–27370.

Fandrey, J. (2004). Oxygen-dependent and tissue-specific regulation of erythropoietin gene expression. *American Journal of Physiology - Regulatory, Integrative and Comparative Physiology* *286*, R977–R988.

Faucheux, B.A., Martin, M.-E., Beaumont, C., Hunot, S., Hauw, J.-J., Agid, Y., and Hirsch, E.C. (2002). Lack of up-regulation of ferritin is associated with sustained iron regulatory protein-1 binding activity in the substantia nigra of patients with Parkinson's disease. *Journal of Neurochemistry* *83*, 320–330.

Feder, J.N., Gnirke, A., Thomas, W., Tsuchihashi, Z., Ruddy, D.A., Basava, A., Dormishian, F., Domingo, R.J., Ellis, M.C., Fullan, A., et al. (1996). A novel MHC class I-like gene is mutated in patients with hereditary haemochromatosis. *Nature Genetics* *13*, 399–408.

Ferreira, C., Bucchini, D., Martin, M.-E., Levi, S., Arosio, P., Grandchamp, B., and Beaumont, C. (2000). Early Embryonic Lethality of H Ferritin Gene Deletion in Mice. *Journal of Biological Chemistry* *275*, 3021–3024.

Ferreira, C., Santambrogio, P., Martin, M.-E., Andrieu, V., Feldmann, G., Hénin, D., and Beaumont, C. (2001). H ferritin knockout mice: a model of hyperferritinemia in the absence of iron overload. *Blood* *98*, 525–532.

Ferring-Appel, D., Hentze, M.W., and Galy, B. (2009). Cell-autonomous and systemic context-dependent functions of iron regulatory protein 2 in mammalian iron metabolism. *Blood* *113*, 679–687.

Finberg, K.E. (2009). Iron-Refractory Iron Deficiency Anemia. *Seminars in Hematology* *46*, 378–386.

Fleming, M.D., Romano, M.A., Su, M.A., Garrick, L.M., Garrick, M.D., and Andrews, N.C. (1998). Nramp2 is mutated in the anemic Belgrade (b) rat: Evidence of a role for Nramp2 in endosomal iron transport. *Proceedings of the National Academy of Sciences* 95, 1148–1153.

Fleming, M.D., Trenor, C.C., Su, M.A., Foernzler, D., Beier, D.R., Dietrich, W.F., and Andrews, N.C. (1997). Microcytic anaemia mice have a mutation in Nramp2, a candidate iron transporter gene. *Nature Genetics* 16, 383–386.

Fleming, R.E., Feng, Q., and Britton, R.S. (2011). Knockout mouse models of iron homeostasis. *Annual Review of Nutrition* 31, 117–137.

Fleming, R.E., and Ponka, P. (2012). Iron Overload in Human Disease. *New England Journal of Medicine* 366, 348–359.

Fraser, J., Lin, F., and Berridge, M. (1988). Expression of high affinity receptors for erythropoietin on human bone marrow cells and on the human erythroleukemic cell line, HEL. *Experimental Hematology* 16, 836.

Friedlich, A.L., Tanzi, R.E., and Rogers, J.T. (2007). The 5'[[prime]]-untranslated region of Parkinson's disease  $\alpha$ -synuclein messengerRNA contains a predicted iron responsive element. *Molecular Psychiatry* 12, 222–223.

Galaris, D., and Pantopoulos, K. (2008). Oxidative stress and iron homeostasis: mechanistic and health aspects. *Critical Reviews in Clinical Laboratory Sciences* 45, 1–23.

Galy, B., Ferring, D., Benesova, M., Benes, V., and Hentze, M.W. (2004). Targeted mutagenesis of the murine IRP1 and IRP2 genes reveals context-dependent RNA processing differences in vivo. *RNA* 10, 1019–1025.

Galy, B., Ferring, D., and Hentze, M.W. (2005a). Generation of conditional alleles of the murine iron regulatory protein (IRP)-1 and -2 genes. *Genesis* 43, 181–188.

Galy, B., Ferring, D., Minana, B., Bell, O., Janser, H.G., Muckenthaler, M., Schümann, K., and Hentze, M.W. (2005b). Altered body iron distribution and microcytosis in mice deficient in iron regulatory protein 2 (IRP2). *Blood* 106, 2580–2589.

Galy, B., Ferring-Appel, D., Kaden, S., Gröne, H.-J., and Hentze, M.W. (2008). Iron Regulatory Proteins Are Essential for Intestinal Function and Control Key Iron Absorption Molecules in the Duodenum. *Cell Metabolism* 7, 79–85.

Galy, B., Ferring-Appel, D., Sauer, S.W., Kaden, S., Lyoumi, S., Puy, H., Kölker, S., Gröne, H.-J., and Hentze, M.W. (2010). Iron Regulatory Proteins Secure Mitochondrial Iron Sufficiency and Function. *Cell Metabolism* 12, 194–201.

Ganz, T., and Nemeth, E. (2012). Hepcidin and iron homeostasis. *Biochimica Et Biophysica Acta (BBA) - Molecular Cell Research* 1823, 1434–1443.

Girelli, D., Corrocher, R., Bisceglia, L., Olivieri, O., Franceschi, L. De, Zelante, L., and Gasparini, P. (1995). Molecular basis for the recently described hereditary hyperferritinemia-cataract syndrome: a mutation in the iron-responsive element of ferritin L-subunit gene (the “Verona mutation”). *Blood* 86, 4050–4053.

Goforth, J.B., Anderson, S.A., Nizzi, C.P., and Eisenstein, R.S. (2010). Multiple determinants within iron-responsive elements dictate iron regulatory protein binding and regulatory hierarchy. *RNA* 16, 154–169.

Gray, N.K., Pantopoulos, K., Dandekar, T., Ackrell, B.A., and Hentze, M.W. (1996). Translational regulation of mammalian and *Drosophila* citric acid cycle enzymes via iron-responsive elements. *Proceedings of the National Academy of Sciences of the United States of America* 93, 4925–4930.

Gregory, A., and Hayflick, S.J. (2011). Genetics of Neurodegeneration with Brain Iron Accumulation. *Current Neurology and Neuroscience Reports* 11, 254–261.

Gruber, M., Hu, C.-J., Johnson, R.S., Brown, E.J., Keith, B., and Simon, M.C. (2007). Acute postnatal ablation of *Hif-2 $\alpha$*  results in anemia. *Proceedings of the National Academy of Sciences* 104, 2301–2306.

Gruer, M.J., Artymiuk, P.J., and Guest, J.R. (1997). The aconitase family: three structural variations on a common theme. *Trends in Biochemical Sciences* 22, 3–6.

Gunshin, H., Allerson, C.R., Polycarpou-Schwarz, M., Rofts, a, Rogers, J.T., Kishi, F., Hentze, M.W., Rouault, T. a, Andrews, N.C., and Hediger, M. a (2001). Iron-dependent regulation of the divalent metal ion transporter. *FEBS Letters* 509, 309–316.

Gunshin, H., Fujiwara, Y., Custodio, A.O., DiRenzo, C., Robine, S., and Andrews, N.C. (2005). Slc11a2 is required for intestinal iron absorption and erythropoiesis but dispensable in placenta and liver. *Journal of Clinical Investigation* 115, 1258–1266.

Hall, R.E., Henriksson, K.G., Lewis, S.F., Haller, R.G., and Kennaway, N.G. (1993). Mitochondrial myopathy with succinate dehydrogenase and aconitase deficiency. Abnormalities of several iron-sulfur proteins. *Journal of Clinical Investigation* 92, 2660–2666.

Hallberg, L. (1981). Bioavailability of Dietary Iron in Man. *Annual Review of Nutrition* 1, 123–147.

Haller, R.G., Henriksson, K.G., Jorfeldt, L., Hultman, E., Wibom, R., Sahlin, K., Areskog, N.H., Gunder, M., Ayyad, K., and Blomqvist, C.G. (1991). Deficiency of skeletal muscle succinate dehydrogenase and aconitase. Pathophysiology of exercise in a novel human muscle oxidative defect. *The Journal of Clinical Investigation* 88, 1197–1206.

Halliwell, B., and Gutteridge, J.M.C. (1992). Biologically relevant metal ion-dependent hydroxyl radical generation An update. *FEBS Letters* 307, 108–112.

Harris, Z.L., Durley, A.P., Man, T.K., and Gitlin, J.D. (1999). Targeted gene disruption reveals an essential role for ceruloplasmin in cellular iron efflux. *Proceedings of the National Academy of Sciences* 96, 10812–10817.

Harrison, P.M., and Arosio, P. (1996). The ferritins: molecular properties, iron storage function and cellular regulation. *Biochimica Et Biophysica Acta* 1275, 161–203.

Hashimoto, S., Suzuki, T., Dong, H.-Y., Yamazaki, N., and Matsushima, K. (1999). Serial Analysis of Gene Expression in Human Monocytes and Macrophages. *Blood* 94, 837–844.

Hentze, M.W., Caughman, S.W., Casey, J.L., Kodier, D.M., Rouault, T.A., Harford, J.B., and Klausner, R.D. (1988). A model for the structure and functions of iron-responsive elements. *Gene* 72, 201–208.

## 5. BIBLIOGRAPHY

---

Hentze, M.W., and Kuhnt, L.C. (1996). Review Molecular control of vertebrate iron metabolism□: mRNA-based regulatory circuits operated by iron , nitric oxide , and oxidative stress. *93*, 8175–8182.

Hentze, M.W., Muckenthaler, M.U., and Andrews, N.C. (2004). Balancing Acts: Molecular Control of Mammalian Iron Metabolism. *Cell 117*, 285–297.

Hentze, M.W., Muckenthaler, M.U., Galy, B., and Camaschella, C. (2010). Two to Tango: Regulation of Mammalian Iron Metabolism. *Cell 142*, 24–38.

Herrmann, T., Muckenthaler, M., Van der Hoeven, F., Brennan, K., Gehrke, S.G., Hubert, N., Sergi, C., Gröne, H.-J., Kaiser, I., Gosch, I., et al. (2004). Iron overload in adult Hfe-deficient mice independent of changes in the steady-state expression of the duodenal iron transporters DMT1 and Ireg1/ferroportin. *Journal of Molecular Medicine (Berlin, Germany) 82*, 39–48.

Hirling, H., Henderson, B.R., and Kühn, L.C. (1994). Mutational analysis of the [4Fe-4S]-cluster converting iron regulatory factor from its RNA-binding form to cytoplasmic aconitase. *The EMBO Journal 13*, 453–461.

Huang, F.W. (2005). A mouse model of juvenile hemochromatosis. *Journal of Clinical Investigation 115*, 2187–2191.

Hubert, N., and Hentze, M.W. (2002). Previously uncharacterized isoforms of divalent metal transporter (DMT)-1: implications for regulation and cellular function. *Proceedings of the National Academy of Sciences of the United States of America 99*, 12345–12350.

Hvidberg, V., Maniecki, M.B., Jacobsen, C., Højrup, P., Møller, H.J., and Moestrup, S.K. (2005). Identification of the receptor scavenging hemopexin-heme complexes. *Blood 106*, 2572–2579.

Ishikawa, H., Kato, M., Hori, H., Ishimori, K., Kirisako, T., Tokunaga, F., and Iwai, K. (2005). Involvement of Heme Regulatory Motif in Heme-Mediated Ubiquitination and Degradation of IRP2. *Molecular Cell 19*, 171–181.

Iwai, K., Drake, S.K., Wehr, N.B., Weissman, A.M., LaVaute, T., Minato, N., Klausner, R.D., Levine, R.L., and Rouault, T.A. (1998). Iron-dependent oxidation, ubiquitination, and

degradation of iron regulatory protein 2: Implications for degradation of oxidized proteins. *Proceedings of the National Academy of Sciences* 95, 4924–4928.

Kallio, P.J., Wilson, W.J., O'Brien, S., Makino, Y., and Poellinger, L. (1999). Regulation of the hypoxia-inducible transcription factor 1alpha by the ubiquitin-proteasome pathway. *The Journal of Biological Chemistry* 274, 6519–6525.

Kato, J., Fujikawa, K., Kanda, M., Fukuda, N., Sasaki, K., Takayama, T., Kobune, M., Takada, K., Takimoto, R., Hamada, H., et al. (2001). A Mutation, in the Iron-Responsive Element of H Ferritin mRNA, Causing Autosomal Dominant Iron Overload. *American Journal of Human Genetics* 69, 191–197.

Kawabata, H., Fleming, R.E., Gui, D., Moon, S.Y., Saitoh, T., O'Kelly, J., Umehara, Y., Wano, Y., Said, J.W., and Koeffler, H.P. (2005). Expression of hepcidin is down-regulated in TfR2 mutant mice manifesting a phenotype of hereditary hemochromatosis. *Blood* 105, 376–381.

Keel, S.B., Doty, R.T., Yang, Z., Quigley, J.G., Chen, J., Knoblauch, S., Kingsley, P.D., De Domenico, I., Vaughn, M.B., Kaplan, J., et al. (2008). A Heme Export Protein Is Required for Red Blood Cell Differentiation and Iron Homeostasis. *Science* 319, 825–828.

Kennedy, M.C., Mende-Mueller, L., Blondin, G.A., and Beinert, H. (1992). Purification and characterization of cytosolic aconitase from beef liver and its relationship to the iron-responsive element binding protein. *Proceedings of the National Academy of Sciences* 89, 11730–11734.

Kidane, T.Z., Sauble, E., and Linder, M.C. (2006). Release of iron from ferritin requires lysosomal activity. *American Journal of Physiology - Cell Physiology* 291, C445–C455.

Kim, H.-Y., LaVaute, T., Iwai, K., Klausner, R.D., and Rouault, T.A. (1996). Identification of a Conserved and Functional Iron-responsive Element in the 5'-Untranslated Region of Mammalian Mitochondrial Aconitase. *Journal of Biological Chemistry* 271, 24226–24230.

Kispal, G., Csere, P., Guiard, B., and Lill, R. (1997). The ABC transporter Atm1p is required for mitochondrial iron homeostasis. *FEBS Letters* 418, 346–350.

- Knutson, M.D., Vafa, M.R., Haile, D.J., and Wessling-Resnick, M. (2003). Iron loading and erythrophagocytosis increase ferroportin 1 (FPN1) expression in J774 macrophages. *Blood* 102, 4191–4197.
- Kohler, S.A., Henderson, B.R., and Kühn, L.C. (1995). Succinate Dehydrogenase b mRNA of *Drosophila melanogaster* Has a Functional Iron-responsive Element in Its 5'-Untranslated Region. *Journal of Biological Chemistry* 270, 30781–30786.
- Koury, M.J., and Ponka, P. (2004). New insights into erythropoiesis: the roles of folate, vitamin B12, and iron. *Annual Review of Nutrition* 24, 105–131.
- Koury, S.T., Bondurant, M.C., Koury, M.J., and Semenza, G.L. (1991). Localization of cells producing erythropoietin in murine liver by in situ hybridization. *Blood* 77, 2497–2503.
- Krause, A., Neitz, S., Mägert, H.-J., Schulz, A., Forssmann, W.-G., Schulz-Knappe, P., and Adermann, K. (2000). LEAP-1, a novel highly disulfide-bonded human peptide, exhibits antimicrobial activity. *FEBS Letters* 480, 147–150.
- Kristiansen, M., Graversen, J.H., Jacobsen, C., Sonne, O., Hoffman, H.J., Law, S.K., and Moestrup, S.K. (2001). Identification of the haemoglobin scavenger receptor. *Nature* 409, 198–201.
- Lamoril, J., Boulechfar, S., De Verneuil, H., Grandchamp, B., Nordmann, Y., and Deybach, J.-C. (1991). Human Erythropoietic Protoporphyrin: Two point mutations in the ferrochelatase gene. *Biochemical and Biophysical Research Communications* 181, 594–599.
- Latunde-Dada, G.O., Van der Westhuizen, J., Vulpe, C.D., Anderson, G.J., Simpson, R.J., and McKie, A.T. (2002). Molecular and Functional Roles of Duodenal Cytochrome B (Dcytb) in Iron Metabolism. *Blood Cells, Molecules and Diseases* 29, 356–360.
- LaVaute, T., Smith, S., Cooperman, S., Iwai, K., Land, W., Meyron-Holtz, E., Drake, S.K., Miller, G., Abu-Asab, M., Tsokos, M., et al. (2001). Targeted deletion of the gene encoding iron regulatory protein-2 causes misregulation of iron metabolism and neurodegenerative disease in mice. *Nature Genetics* 27, 209–214.

Lei, P., Ayton, S., Finkelstein, D.I., Spoorri, L., Ciccotosto, G.D., Wright, D.K., Wong, B.X.W., Adlard, P.A., Cherny, R.A., Lam, L.Q., et al. (2012). Tau deficiency induces parkinsonism with dementia by impairing APP-mediated iron export. *Nature Medicine* *18*, 291–295.

Lesbordes-Brion, J.-C., Viatte, L., Bennoun, M., Lou, D.-Q., Ramey, G., Houbron, C., Hamard, G., Kahn, A., and Vaulont, S. (2006). Targeted disruption of the hepcidin 1 gene results in severe hemochromatosis. *Blood* *108*, 1402–1405.

Levi, S., Corsi, B., Bosisio, M., Invernizzi, R., Volz, A., Sanford, D., Arosio, P., and Drysdale, J. (2001). A Human Mitochondrial Ferritin Encoded by an Intronless Gene. *Journal of Biological Chemistry* *276*, 24437–24440.

Levy, J.E., Jin, O., Fujiwara, Y., Kuo, F., and Andrews, N.C. (1999). Transferrin receptor is necessary for development of erythrocytes and the nervous system. *Nature Genetics* *21*, 396–399.

Liew, Y.-F., and Shaw, N.-S. (2005). Mitochondrial Cysteine Desulfurase Iron-Sulfur Cluster S and Aconitase Are Post-transcriptionally Regulated by Dietary Iron in Skeletal Muscle of Rats. *The Journal of Nutrition* *135*, 2151–2158.

Lill, R., and Mühlenhoff, U. (2008). Maturation of iron-sulfur proteins in eukaryotes: mechanisms, connected processes, and diseases. *Annual Review of Biochemistry* *77*, 669–700.

Lind, M.I., Missirlis, F., Melefors, O., Uhrigshardt, H., Kirby, K., Phillips, J.P., Söderhäll, K., and Rouault, T. a (2006). Of two cytosolic aconitases expressed in *Drosophila*, only one functions as an iron-regulatory protein. *The Journal of Biological Chemistry* *281*, 18707–18714.

Lobmayr, L., Brooks, D.G., and Wilson, R.B. (2005). Increased IRP1 activity in Friedreich ataxia. *Gene* *354*, 157–161.

Mastrogiannaki, M., Matak, P., Keith, B., Simon, M.C., Vaulont, S., and Peyssonnaud, C. (2009). HIF-2 $\alpha$ , but not HIF-1 $\alpha$ , promotes iron absorption in mice. *J Clin Invest* *119*, 1159–1166.

McKie, A.T., Marciani, P., Rolfs, A., Brennan, K., Wehr, K., Barrow, D., Miret, S., Bomford, A., Peters, T.J., Farzaneh, F., et al. (2000). A Novel Duodenal Iron-Regulated Transporter, IREG1, Implicated in the Basolateral Transfer of Iron to the Circulation. *Molecular Cell* *5*, 299–309.

## 5. BIBLIOGRAPHY

---

Merkofer, M., Kissner, R., Hider, R.C., Brunk, U.T., and Koppenol, W.H. (2006). Fenton Chemistry and Iron Chelation under Physiologically Relevant Conditions: Electrochemistry and Kinetics. *Chemical Research in Toxicology* *19*, 1263–1269.

Meyron-Holtz, E.G., Ghosh, M.C., Iwai, K., LaVaute, T., Brazzolotto, X., Berger, U. V, Land, W., Ollivierre-Wilson, H., Grinberg, A., Love, P., et al. (2004a). Genetic ablations of iron regulatory proteins 1 and 2 reveal why iron regulatory protein 2 dominates iron homeostasis. *The EMBO Journal* *23*, 386–395.

Meyron-Holtz, E.G., Ghosh, M.C., and Rouault, T. a (2004b). Mammalian tissue oxygen levels modulate iron-regulatory protein activities in vivo. *Science (New York, N.Y.)* *306*, 2087–2090.

Meyron-Holtz, E.G., Moshe-Belizowski, S., and Cohen, L.A. (2011). A possible role for secreted ferritin in tissue iron distribution. *Journal of Neural Transmission* *118*, 337–347.

Mims, M.P., Guan, Y., Pospisilova, D., Priwitzerova, M., Indrak, K., Ponka, P., Divoky, V., and Prchal, J.T. (2005). Identification of a human mutation of DMT1 in a patient with microcytic anemia and iron overload. *Blood* *105*, 1337–1342.

Missirlis, F., Hu, J., Kirby, K., Hilliker, A.J., Rouault, T.A., and Phillips, J.P. (2003). Compartment-specific Protection of Iron-Sulfur Proteins by Superoxide Dismutase. *Journal of Biological Chemistry* *278*, 47365–47369.

Mochel, F., Knight, M.A., Tong, W.-H., Hernandez, D., Ayyad, K., Taivassalo, T., Andersen, P.M., Singleton, A., Rouault, T.A., Fischbeck, K.H., et al. (2008). Splice Mutation in the Iron-Sulfur Cluster Scaffold Protein ISCU Causes Myopathy with Exercise Intolerance. *American Journal of Human Genetics* *82*, 652–660.

Mok, H., Jelinek, J., Pai, S., Cattanaach, B.M., Prchal, J.T., Youssoufian, H., and Schumacher, A. (2004). Disruption of Ferroportin 1 Regulation Causes Dynamic Alterations in Iron Homeostasis and Erythropoiesis in Polycythaemia Mice. *Development* *131*, 1859–1868.

Montosi, G., Donovan, A., Totaro, A., Garuti, C., Pignatti, E., Cassanelli, S., Trenor, C.C., Gasparini, P., Andrews, N.C., and Pietrangelo, A. (2001). Autosomal-dominant hemochromatosis is associated with a mutation in the ferroportin (SLC11A3) gene. *Journal of Clinical Investigation* *108*, 619–623.

Moroishi, T., Nishiyama, M., Takeda, Y., Iwai, K., and Nakayama, K.I. (2011). The FBXL5-IRP2 axis is integral to control of iron metabolism in vivo. *Cell Metabolism* *14*, 339–351.

Muckenthaler, M., Gray, N.K., and Hentze, M.W. (1998). IRP-1 Binding to Ferritin mRNA Prevents the Recruitment of the Small Ribosomal Subunit by the Cap-Binding Complex eIF4F. *Molecular Cell* *2*, 383–388.

Muir, A.R., and Golberg, L. (1961). Observations on Subcutaneous Macrophages. Phagocytosis of Iron-Dextran and Ferritin Synthesis. *Experimental Physiology* *46*, 289–298.

Mühlenhoff, U., Gerber, J., Richhardt, N., and Lill, R. (2003). Components involved in assembly and dislocation of iron-sulfur clusters on the scaffold protein Isu1p. *The EMBO Journal* *22*, 4815–4825.

Mühlenhoff, U., Richhardt, N., Ristow, M., Kispal, G., and Lill, R. (2002). The yeast frataxin homolog Yfh1p plays a specific role in the maturation of cellular Fe/S proteins. *Human Molecular Genetics* *11*, 2025–2036.

Nemeth, E., Tuttle, M.S., Powelson, J., Vaughn, M.B., Donovan, A., Ward, D.M., Ganz, T., and Kaplan, J. (2004). Hepcidin Regulates Cellular Iron Efflux by Binding to Ferroportin and Inducing Its Internalization. *Science* *306*, 2090–2093.

Nicolas, G., Chauvet, C., Viatte, L., Danan, J.L., Bigard, X., Devaux, I., Beaumont, C., Kahn, A., and Vaulont, S. (2002). The gene encoding the iron regulatory peptide hepcidin is regulated by anemia, hypoxia, and inflammation. *Journal of Clinical Investigation* *110*, 1037–1044.

Niederkofler, V. (2005). Hemojuvelin is essential for dietary iron sensing, and its mutation leads to severe iron overload. *Journal of Clinical Investigation* *115*, 2180–2186.

Njajou, O.T., Vaessen, N., Joosse, M., Berghuis, B., Dongen, J.W.F. van, Breuning, M.H., Snijders, P.J.L.M., Rutten, W.P.F., Sandkuijl, L.A., Oostra, B.A., et al. (2001). A mutation in SLC11A3 is associated with autosomal dominant hemochromatosis. *Nature Genetics* *28*, 213–214.

## 5. BIBLIOGRAPHY

---

Ohgami, R.S., Campagna, D.R., Antiochos, B., Wood, E.B., Sharp, J.J., Barker, J.E., and Fleming, M.D. (2005). nm1054: a spontaneous, recessive, hypochromic, microcytic anemia mutation in the mouse. *Blood* *106*, 3625–3631.

Ohgami, R.S., Campagna, D.R., McDonald, A., and Fleming, M.D. (2006). The Steap proteins are metalloreductases. *Blood* *108*, 1388–1394.

Ohkawa, H., Ohishi, N., and Yagi, K. (1979). Assay for lipid peroxides in animal tissues by thiobarbituric acid reaction. *Analytical Biochemistry* *95*, 351–358.

Olsson, A., Lind, L., Thornell, L.-E., and Holmberg, M. (2008). Myopathy with lactic acidosis is linked to chromosome 12q23.3–24.11 and caused by an intron mutation in the ISCU gene resulting in a splicing defect. *Human Molecular Genetics* *17*, 1666–1672.

Ordway, G.A., and Garry, D.J. (2004). Myoglobin: an essential hemoprotein in striated muscle. *Journal of Experimental Biology* *207*, 3441–3446.

Pak, M., Lopez, M.A., Gabayan, V., Ganz, T., and Rivera, S. (2006). Suppression of hepcidin during anemia requires erythropoietic activity. *Blood* *108*, 3730–3735.

Pandolfo, M. (2003). Friedreich ataxia. *Seminars in Pediatric Neurology* *10*, 163–172.

Pantopoulos, K., Mueller, S., Atzberger, a, Ansorge, W., Stremmel, W., and Hentze, M.W. (1997). Differences in the regulation of iron regulatory protein-1 (IRP-1) by extra- and intracellular oxidative stress. *The Journal of Biological Chemistry* *272*, 9802–9808.

Pantopoulos, K., Porwal, S.K., Tartakoff, A., and Devireddy, L. (2012). Mechanisms of Mammalian Iron Homeostasis. *Biochemistry* *51*, 5705–5724.

Papanikolaou, G., Samuels, M.E., Ludwig, E.H., MacDonald, M.L.E., Franchini, P.L., Dubé, M.-P., Andres, L., MacFarlane, J., Sakellaropoulos, N., Politou, M., et al. (2003). Mutations in HFE2 cause iron overload in chromosome 1q-linked juvenile hemochromatosis. *Nature Genetics* *36*, 77–82.

Paradkar, P.N., Zumbrennen, K.B., Paw, B.H., Ward, D.M., and Kaplan, J. (2009). Regulation of mitochondrial iron import through differential turnover of mitoferrin 1 and mitoferrin 2. *Molecular and Cellular Biology* *29*, 1007–1016.

Paraskeva, E., and Hentze, M.W. (1996). Iron-sulphur clusters as genetic regulatory switches: the bifunctional iron regulatory protein-1. *FEBS Letters* 389, 40–43.

Park, C.H., Valore, E. V, Waring, a J., and Ganz, T. (2001). Heparin, a urinary antimicrobial peptide synthesized in the liver. *The Journal of Biological Chemistry* 276, 7806–7810.

Peyssonnaud, C., Zinkernagel, A.S., Schuepbach, R.A., Rankin, E., Vaulont, S., Haase, V.H., Nizet, V., and Johnson, R.S. (2007). Regulation of iron homeostasis by the hypoxia-inducible transcription factors (HIFs). *Journal of Clinical Investigation* 117, 1926–1932.

Philpott, C.C., Haile, D., Rouault, T.A., and Klausner, R.D. (1993). Modification of a free Fe-S cluster cysteine residue in the active iron-responsive element-binding protein prevents RNA binding. *Journal of Biological Chemistry* 268, 17655–17658.

Philpott, C.C., Klausner, R.D., and Rouault, T.A. (1994). The bifunctional iron-responsive element binding protein/cytosolic aconitase: the role of active-site residues in ligand binding and regulation. *Proceedings of the National Academy of Sciences* 91, 7321–7325.

Piccinelli, P., and Samuelsson, T. (2007). Evolution of the iron-responsive element. *RNA* 13, 952–966.

Pietrangelo, A. (2010). Hereditary Hemochromatosis: Pathogenesis, Diagnosis, and Treatment. *Gastroenterology* 139, 393–408.e2.

Ponka, P. (1997). Tissue-Specific Regulation of Iron Metabolism and Heme Synthesis: Distinct Control Mechanisms in Erythroid Cells. *Blood* 89, 1–25.

Poss, K.D., and Tonegawa, S. (1997). Heme oxygenase 1 is required for mammalian iron reutilization. *Proceedings of the National Academy of Sciences* 94, 10919–10924.

Puccio, H., Simon, D., Cossée, M., Criqui-Filipe, P., Tiziano, F., Melki, J., Hindelang, C., Matyas, R., Rustin, P., and Koenig, M. (2001). Mouse models for Friedreich ataxia exhibit cardiomyopathy, sensory nerve defect and Fe-S enzyme deficiency followed by intramitochondrial iron deposits. *Nature Genetics* 27, 181–186.

- Rajagopal, A., Rao, A.U., Amigo, J., Tian, M., Upadhyay, S.K., Hall, C., Uhm, S., Mathew, M.K., Fleming, M.D., Paw, B.H., et al. (2008). Haem homeostasis is regulated by the conserved and concerted functions of HRG-1 proteins. *Nature* *453*, 1127–1131.
- Ramos, E., Kautz, L., Rodriguez, R., Hansen, M., Gabayan, V., Ginzburg, Y., Roth, M.-P., Nemeth, E., and Ganz, T. (2011). Evidence for distinct pathways of hepcidin regulation by acute and chronic iron loading. *Hepatology (Baltimore, Md.)* *53*, 1333–1341.
- Rankin, E.B., Biju, M.P., Liu, Q., Unger, T.L., Rha, J., Johnson, R.S., Simon, M.C., Keith, B., and Haase, V.H. (2007). Hypoxia-inducible factor–2 (HIF-2) regulates hepatic erythropoietin in vivo. *Journal of Clinical Investigation* *117*, 1068–1077.
- Rauen, U., Springer, A., Weisheit, D., Petrat, F., Korth, H.-G., De Groot, H., and Sustmann, R. (2007). Assessment of Chelatable Mitochondrial Iron by Using Mitochondrion-Selective Fluorescent Iron Indicators with Different Iron-Binding Affinities. *ChemBioChem* *8*, 341–352.
- Richardson, D.R., Lane, D.J.R., Becker, E.M., Huang, M.L.-H., Whitnall, M., Suryo Rahmanto, Y., Sheftel, A.D., and Ponka, P. (2010). Mitochondrial iron trafficking and the integration of iron metabolism between the mitochondrion and cytosol. *Proceedings of the National Academy of Sciences of the United States of America* *107*, 10775–10782.
- Roetto, A., Papanikolaou, G., Politou, M., Alberti, F., Girelli, D., Christakis, J., Loukopoulos, D., and Camaschella, C. (2002). Mutant antimicrobial peptide hepcidin is associated with severe juvenile hemochromatosis. *Nature Genetics* *33*, 21–22.
- Rogers, J.T., Randall, J.D., Cahill, C.M., Eder, P.S., Huang, X., Gunshin, H., Leiter, L., McPhee, J., Sarang, S.S., Utsuki, T., et al. (2002). An iron-responsive element type II in the 5'-untranslated region of the Alzheimer's amyloid precursor protein transcript. *The Journal of Biological Chemistry* *277*, 45518–45528.
- Rouault, T. a, and Tong, W.H. (2008). Iron-sulfur cluster biogenesis and human disease. *Trends in Genetics: TIG* *24*, 398–407.
- Rouault, T.A. (2006). The role of iron regulatory proteins in mammalian iron homeostasis and disease. *Nature Chemical Biology* *2*, 406–414.

Rouault, T.A., Haile, D.J., Downey, W.E., Philpott, C.C., Tang, C., Samaniego, F., Chin, J., Paul, I., Orloff, D., Harford, J.B., et al. (1992). An iron-sulfur cluster plays a novel regulatory role in the iron-responsive element binding protein. *Biometals* 5, 131–140.

Rouault, T.A., Stout, C.D., Kaptain, S., Harford, J.B., and Klausner, R.D. (1991). Structural relationship between an iron-regulated RNA-binding protein (IRE-BP) and aconitase: Functional implications. *Cell* 64, 881–883.

Roy, C.N., and Enns, C.A. (2000). Iron homeostasis: new tales from the crypt. *Blood* 96, 4020–4027.

Rudeck, M., Volk, T., Sitte, N., and Grune, T. (2000). Ferritin Oxidation in Vitro: Implication of Iron Release and Degradation by the 20S Proteasome. *IUBMB Life* 49, 451–456.

Salahudeen, A.A., Thompson, J.W., Ruiz, J.C., Ma, H.-W., Kinch, L.N., Li, Q., Grishin, N. V., and Bruick, R.K. (2009). An E3 Ligase Possessing an Iron-Responsive Hemerythrin Domain Is a Regulator of Iron Homeostasis. *Science* 326, 722–726.

Sanchez, M., Galy, B., Dandekar, T., Bengert, P., Vainshtein, Y., Stolte, J., Muckenthaler, M.U., and Hentze, M.W. (2006). Iron Regulation and the Cell Cycle Identification of an Iron-Responsive Element in the 3'-Untranslated Region of Human Cell Division Cycle 14A by a Refined Microarray-based Screening Strategy. *Journal of Biological Chemistry* 281, 22865–22874.

Sanchez, M., Galy, B., Hentze, M.W., and Muckenthaler, M.U. (2007a). Identification of target mRNAs of regulatory RNA-binding proteins using mRNP immunopurification and microarrays. *Nature Protocols* 2, 2033–2042.

Sanchez, M., Galy, B., Muckenthaler, M.U., and Hentze, M.W. (2007b). Iron-regulatory proteins limit hypoxia-inducible factor-2 $\alpha$  expression in iron deficiency. *Nature Structural & Molecular Biology* 14, 420–426.

Sanchez, M., Galy, B., Schwanhaeusser, B., Blake, J., Bähr-Ivacevic, T., Benes, V., Selbach, M., Muckenthaler, M.U., and Hentze, M.W. (2011). Iron Regulatory Protein-1 and -2: Transcriptome-Wide Definition of Binding mRNAs and Shaping of the Cellular Proteome by Iron Regulatory Proteins. *Blood* 118, e168–79.

## 5. BIBLIOGRAPHY

---

Schranzhofer, M., Schifrer, M., Cabrera, J.A., Kopp, S., Chiba, P., Beug, H., and Müllner, E.W. (2006). Remodeling the regulation of iron metabolism during erythroid differentiation to ensure efficient heme biosynthesis. *Blood* *107*, 4159–4167.

Schumann, K., Szegner, B., Kohler, B., Pfaffl, M.W., and Ertle, T. (2007). A method to assess <sup>59</sup>Fe in residual tissue blood content in mice and its use to correct <sup>59</sup>Fe-distribution kinetics accordingly. *Toxicology* *241*, 19–32.

Scortegagna, M., Ding, K., Oktay, Y., Gaur, A., Thurmond, F., Yan, L.-J., Marck, B.T., Matsumoto, A.M., Shelton, J.M., Richardson, J.A., et al. (2003a). Multiple organ pathology, metabolic abnormalities and impaired homeostasis of reactive oxygen species in *Epas1*<sup>-/-</sup> mice. *Nature Genetics* *35*, 331–340.

Scortegagna, M., Morris, M.A., Oktay, Y., Bennett, M., and Garcia, J.A. (2003b). The HIF family member EPAS1/HIF-2 $\alpha$  is required for normal hematopoiesis in mice. *Blood* *102*, 1634–1640.

Semenza, G.L. (2011). Oxygen Sensing, Homeostasis, and Disease. *New England Journal of Medicine* *365*, 537–547.

Shaw, G.C., Cope, J.J., Li, L., Corson, K., Hersey, C., Ackermann, G.E., Gwynn, B., Lambert, A.J., Wingert, R. a, Traver, D., et al. (2006). Mitoferrin is essential for erythroid iron assimilation. *Nature* *440*, 96–100.

Sheftel, A., Stehling, O., and Lill, R. (2010). Iron–sulfur proteins in health and disease. *Trends in Endocrinology & Metabolism* *21*, 302–314.

Shi, H., Bencze, K.Z., Stemmler, T.L., and Philpott, C.C. (2008). A cytosolic iron chaperone that delivers iron to ferritin. *Science (New York, N.Y.)* *320*, 1207–1210.

Shu, C., Sung, M.W., Stewart, M.D., Igumenova, T.I., Tan, X., and Li, P. (2012). The Structural Basis of Iron Sensing by the Human F-box Protein FBXL5. *ChemBioChem* *13*, 788–791.

Simon, M., Bourel, M., Genetet, B., and Fauchet, R. (1977). Idiopathic hemochromatosis. Demonstration of recessive transmission and early detection by family HLA typing. *The New England Journal of Medicine* *297*, 1017–1021.

Sinha, S., Anderson, J.P., Barbour, R., Basi, G.S., Caccavello, R., Davis, D., Doan, M., Dovey, H.F., Frigon, N., Hong, J., et al. (1999). Purification and cloning of amyloid precursor protein beta-secretase from human brain. *Nature* *402*, 537–540.

Smith, M.A., Wehr, K., Harris, P.L.R., Siedlak, S.L., Connor, J.R., and Perry, G. (1998). Abnormal localization of iron regulatory protein in Alzheimer's disease. *Brain Research* *788*, 232–236.

Smith, S.R., Cooperman, S., Lavaute, T., Tresser, N., Ghosh, M., Meyron-Holtz, E., Land, W., Ollivierre, H., Jortner, B., Switzer, R., et al. (2004). Severity of Neurodegeneration Correlates with Compromise of Iron Metabolism in Mice with Iron Regulatory Protein Deficiencies. *Annals of the New York Academy of Sciences* *1012*, 65–83.

Smith, S.R., Ghosh, M.C., Ollivierre-Wilson, H., Hang Tong, W., and Rouault, T.A. (2006). Complete loss of iron regulatory proteins 1 and 2 prevents viability of murine zygotes beyond the blastocyst stage of embryonic development. *Blood Cells, Molecules, and Diseases* *36*, 283–287.

Srinivas, S., Watanabe, T., Lin, C.-S., William, C.M., Tanabe, Y., Jessell, T.M., and Costantini, F. (2001). Cre reporter strains produced by targeted insertion of EYFP and ECFP into the ROSA26 locus. *BMC Developmental Biology* *1*, 4.

Suega, K., Bakta, M., Dharmayudha, T.G., Lukman, J.S., and Suwitra, K. (2005). Profile of anemia in chronic renal failure patients: comparison between predialyzed and dialyzed patients at the Division of Nephrology, Department of Internal Medicine, Sanglah Hospital, Denpasar, Bali, Indonesia. *Acta Medica Indonesiana* *37*, 190–194.

Surdej, P., Richman, L., and Kühn, L.C. (2008). Differential translational regulation of IRE-containing mRNAs in *Drosophila melanogaster* by endogenous IRP and a constitutive human IRP1 mutant. *Insect Biochemistry and Molecular Biology* *38*, 891–894.

Talbot, A.-L., Bullock, G.C., Delehanty, L.L., Sattler, M., Zhao, Z.J., and Goldfarb, A.N. (2011). Aconitase Regulation of Erythropoiesis Correlates with a Novel Licensing Function in Erythropoietin-Induced ERK Signaling. *PLoS ONE* *6*, e23850.

Tang, S.-H.E., Silva, F.J., Tsark, W.M.K., and Mann, J.R. (2002). A cre/loxP-deleter transgenic line in mouse strain 129S1/SvImJ. *Genesis* *32*, 199–202.

- Theil, E.C. (1994). Iron regulatory elements (IREs): a family of mRNA non-coding sequences. *Biochemical Journal* 304, 1–11.
- Theurl, I., Ludwiczek, S., Eller, P., Seifert, M., Artner, E., Brunner, P., and Weiss, G. (2005). Pathways for the regulation of body iron homeostasis in response to experimental iron overload. *Journal of Hepatology* 43, 711–719.
- Thompson, J.W., and Bruick, R.K. (2012). Protein degradation and iron homeostasis. *Biochimica Et Biophysica Acta* 1823, 1484–1490.
- Torti, F.M., and Torti, S. V. (2002). Regulation of ferritin genes and protein. *Blood* 99, 3505–3516.
- Torti, S. V, and Torti, F.M. (1994). Iron and ferritin in inflammation and cancer. *Advances in Inorganic Biochemistry* 10, 119–137.
- Trenor, C.C., Campagna, D.R., Sellers, V.M., Andrews, N.C., and Fleming, M.D. (2000). The molecular defect in hypotransferrinemic mice. *Blood* 96, 1113–1118.
- Truett, G.E., Heeger, P., Mynatt, R.L., Truett, A.A., Walker, J.A., and Warman, M.L. (2000). Preparation of PCR-quality mouse genomic DNA with hot sodium hydroxide and tris (HotSHOT). *BioTechniques* 29, 52, 54.
- Truty, J., Malpe, R., and Linder, M.C. (2001). Iron Prevents Ferritin Turnover in Hepatic Cells. *Journal of Biological Chemistry* 276, 48775–48780.
- Vashisht, A.A., Zumbrennen, K.B., Huang, X., Powers, D.N., Durazo, A., Sun, D., Bhaskaran, N., Persson, A., Uhlen, M., Sangfelt, O., et al. (2009). Control of Iron Homeostasis by an Iron-Regulated Ubiquitin Ligase. *Science* 326, 718–721.
- Vickery, L.E., and Cupp-Vickery, J.R. (2007). Molecular chaperones HscA/Ssq1 and HscB/Jac1 and their roles in iron-sulfur protein maturation. *Critical Reviews in Biochemistry and Molecular Biology* 42, 95–111.
- Vujić Spasić, M., Kiss, J., Herrmann, T., Galy, B., Martinache, S., Stolte, J., Gröne, H.-J., Stremmel, W., Hentze, M.W., and Muckenthaler, M.U. (2008). Hfe Acts in Hepatocytes to Prevent Hemochromatosis. *Cell Metabolism* 7, 173–178.

Vulpe, C.D., Kuo, Y.-M., Murphy, T.L., Cowley, L., Askwith, C., Libina, N., Gitschier, J., and Anderson, G.J. (1999). Hephaestin, a ceruloplasmin homologue implicated in intestinal iron transport, is defective in the sla mouse. *Nature Genetics* 21, 195–199.

Walden, W.E., Selezneva, A.I., Dupuy, J., Volbeda, A., Fontecilla-Camps, J.C., Theil, E.C., and Volz, K. (2006). Structure of Dual Function Iron Regulatory Protein 1 Complexed with Ferritin IRE-RNA. *Science* 314, 1903–1908.

Wang, J., and Pantopoulos, K. (2002). Conditional Derepression of Ferritin Synthesis in Cells Expressing a Constitutive IRP1 Mutant. *Molecular and Cellular Biology* 22, 4638–4651.

Wang, J., and Pantopoulos, K. (2011). Regulation of cellular iron metabolism. *The Biochemical Journal* 434, 365–381.

Warnecke, C., Zaborowska, Z., Kurreck, J., Erdmann, V.A., Frei, U., Wiesener, M., and Eckardt, K.-U. (2004). Differentiating the functional role of hypoxia-inducible factor (HIF)-1 $\alpha$  and HIF-2 $\alpha$  (EPAS-1) by the use of RNA interference: erythropoietin is a HIF-2 $\alpha$  target gene in Hep3B and Kelly cells. *The FASEB Journal* 18, 1462–1464.

Weiss, G., and Goodnough, L.T. (2005). Anemia of Chronic Disease. *New England Journal of Medicine* 352, 1011–1023.

WHO (2005). Worldwide prevalence of anaemia 1993–2005. WHO global database on anaemia / Edited by Bruno de Benoist, Erin McLean, Ines Egli and Mary Cogswell.

Wingert, R.A., Galloway, J.L., Barut, B., Foott, H., Fraenkel, P., Axe, J.L., Weber, G.J., Dooley, K., Davidson, A.J., Schmid, B., et al. (2005). Deficiency of glutaredoxin 5 reveals Fe-S clusters are required for vertebrate haem synthesis. *Nature* 436, 1035–1039.

Ye, H., and Rouault, T.A. (2010). Human Iron–Sulfur Cluster Assembly, Cellular Iron Homeostasis, and Disease. *Biochemistry* 49, 4945–4956.

Youdim, M.B.H. (2008). Brain iron deficiency and excess; cognitive impairment and neurodegeneration with involvement of striatum and hippocampus. *Neurotoxicity Research* 14, 45–56.

## 5. BIBLIOGRAPHY

---

Zambrowicz, B.P., Imamoto, A., Fiering, S., Herzenberg, L.A., Kerr, W.G., and Soriano, P. (1997). Disruption of overlapping transcripts in the ROSA  $\beta$ geo 26 gene trap strain leads to widespread expression of  $\beta$ -galactosidase in mouse embryos and hematopoietic cells. *Proceedings of the National Academy of Sciences of the United States of America* *94*, 3789–3794.

Zhang, D.-L., Hughes, R.M., Ollivierre-Wilson, H., Ghosh, M.C., and Rouault, T.A. (2009). A Ferroportin Transcript that Lacks an Iron-Responsive Element Enables Duodenal and Erythroid Precursor Cells to Evade Translational Repression. *Cell Metabolism* *9*, 461–473.

Zhang, D.-L., Senecal, T., Ghosh, M.C., Ollivierre-Wilson, H., Tu, T., and Rouault, T. a (2011). Hepcidin regulates ferroportin expression and intracellular iron homeostasis of erythroblasts. *Blood* *118*, 2868–2877.

Zhang, Y., Mikhael, M., Xu, D., Li, Y., Soe-Lin, S., Ning, B., Li, W., Nie, G., Zhao, Y., and Ponka, P. (2010). Lysosomal Proteolysis Is the Primary Degradation Pathway for Cytosolic Ferritin and Cytosolic Ferritin Degradation Is Necessary for Iron Exit. *Antioxidants & Redox Signaling* *13*, 999–1009.

Zohn, I.E., De Domenico, I., Pollock, A., Ward, D.M., Goodman, J.F., Liang, X., Sanchez, A.J., Niswander, L., and Kaplan, J. (2007). The flatiron mutation in mouse ferroportin acts as a dominant negative to cause ferroportin disease. *Blood* *109*, 4174–4180.

Zumbrennen, K.B., Wallander, M.L., Romney, S.J., and Leibold, E. a (2009). Cysteine oxidation regulates the RNA-binding activity of iron regulatory protein 2. *Molecular and Cellular Biology* *29*, 2219–2229.

---



## 6. APPENDIX

This chapter includes experiments that were performed at the Mouse Clinic Institut (ICS, Strasbourg) and are not shown in the main body of this thesis. The description of the experimental procedures as well as of the data has been adopted from a written report provided by the ICS.

### 6.1 STUDY DESIGN

A first cohort of mice was used for metabolic and cardiac exploration, as well as for blood analysis. This pipeline was constituted of 36 mice, 18 wild type control mice (WT) (9 males and 9 females) and 18 IRP1\* mice (9 males and 9 females) fed with a standard chow diet. Body weight and food intake were recorded once a week from the age of 10 to 18 weeks. At the age of 10 weeks, body composition (lean, fat and free body fluid content) was evaluated on conscious mice by quantitative nuclear magnetic resonance (qNMR). At the age of 11 weeks mice were housed individually in TSE cages for evaluation of energy expenditure by indirect calorimetry. At the end of the experiment, 48 hours feces were collected for evaluation of the food efficiency by a calorimetric bomb. Cardiac electrical activity was assessed by electrocardiography (ECG) at the age of 12 weeks. 3 weeks later, an oral glucose tolerance test (OGTT) was performed after 16 hours fasting. At the age of 17 weeks, insulin sensitivity was evaluated by an intraperitoneal insulin sensitivity test (IPIST) after 2 hours fasting. At the end of the study (at 19 weeks of age) blood was collected on 4h fasted mice by retro orbital puncture under isoflurane anaesthesia. Mice were sacrificed for visual inspection and measurement of body weight and body length.

For the neurobehavioral assessments, a second cohort of 12 WT and 12 IRP1\* male mice was used. Following their arrival to the testing area, animals were group housed in MICE cages and maintained in a room with controlled temperature (21-22°C) under a 12-12 light-dark cycle (light on at 07 a.m.), with food and water available *ad libitum*. All experiments were carried out in accordance with the European Communities Council Directive of 24 November 1986.

## **6.2 MATERIALS AND METHODS**

### **6.2.1. Body weight, food intake and body composition**

Body weight and food intake were recorded once a week from the age of 10 to 18 weeks. qNMR analysis was performed at 10 weeks of age to give precise analysis of the body composition for fat content, lean tissues and free body fluid. This was conducted using a the Minispec+ analyzer (Bruker) by Nuclear Magnetic Resonance (NMR) and during light period on conscious fed mice.

### **6.2.2 Energy expenditure**

Energy expenditure was evaluated at 11 weeks of age through indirect calorimetry. Oxygen consumption was assessed with an open flow respirometric system (TSE system, Labmaster, Germany). The system contains CO<sub>2</sub> and O<sub>2</sub> sensors to measure the difference in CO<sub>2</sub> and O<sub>2</sub> concentrations in air volumes flowing through control or animal cages. The amount of oxygen consumed over a given period of time was calculated, knowing the volume of the air flow. Data from gas exchange were expressed as Kcal/h/kg<sup>0.75</sup>. CO<sub>2</sub> production was also monitored and both the respiratory exchange ratio (RER; which define fuel preference between glucose and lipid metabolism) and heat production (Kcal/h/kg<sup>0.75</sup>) calculated. An activity and food intake monitoring system was integrated to measure activity and feeding/drinking behaviors, which are involved in the energy expenditure. Following a 24h-acclimatization period, the experiment was performed over 24 hours, overlapping both with light period of day 1 and day 2 (from 3:00pm Day 1 to 3:00pm Day 2), under a 12h light: 12h dark photoperiod, at ambient temperature (21°C ± 2).

### **6.2.3 Calorimeter bomb**

The feces were collected during 48 hours at the age of 11 weeks in the TSE cages. The energy content of the stools was evaluated in a bomb calorimeter (C503 control, IKA). The sample was burned in an oxygen-rich atmosphere inside a sealed chamber surrounded by a jacket containing a known volume of water. The rise in temperature of the water was recorded and used to calculate the amount of heat produced. The assay was performed on stools to evaluate the energy digested by mice and then, indirectly, the intestinal function. The energy digested was calculated by the difference between the total calories ingested and excreted in feces and expressed as “food efficiency”.

#### **6.2.4 Oral glucose tolerance test with insulin measurement**

An oral glucose tolerance test was performed at 15 weeks of age to evaluate the regulation of the glycemia. Acute hyperglycemia was induced by administration of a standardized glucose bolus (2g/kg). The glucose was administered by oral gavage and blood glucose measured at different time points, over 180 minutes after the administration, using blood glucose monitor and glucose test strips (Roche Diagnostics, Accu-Chek). Tail bleeding was performed to collect blood measurement of the plasmatic insulin level at T0, T15 and T30 minutes after glucose administration. The test was conducted during the light period, after overnight fasting (16h fasted mice).

#### **6.2.5 Intra peritoneal insulin sensitivity test**

An intra peritoneal insulin sensitivity test was performed at 17 weeks of age to measure the regulation of the glycemia after administration of a standardized insulin load (0.5 UI/kg). The insulin was administered by intraperitoneal injection and blood glucose measured at different time points over 90 minutes after the administration, using blood glucose monitor and glucose test strips (Roche Diagnostics, Accu-Chek). The test was conducted during the light period, after 2h fasting.

#### **6.2.6 Blood analysis**

Blood was collected by retro orbital puncture under isoflurane anesthesia after 4 hours fasting, at the age of 19 weeks. Blood chemistry was performed on an OLYMPUS AU-400 automated laboratory work station (Olympus France SA, Rungis, France) using commercial reagents (Olympus Diagnostica GmbH, Lismeehan, Ireland). A complete blood count was performed on an Advia 120 Vet. (Siemens). All the data are expressed as mean +/- SEM. All comparison between IRP1\* and WT mice were performed using Anova test followed by a Student t test. A statistically significant difference was considered for  $p < 0.05$ .

#### **6.2.7 Gross neurological examination**

The general health and basic sensory motor functions were evaluated using a modified SHIRPA protocol (EMPreSS, eumorphia.org). This analysis provides an overview of physical appearance, body weight, body temperature, neurological reflexes and sensory abilities. Spontaneous activity was measured using 24 individual boxes equipped with infra-red captors allowing automatic measurement of ambulatory locomotor activity and rears (Imetronic, Pessac,

France). Mice were tested for 2 hours and the evolution of global locomotion and rears was followed per 10-min bins over the testing period.

### **6.2.8 Open field test**

The openfield test allows evaluation of anxiety and exploratory drive. Mice were tested in automated open fields (Panlab, Barcelona, Spain), each virtually divided into central and peripheral regions. The open fields were placed in a room homogeneously illuminated at 150 Lux. Each mouse was placed in the periphery of the open field and allowed to explore freely the apparatus for 30 min, with the experimenter out of the animal's sight. The distance traveled, the number of rears, and time spent in the central and peripheral regions were recorded over the test session. The latency and number of crosses into as well as the percent time spent in center area were used as indices of emotionality/anxiety.

### **6.2.9 Histology**

For histopathological analysis, heart, anterior tibialis and gastrocnemius + soleus muscles were collected on 6 mice per group. All tissues were paraffin embedded and hematoxylin-heosin-(HE) stained.

## **6.3 RESULTS**

### **6.3.1 Body weights and food intake**

Body weights tended to be lower in IRP1\* mice than in the controls; however the difference was not significant between IRP1\* and WT mice (in both genders) (Fig. 6.1a, top). The food intake tended to be slightly lower in IRP1\* mice than in the controls; however the difference was not significant between the 2 groups (Fig. 1a, bottom).

While body weights were comparable, IRP1\* mice showed a slight increase in the percentage of fat; however their fat mass in gram was comparable to the controls. Lean and free body fluid content were not significantly changed in male IRP1\* mice. Female IRP1\* mice did not showed any significant change in their body composition (lean, fat and free body fluid content). (Fig. 6.1b)

### **6.3.2 Energy expenditure, activity, food and water intake**

Oxygen consumption, RER and heat production were not significantly changed in female IRP1\* mice. Male IRP1\* mice showed a slight increase in oxygen consumption and in heat production only during the light period, which could be considered as a physiological change (Fig. 6.a). Ambulatory activity was comparable between IRP1\* and WT mice (Fig. 6.2b). Food and water consumption were also similar (Fig. 6.2c).

### **6.3.3 Calorimetric bomb**

The feces energy content, the total energy excreted and ingested by day and the food efficiency were similar between IRP1\* and WT mice (Fig. 6.3).

### **6.3.4 Oral glucose tolerance test**

After 16 hours fasting, body weights were similar between IRP1\* and WT mice. All the parameters of the OGTT were comparable between IRP1\* and WT mice. Time 0 glucose and the area under the glucose curve (AUC) were not significantly changed in IRP1\* mice (Fig. 6.4a). Insulin levels at time 0, 15 and 30 minutes were also similar between IRP1\* and WT mice (Fig. 6.4b).

### **6.3.5 Insulin sensitivity test**

At the age of the test, body weights were similar between IRP1\* and WT mice. T0 glucose levels and the slope of glucose decrease during the IPIST were similar between male IRP1\* and

WT mice (Fig. 6.5, left). T0 glucose levels were similar between female IRP1\* and WT mice; however the slope of glucose decrease after insulin injection was slightly higher in female IRP1\* mice than in the controls (Fig. 6.5, right).

### **6.3.6 Blood analysis**

Erythrocytes number was significantly lower in male and female IRP1\* mice than in the controls. In addition hemoglobin, and hematocrit levels were decreased in IRP1\* mice, while the MCV was higher in IRP1\* mice than in the controls (Fig. 6.6a).

Regarding blood chemistry parameters and enzymatic activities: glucose, total, HDL and LDL cholesterol, triglycerides, free fatty acids (FFA), and glycerol levels were comparable between IRP1\* and WT mice (Fig. 6.6b).

### **6.3.7 General health and specific motor abilities**

IRP1\* males had good general health, showing normal body weight, normal body temperature and locomotor activity (Fig. 6.7). Gross neurological evaluation of mice did not reveal any obvious sign of altered sensory or vestibular functions in IRP1\* mice (not shown).

### **6.3.8 The openfield test**

In the openfield test, overall locomotor activity and rears were comparable between WT and IRP1\* males ( $t_{22} \leq 0.72$ , NS) (Fig. 6.8, top). Exploration of the central part of the openfield arena (% time in the centre and the number of entries) was also comparable between genotypes ( $t_{22} \leq 0.99$ , NS), suggesting that IRP1\* did not affect anxiety in this test (Fig. 6.8, bottom).

### **6.3.9 Histology**

No significant microscopic lesions were detected in any of the organs proposed for analysis. As to skeletal muscles (Fig 6.9), the diameter of the fibers was equivalent in IRP1\* mice compared to controls; nuclei were peripheric, and striation was present. No significant interstitial inflammation was detected.

## 6.4 CONCLUSION

Mice with gain of IRP1 function did not display major changes in body weight, body composition, energy expenditure and food efficiency. Their glucose metabolism did not appear significantly modified and no changes were observed in their circulating lipid levels. IRP1\* mice displayed a macrocytic anemia. General health, spontaneous locomotor activity and anxiety related behavior were not affected in IRP1\* mice under the experimental conditions. No major lesions were detected in any tissues submitted for analysis.

6.5 FIGURES

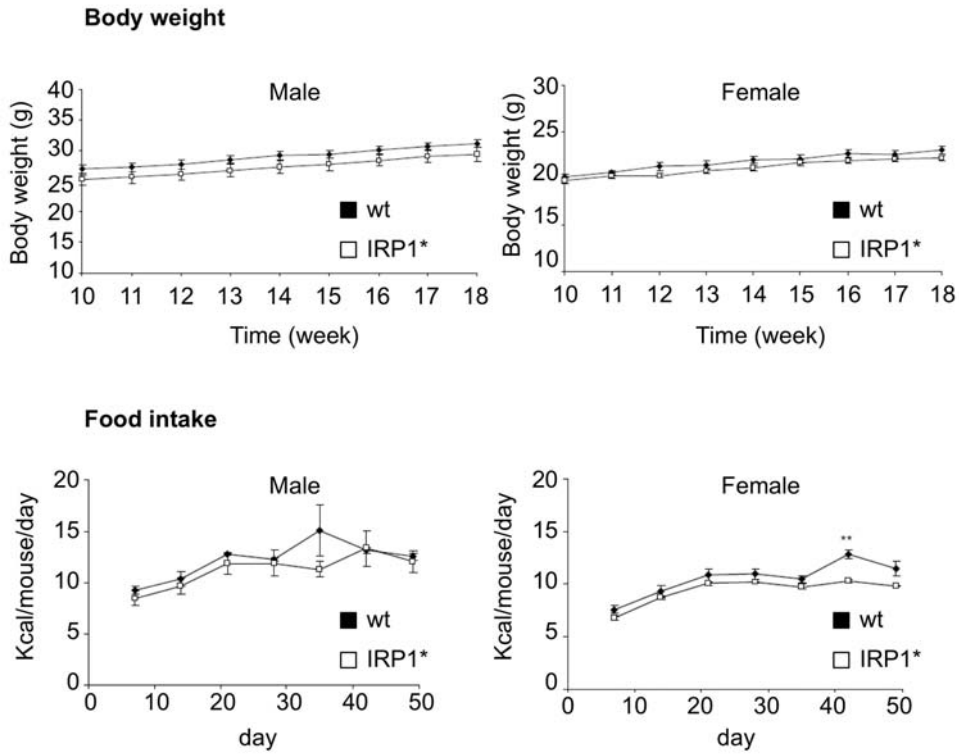


Figure 6.1a

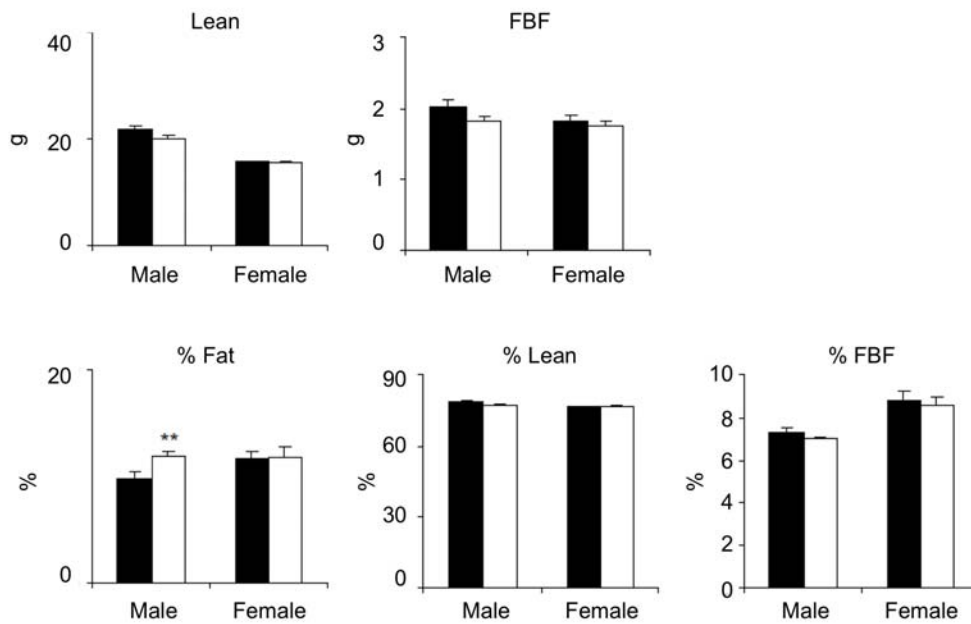


Figure 6.1b

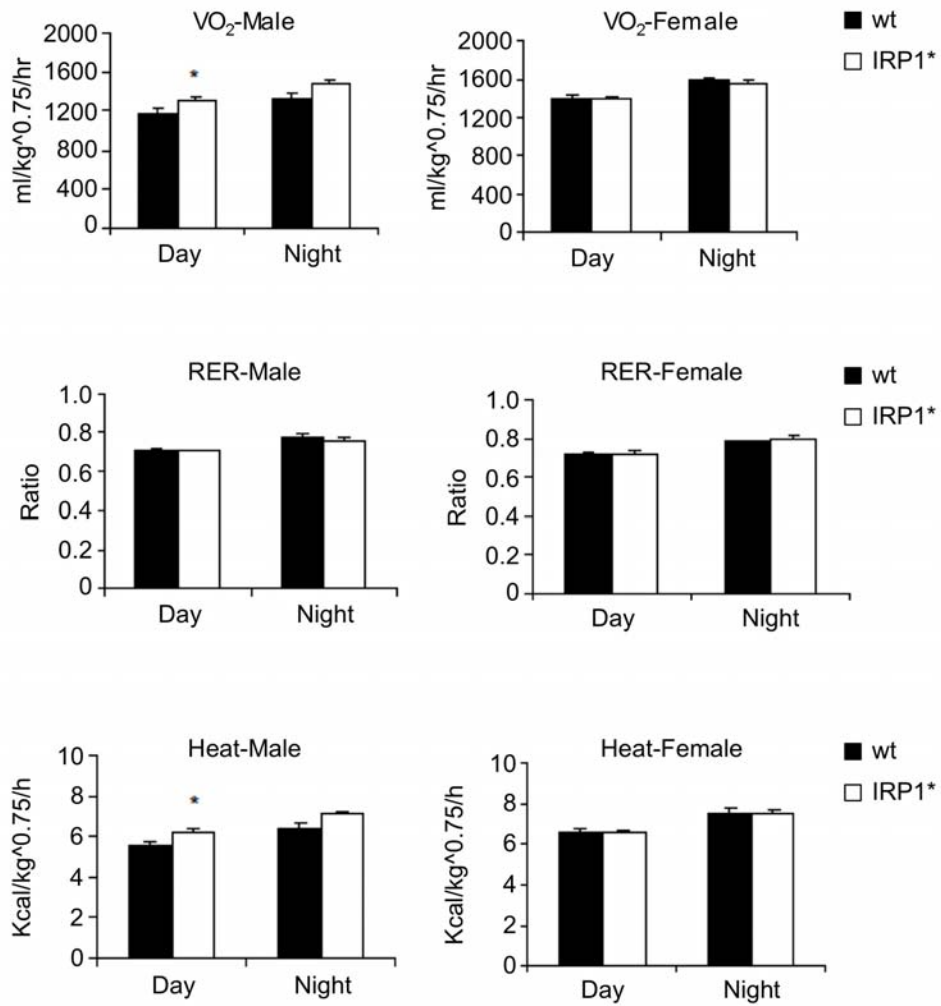


Figure 6.2a

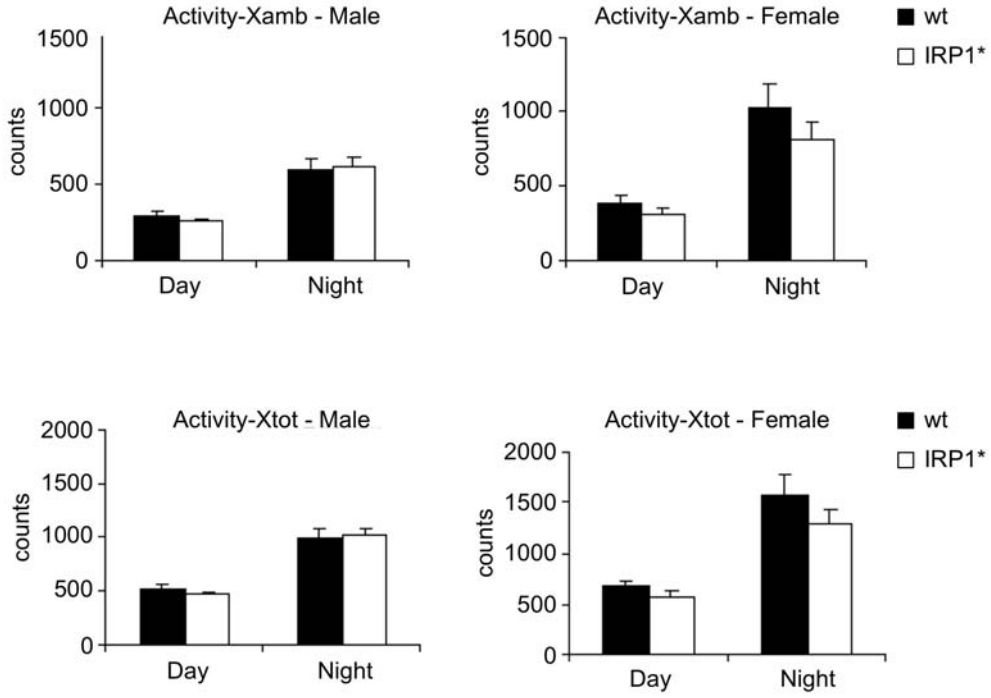


Figure 6.2b

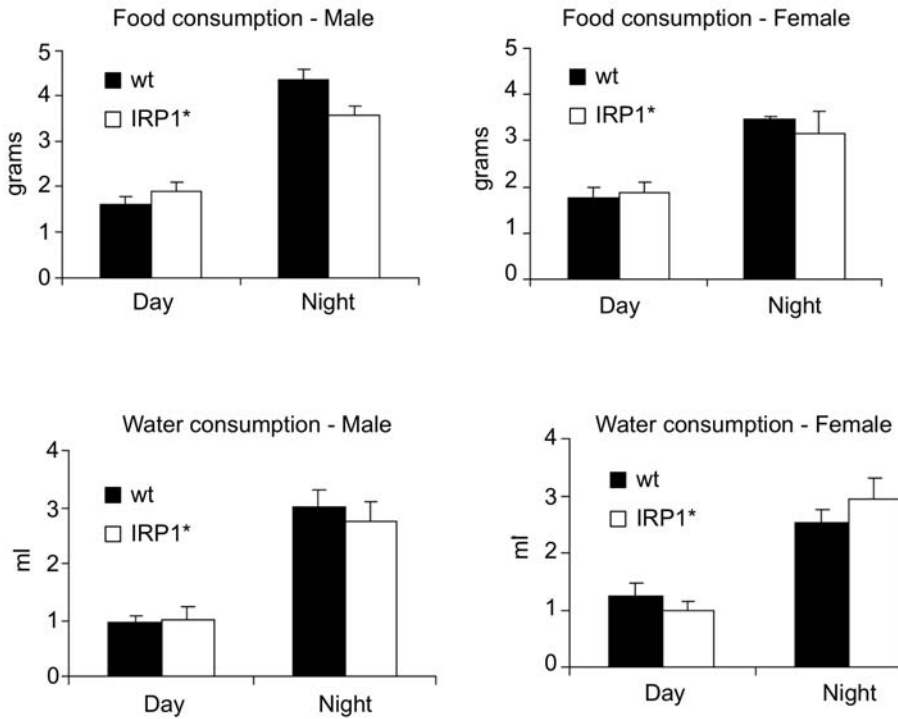


Figure 6.2c

## Calorimetric bomb

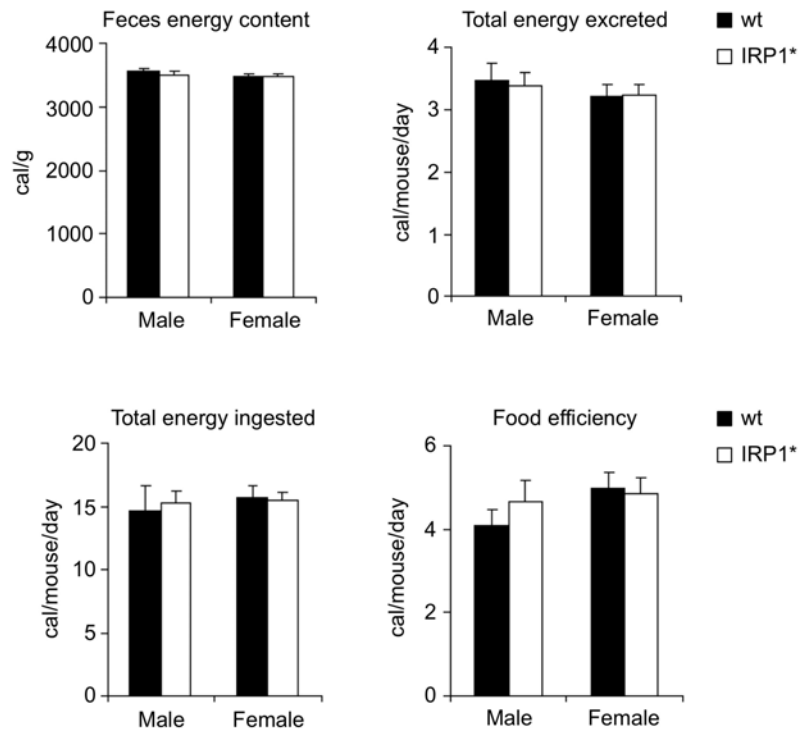


Figure 6.3

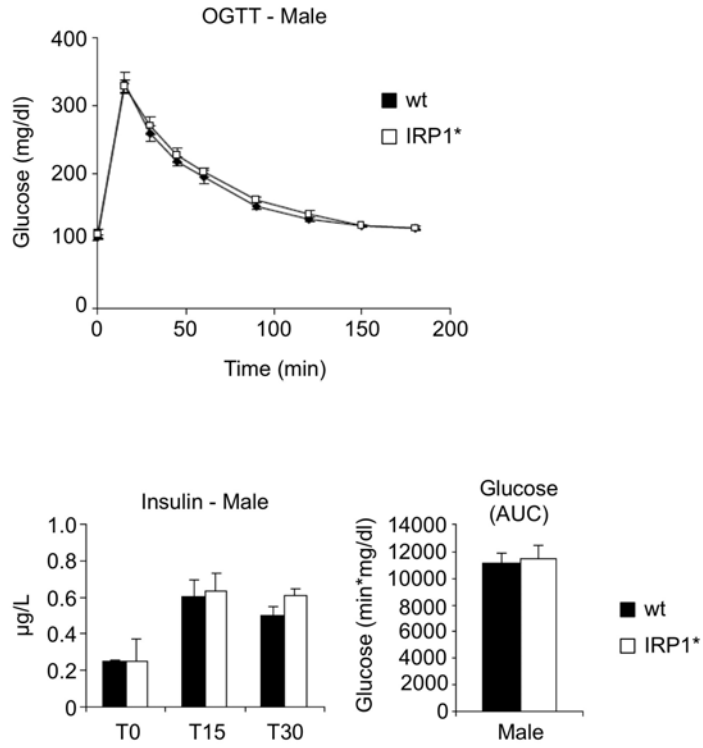


Figure 6.4a

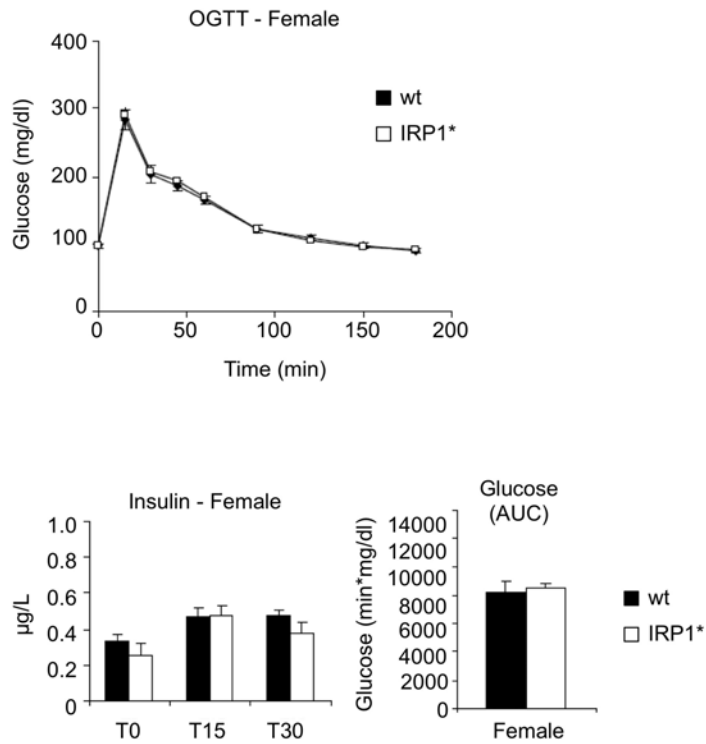


Figure 6.4b

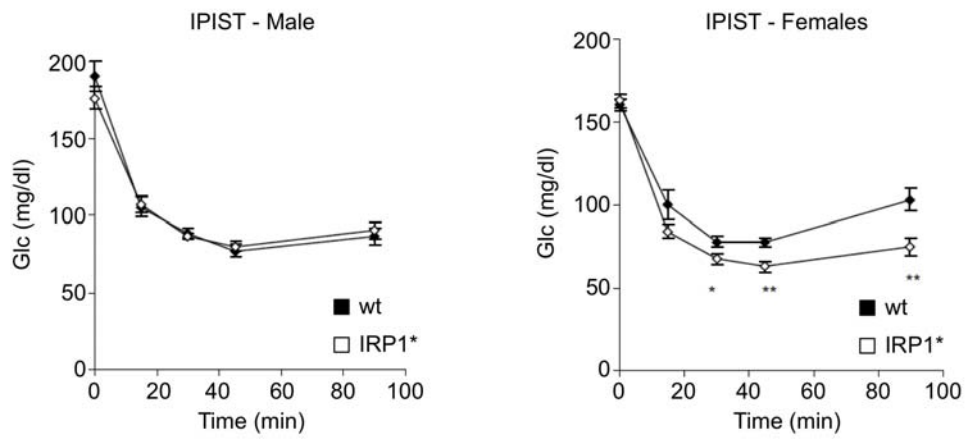


Figure 6.5

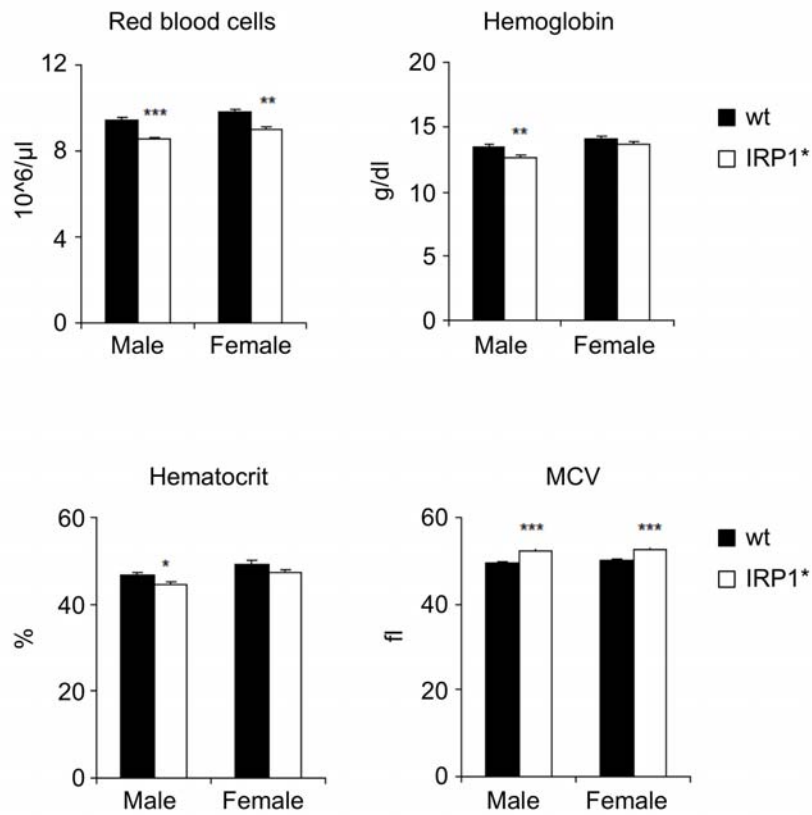


Figure 6.6a

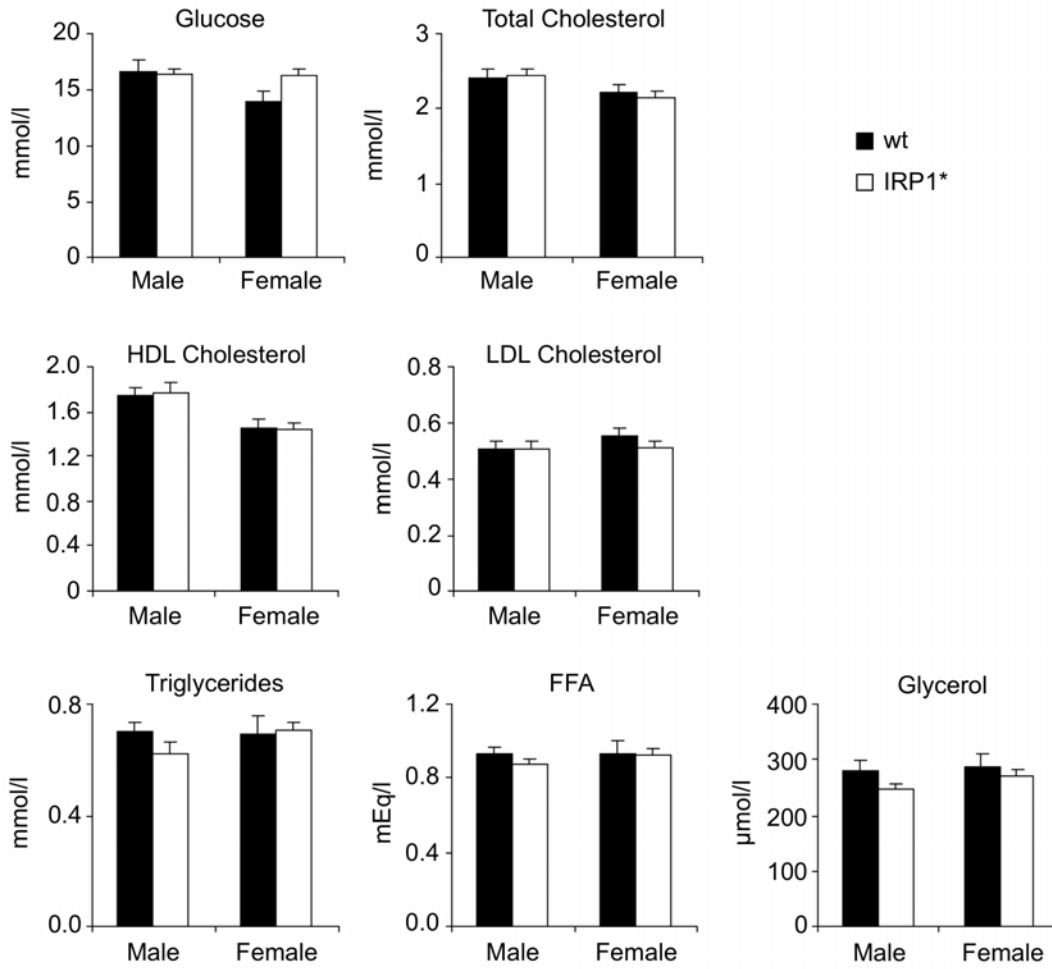


Figure 6.6b

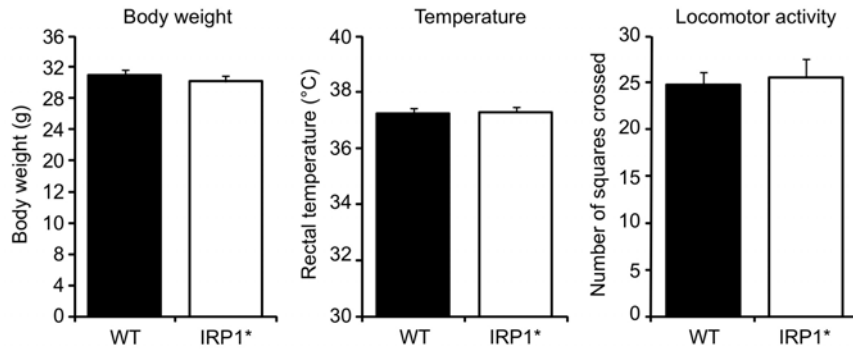


Figure 6.7

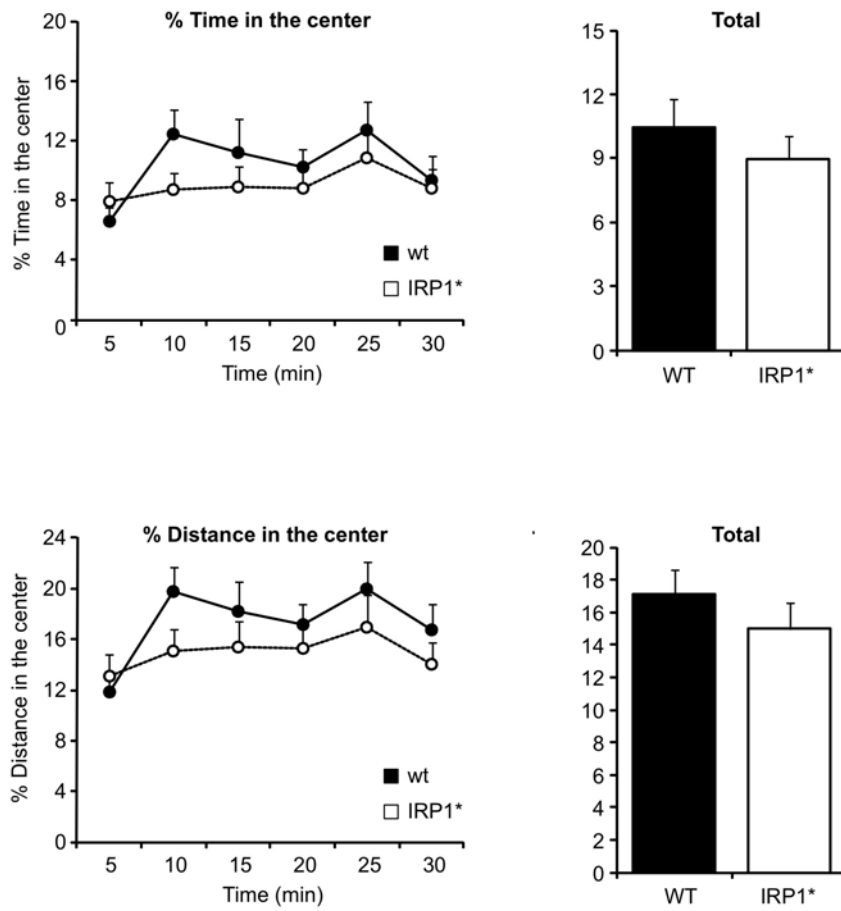


Figure 6.8a

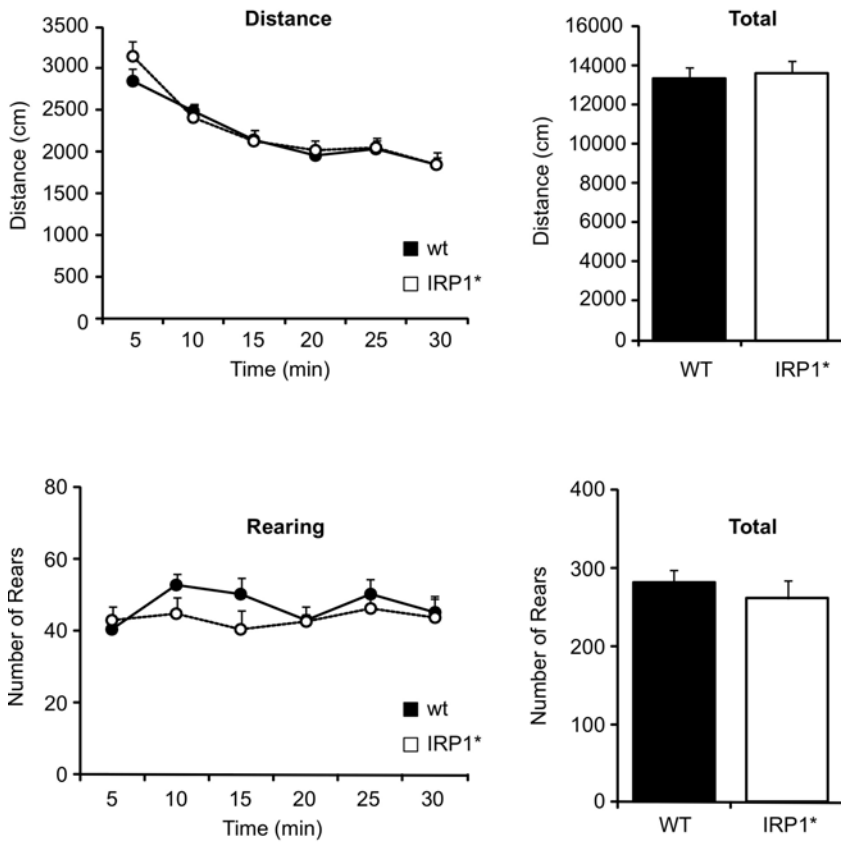


Figure 6.8b

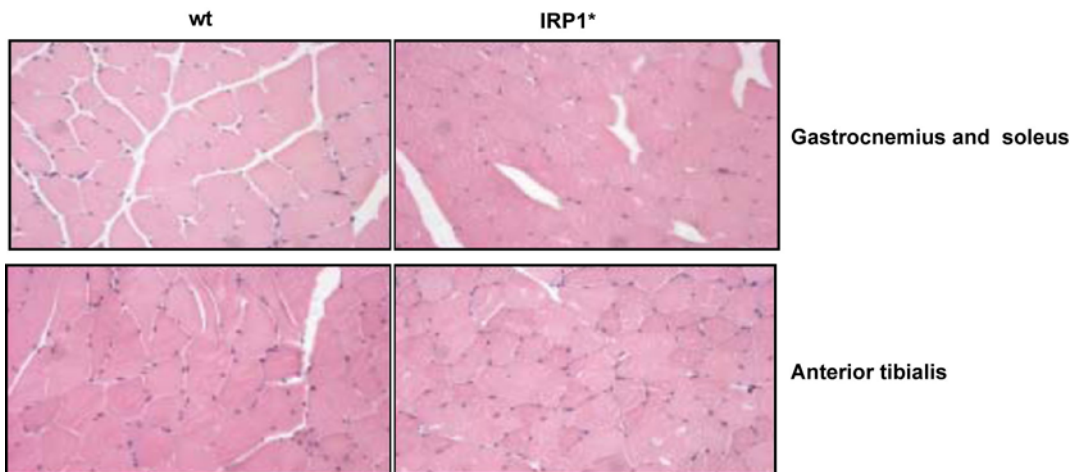


Figure 6.9

---



## 7. PRESENTATIONS AND PUBLICATIONS

### 7.1 PRESENTATIONS

**D. Casarrubea**, L. Viatte, R. Eisenstein, B. Galy, M. W. Hentze. “Generation of a mouse strain with inducible IRP1 overexpression: a new model for understanding iron metabolism disorders” International Bioiron Society (IBIS) meeting, June 2009, Porto. Poster presentation.

**D. Casarrubea**, L. Viatte, R. Eisenstein, B. Galy and M.W. Hentze. “A new mouse model with gain of IRP function to investigate the in vivo role of the IRP/IRE system in normal and pathological iron metabolism. European Iron Club (EIC), Nijmegen 2010. Poster presentation.

**Daniela Casarrubea, MS**, L. Viatte, T. Hallas, A. Vasanthakumar, R. Eisenstein, K. Schümann, B. Galy and M.W. Hentze. “A new mouse model with gain of IRP function to investigate the in vivo role of the IRP/IRE system”. International Bioiron Society (IBIS) meeting, May 2010, Vancouver. Podium presentation.

### 7.2 PUBLICATIONS

Most results presented in this dissertation are part of a manuscript submitted for publication and currently under review process. Some text passages of the submitted manuscript have been adopted in this dissertation.



## 8. ACKNOWLEDGEMENTS

I want to thank all the people who contributed to the success of this work.

First of all, I like to thank Matthias for giving me the possibility to do my PhD in such a great research institute as EMBL. In particular, I want to thank him for his faith and great encouragement over the last years.

I am especially indebted to Bruno, for his interest in my work, his inspiration, his suggestions and the time he took for discussion.

Many thanks to Darren Gilmour, François Spitz and Klaus Unsicker, who followed with interest the development of my work throughout these years.

I would like to thank Ralf Bartenschlager for kindly taking part to my thesis defense committee.

I want to acknowledge the laboratory of animal resources (LAR) and the transgenic service. In particular I would like to thank Conny Henkel for taking daily care of our animals and Klaus Schmidt for being always so eager to help with mouse experiments. The flow cytometry facility, and in particular Alexis, helped a lot for part of this work.

I also want to thank S. Srinivas for donation of the plasmids pBigT and pROSA26PA, as well as Maja Vujić and Martina Muckenthaler for the kind gift of the HFE mouse line.

Thanks to our collaborators Rick Eisenstein, Klaus Schuman, the ICS and prof. J.H. Groene for sharing their expertise and for their contribution to this work. Also, I want to thank Lydie Viatte who started this project before my arrival to the lab.

## 8. ACKNOWLEDGEMENTS

---

If the experimental work was particularly challenging, I was glad that I could always count on Dunja for technical assistance and for sharing all her tips and tricks. I would also like to thank Sandro, who even from downtown was so open for discussion and help.

I am grateful to all the people who proof-read my thesis and gave useful comments, including Bruno, Matthias, Elli, Rasti, Suzie, Per, Dunja, Amy, Robert and Rodolfo. In particular, I am thankful to Suzie for her critical support during this last intense lap of my PhD, for very useful discussion and help. Also, I want to thank Bene for translating the summary of this thesis into this evil language (a.k.a. German).

Alongside, I would like to thank all the previous and current members of the Hentze lab, for the science they shared but also for the friendship and the great atmosphere they created in the lab. Among the previous, I want to especially thank Francesca and Aurelie, and among the current ones I cannot fail to mention Alfredo, since he showed me that “he has changed”. Thanks all of you for the crazy and fun atmosphere of the “main lab” (V211), and also of the other lab V210 (now it’s stated in an official document).

My stay in Heidelberg would not have been so enjoyable and unique if I had not met nice people with whom I shared friendship, trips, troubles and parties. Among those, I want to especially thank my great friends Francesca, Luca, Angelica and Andreas. Also, it was great to share, among other things, a passion for swing dance with my friends Erika and Enrico. I want to thank all the predocs of my year, for the fun and trips, as well as my dear roomies, Johanna, Esme and Caro, for being so incredibly caring and supportive like a real family.

These last six months would have been much harder if Per was not next to me, with all his affection, great support, patience and encouragement. Thanks so much.

Grazie a mia madre, per la sua testarda irragionevolezza nel continuare a credere in me.

---

This work was partially supported by an EEC FP6 grant (LSHM-CT-2006-037296 Euroiron1) and a Virtual Liver Network grant (funding number 315740) to M.W.H..